Spring 1990

Experimental Studies of Bulk Optically Controlled GaAs Switches Utilizing Fast Infrared Quenching

Michael S. Mazzola
Old Dominion University

EXPERIMENTAL STUDIES OF BULK OPTICALLY CONTROLLED GaAs SWITCHES UTILIZING FAST INFRARED QUENCHING

by

Michael S. Mazzola
B.S.E.E. December 1984, Old Dominion University
M.E. December 1986, Old Dominion University

A Dissertation Submitted to the Faculty of
Old Dominion University in Partial Fulfillment of the
Requirements for the Degree of

DOCTOR OF PHILOSOPHY

ELECTRICAL ENGINEERING

OLD DOMINION UNIVERSITY
May 1990

Approved by:

Karl H. Schoenbach (Director)

ABSTRACT

EXPERIMENTAL STUDIES OF BULK OPTICALLY CONTROLLED GaAs SWITCHES UTILIZING FAST INFRARED QUENCHING

Michael S. Mazzola
Old Dominion University, 1990
Director: Dr. Karl H. Schoenbach

This dissertation describes some of the properties of copper-compensated, silicon-doped GaAs (Cu:Si:GaAs) with the purpose of demonstrating the feasibility of the Bulk Optically Controlled Switch (BOSS) concept. The BOSS concept involves the excitation of electrons or holes from selected deep centers in the band gap of a bulk Cu:Si:GaAs photoconductor. The conductivity of the Cu:Si:GaAs crystal can be increased or decreased on command by irradiating the crystal with laser light of different wavelengths in the infrared. Photoconductivities as large as 1 $(\Omega\ cm)^{-1}$ were measured to persist for microseconds after illumination by a 7 ns laser pulse with wavelength λ = 1064 nm. Strong optical quenching of this photoconductivity over a nanosecond time scale has been observed during illumination with a second laser pulse of wavelength $\lambda \geq 1500$ nm. During the conduction phase, currents as large as 10 kA/cm^2 have been measured after the crystal withstood fields as large as 19 kV/cm. Dark conductivities of GaAs crystals grown with a silicon doping density of $5 \times 10^{16}\ cm^{-3}$ have been measured after copper diffusion to range from 1.5×10^{-2} $(\Omega\ cm)^{-1}$ to as low as 1.4×10^{-6} $(\Omega\ cm)^{-1}$. These differences are interpreted to be the result of controlled compensation of the crystal resulting in the conversion of the

crystal from strongly n-type (undercompensated) to weakly p-type (over-compensated). The actual level of compensation at thermal equilibrium is shown to have an important effect on the photoconductivity properties of the crystal.

ACKNOWLEDGEMENTS

I thank first my advisor, Dr. Karl Schoenbach, who has guided me over the past several years with much thought, decisiveness, and, most important, patience.

I also thank my committee, Dr. V. Lakdawala, Dr. D. Cook, Dr. G. McRee, and Dr. R. Joshi, for their thorough consideration of this document.

To Dr. Guillermo Loubriel, who made my stay at Sandia National Laboratories over the summer of 1988 both enjoyable and fruitful, I extend my most sincere appreciation.

In addition I must mention Mr. John Wigginton and Mr. Randy Roush for their considerable help and skill during development and optimization of the diffusion apparatus. Also, I thank Dr. Sung Ko and Mr. Steven Pronko for their ideas on switch development and laser design and construction. Last but not least, I thank Mr. David Stoudt for completing his thesis first so that I could benefit from his research in topics related to high-power switching with bulk gallium arsenide.

Finally, my most loving gratitude goes to my wife, Janice, for five years of support through long hours and separations, without which my graduate studies would not have been completed.

TABLE OF CONTENTS

TABLE OF CONTENTS - Concluded

LIST OF TABLES

LIST OF FIGURES

LIST OF FIGURES - continued

LIST OF FIGURES - concluded

CHAPTER I

INTRODUCTION

The switching needs of pulsed power machines range widely in power and temporal character. At the extreme of today's needs there are switches that can hold-off millions of volts while breaking down on command to conduct megamperes over a time scale of tens to hundreds of nanoseconds. Perhaps more common are switches that operate between 1 kV and 100 kV, switch 1 kA to 50 kA and operate in the nanosecond regime for closing but recover their dielectric strength over microseconds or longer. Recently, the need for "true" opening switches that can open in nanoseconds as well as close has become apparent [1].

Except for the opening switch, the needs of pulsed power have been met most often with gas filled devices such as thyratrons and spark gaps or with vacuum devices such as vacuum electron tubes. In certain applications requiring relatively slow switching, such as circuit breakers, mechanical switches are used. Increasingly, miniaturization and efficiency are desired to make new applications possible and, as in the case of digital electronics, the obvious approach is to turn to the solid state.

Of course, the solid state materials most likely to be of use as a switch are the semiconductors. Semiconductors can be fabricated into devices that can be switched "on" in nanoseconds or less [2]. Some can be made to open on command, thus raising the possibility of nanosecond to picosecond opening switches for use in

high-repetition-rate, high-bandwidth applications (e.g., impulse radar) [3] or in inductive energy storage, thus allowing for the miniaturization of not only the switch but also the energy storage portion of the pulsed power machine [1].

What semiconductor devices are available for use as high power switches? Since junction devices have traditionally dominated semiconductor technology, it is no surprise that junction devices known as thyristors are the most readily available semiconductor switches for high-power applications (i.e., through-put power greater than 100 kW). However, thyristors based on silicon technology seem to have reached a plateau at a few megawatts, primarily due to voltage hold-off limitations of a few kilovolts [4]. This technology is also inherently slow, limited typically to microsecond closing times. Opening is limited to specialized thyristors such as the gate turn off thristor (GTO) which has relatively low efficiency and long opening times (again, in the mirocseconds) [5]. For many pulsed power applications, these devices are clearly not suitable.

Devices based on MOS transistor technology have been fabricated that demonstrate nanosecond opening and closing; however, the fragile nature of these devices has severely limited their voltage handling capabilities to hundreds of volts [6]. Stacking of these devices to achieve interesting levels of through-put power results in electrical isolation problems for the control electronics driving the gates of the MOS transitors (a problem shared by thyristors), and increases the closing and opening times substantially [6].

Recently, substantial interest has been shown in the pulsed power community for a new type of semiconductor switch, the optically controlled bulk semiconductor switch [3]. An optically controlled bulk switch is based on a highly resistive piece of

semiconductor material (e.g., pure silicon or semi-insulating gallium arsenide) that can be made to conduct by shining light (usually from a laser) on to the region of the semiconductor spanning two ohmic contacts. The resultant current flow can be made to rise in under a nanosecond by application of a suitably fast and intense laser pulse [7]. Since photon absorption is a process occurring over femtoseconds, the activation of the conductivity is considered to be practically devoid of jitter (i.e., timing uncertainty). While the basic idea is not new, advanced concepts will make this type of switch competitive.

One application of bulk optically controlled semiconductor switches that has generated considerable interest is as a nanosecond opening switch (or in some cases, picosecond). This work has focused on direct band gap materials such as gallium arsenide (GaAs) because the electron-hole pair lifetime of silicon is generally too long. For GaAs, the conductivity is generated by shining band gap radiation onto the sample, thus generating a dense electron-hole plasma that conducts the switch current. In properly prepared semi-insulating GaAs, the electron-hole pair lifetime can be subnanosecond [7]; therefore, when the laser pulse has exhausted itself the switch conductivity will rapidly decrease due to electron-hole recombination.

However, the same property which makes the semiconductor material useful as an opening switch also severely limits the quantum efficiency of the closing phase, because so many photons are required to sustain the photoconductivity against the rapid loss of electrons and holes. Since many applications are best suited for relatively long conduction phases (e.g., hundreds of nanoseconds to microseconds) followed by nanosecond opening [8], an unacceptable expenditure of costly laser photons may result from trying to sustain the conductivity. In fact, this problem is

so severe that in applications where relatively short pulses are adequate the required energy of the activating optical radiation may still be unpractical, especially where relatively large area switches are required to handle the through-put power.

Even where fast opening is not required, there are other properties of GaAs that make it a desirable switch material as compared to silicon, such as a wider band gap (to prevent thermal runaway) and a larger electron mobility (for more efficient switching through lower on-state resistance) [9]. In this case, the ability to generate long lifetime photocarriers in GaAs for purely closing applications may be desirable.

Switch concept

A concept that attempts to overcome these obstacles while retaining the advantages of semi-insulating GaAs has been proposed [10]. This proposal, called the Bulk Optically controlled Semiconductor Switch (BOSS), involves the controlled compensation of silicon doped GaAs with copper (Cu:Si:GaAs). Copper forms several deep acceptor levels in GaAs, including levels at 0.14 eV, 0.24 eV, and 0.44 eV above the valence band [11]. Silicon, which forms a shallow donor in GaAs about 6 meV below the conduction band [11], is compensated by the copper acceptors, which results in a highly resistive, semi-insulating semiconductor. The simplified system is illustrated in Fig. I-1.

The copper level at 0.44 eV, labeled as Cu_B in Fig. I-1, has several interesting properties. The capture cross section for free electrons is quite small, while the ratio of the capture cross sections for free holes to free electrons is about 10^6. This makes the level a hole trap [12-13]. In addition, the photoexcitation cross section for holes from the Cu_B state is about an order of magnitude larger than for the photoexcitation of electrons [12]. These cross sections can be exploited to generate

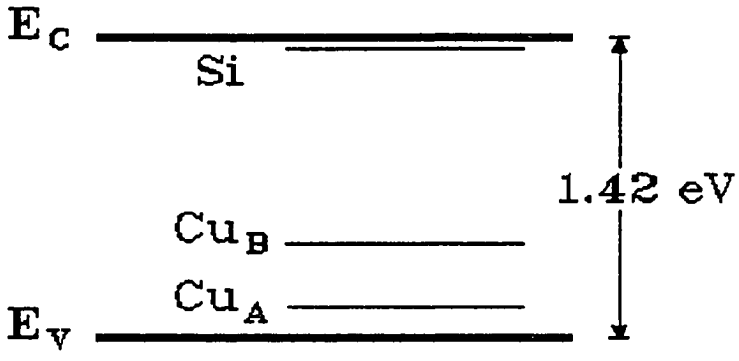

Figure I-1 Simplified energy level diagram of the Cu:Si:GaAs system.

long lifetime photoexcited free electrons to provide for electrical conduction, while allowing the possibility for extinguishing this conductivity by selective photoexcitation of holes from the Cu_B state [10]. This mechanism is described in more detail in the following.

Consider Fig. I-2 (a). A compensated Cu:Si:GaAs crystal is illuminated by radiation with photon energy sufficient to span the gap between the Cu_B state and the conduction band (e.g., with $h\nu$ = 1.1 eV, 1064 nm radiation from a Nd:YAG laser is adequate). This radiation excites both electrons and holes into the conduction band and valence band respectively through a two-step process. As the laser pulse dies away, an initial period of fast recombination occurs; however, a sufficient density of holes are re-trapped back into Cu_B to allow a large free electron density to remain in the conduction band. Because electrons are trapped back into Cu_B only very slowly, the n-type photoconductivity persists for a long time after the laser pulse. This phase is illustrated by Fig. I-2 (b). The conductivity decay rate is probably controlled by the thermal emission of holes from Cu_B, which subsequently recombine with the free electrons, a process that limits the photoconductivity decay to tens of microseconds at room temperature.

The photoconductivity need not be allowed to persist. As shown in Fig. I-2 (c), if the crystal is once again illuminated, but now with radiation of small enough photon energy to exclude Cu_B to conduction band transitions, but large enough to excite holes from Cu_B to the valence band (in practical terms: 0.44 eV < $h\nu$ < 1.0 eV), then the trapped holes in Cu_B will be "stimulated" to recombine with the free electrons and thus extinguish the photoconductivity. Therefore, the BOSS concept utilizes the fast recombination characteristic of semi-insulating GaAs to extinguish

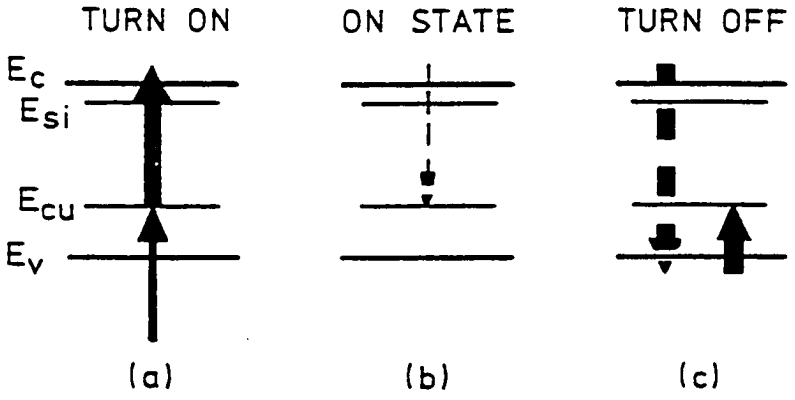

Figure I-2 The BOSS switching cycle showing the generation of tail conductivity in (a); the slow decay of free electrons during tail conduction in (b); and the fast quenching of the tail conductivity by infrared radiation in (c) (from Ref. [10]).

the photoconductivity over nanoseconds or less, while not interfering greatly with the efficient excitation of long-lived photoconductivity. In other words, the Cu:Si:GaAs material could be the basis of an efficient semiconductor based on-command closing and opening switch.

This thesis will demonstrate that the controlled compensation of silicon doped gallium arsenide with copper is possible, thus resulting in a high-resistivity bulk semiconductor suitable for use as an optically controlled switch. In addition, it will be shown that the basic concept described above is sound, and that specific properties of the laser induced photoconductivity of the compensated material, such as the dependence of the photoconductivity on such factors as the degree of compensation, laser wavelength, and laser intensity, is adequately explained by rate equation based models of the bulk material.

Previous work

This review will be restricted to work involving the optical control of bulk semiconductor switches. Three categories of such switches will be identified. The categories are: switches that utilize the diversion of current to control the generated pulse; switches that rely on light to sustain the photoconductivity in the face of recombination; and switches that use two light pulses to both increase and decrease the bulk conductivity of the crystal. It should be noted that the second category could include closing switches based on pure silicon, but since these switches cannot be turned off in a practical sense, they will be omitted.

The Auston switch [14] is perhaps the most well known of the current diversion switches (also known as "crowbars"). The Auston switch is made of a slab of high-resistivity silicon imbedded in a micro-stripline. The slab has two contacts on

the surface which forms a gap between two conductors on top of the stripline. In addition, there is a third contact to the ground plane beneath the slab. A frequency doubled Nd:YAG laser pulse (λ = 532 nm) is applied to the gap on the top surface of the slab, which penetrates only slightly into the semiconductor (~ 1 μm) because the photon energy of the light exceeds the band gap of the material. The generation of free carriers between the two contacts on the surface closes the switch and launches a current pulse to the load which is connected from the top conductor of the stripline to ground. The current path is insulated, at least for a time, from the ground plane by the highly resistive silicon not illuminated by the light.

As long as the source (e.g., a charged line, capacitor, etc.) can supply the current, the switch will conduct because of the long recombination time of the carriers in relatively pure silicon. If however, a second laser pulse of photon energy less than that required for a direct transition in silicon illuminates the semiconductor, a layer of photoexcited free carriers will be created that extends all the way to the ground plane at the botton of the slab (due to the longer absorption length at this wavelength). As long as the new free carriers are created in sufficient density such that the local conduction path has an impedance much less than the load, then the current pulse will be shunted to ground, thus terminating the pulse delivered to the load (but not the pulse supplied by the source!).

While the Auston switch makes clever use of the differing absorption lengths of radiation in a semiconductor, its applications are limited. Because the switch does not terminate the source current it is not an opening switch, which means it has no application in inductive energy storage. In addition, while the load current can be turned off in picoseconds with a suitable laser, the switch cannot be used in

high-repetition-rate applications because the recovery time of the switch is limited by the recombination of free carriers in both conduction paths. These fundamental limitations exclude the Auston switch from two most interesting pulsed power applications: inductive energy storage and high-rep-rate pulsers.

In contrast, consider the light sustained bulk semiconductor switch. This device is typically based on one of several III-V semiconductors, although specially doped silicon has also been used, because of the easy availablility of semi-insulating wafers that invariably contain a concentration of fast recombination centers. These materials have electron-hole pair lifetimes that range from tens of picoseconds to perhaps tens of nanoseconds [15]. Although some of the III-V semiconductors have direct band gaps, the electron-hole pair lifetime is usually dominated by indirect recombination through centers rather than by direct recombination which results in the emission of a photon.

Because the materials are semi-insulating (defined here as a dark resistivity greater than 10^6 Ω cm) they are naturally in the open state, and thus capable of holding off substantial electric fields. In order to conduct (close the switch) the material must be illuminated with high intensity laser light. This laser radiation usually has a photon energy greater than the band gap of the material, which creates electron-hole pairs in a relatively thin region penetrating into the material. The light illuminates the region between two ohmic contacts which allows the photoconductivity to sustain current delivered to a load. However, when the light intensity is decreased or extinguished, and the electric field is not too high, the photoconductivity rapidly decays due to recombination, and the switch opens.

Perhaps the greatest quantity of work has been performed with semi-insulating GaAs [16-20], but a substantial amount of work has also been performed with InP [22] and gold doped silicon [19]. With one and two inch diameter GaAs wafers in which Ni:Au:Ge alloyed contacts were formed on one surface in a planar geometry, Zutavern and Loubriel [19] have demonstrated that at fields less than about 10 kV/cm the material will conduct hundreds of amperes during illumination by a 532 nm wavelength laser pulse. The current decay was usually limited by the finite decay time of the laser pulse (~ 10-40 ns). In addition, the breakdown strength was usually surface flashover limited to about 50 kV/cm when SF_6 was used as the dielectric, but more than twice that limit when deionized water was used [23]. However, a laser energy of at least 10 mJ was required to drive the switch resistance below 50 Ω [19].

As the field was increased above 10 kV/cm, a different phenomenon was observed, which they named "lock on" [21]. In the lock-on mode, the GaAs switch no longer opened but settled instead on a constant-voltage operating point similar to a Zener diode. The lock-on field for GaAs (determined by the voltage that the switch settles at) ranges from just over 3 kV/cm to about 8.5 kV/cm [23], depending on the sample's doping and growth technique. Since lock on has also been observed in InP but never in Si [24-25], it is believed that the transferred electron effect (known as the Gunn effect) may be a contributing factor. Other properties of lock on also suggest the Gunn effect, which will be discussed in greater detail in later chapters.

As has already been mentioned, the relatively high cost (in terms of photons) of operating the switch just described has led to new techniques for optical control

of bulk semiconductor switches. The BOSS concept is applicable to semiconductor systems other than Cu:Si:GaAs. Germer et al. [26], and Germer and Schoenbach [27] have investigated copper doped cadmium sulfide (Cu:CdS). In these experiments, bulk CdS crystals were illuminated with laser pulses of two different wavelengths [27], one for turn on (λ = 532 nm) and one for turn off (λ = 1064 nm). Both laser pulses had a full width at half maximum (FWHM) of 7 ns. The first laser pulse successfully excited long-lived photoconductivity that lasted microseconds, and the second pulse successfully interrupted this conductivity with a decay time as short as 250 ns [27]. The optical quenching (as the interruption of the photoconductivity is called) was attributed to copper centers in the band gap acting in a manner similar to that described for the case of Cu:Si:GaAs.

The material that is the focus of this thesis has also been investigated to some extent by other researchers, most notably by Blanc et al. [13]. In their work, several Si:GaAs crystals were compensated by the diffusion of copper into the crystals. The resulting high-resistivity crystals were all p-type. The conductivity of the crystals were studied both in the dark and under low intensity irradiation at various temperatures with the goal of eliciting basic data. While the crystals were not used as switches, Blanc et al. demonstrated that some of the crystals were reasonably photosensitive and that the material exhibits strong optical quenching at photon energies in the range $0.4 < h\nu < 1.1$ eV, which corresponds to hole excitation from Cu_B. Controlled compensation was not demonstrated in this work, nor was the effect of differing levels of compensation on the photoconductivity explicitly studied.

Copper-compensated, silicon-doped GaAs has been the subject of active work at Old Dominion University. Experimental optical switching work has been reported

at high power for closing [28], and at low power for both closing and opening [29-30]. In addition, a computer simulation of the photoconductivity of Cu:Si:GaAs, based on a zero dimension rate equation model, has been performed in order to provide interpretation of the experimental data as well as to provide optimization criteria for switch design [31-32]. Finally, characterization techniques have been developed, including Deep Level Transient Spectroscopy (DLTS) [33], Photo Induced Current Transient Spectroscopy (PICTS), and Thermally Induced Conductivity Spectroscopy (TICS), in order to provide basic data for the modeling work. This thesis reports on these activities as they pertain to optical control of Cu:Si:GaAs switches.

Organization

Sample preparation and characterization will be the subject of Chapter II, including a thorough description of the compensation process and results. The experimental apparatus used for optogalvanic (switching) experiments will be described in Chapter III. Chapter IV will present the results of the low power closing and opening experiments and the results of the higher power closing experiments. A discussion of these results will follow in Chapter V in which the experiment will be shown to fit well in a frame work of predictions generated from the computer calculations of S. Ko [33]. Finally, Chapter VI will summarize the important conclusions of this work and provide suggestions for future work in this important field of pulsed power switching.

CHAPTER II

SAMPLE PREPARATION AND CHARACTERIZATION

Without proper attention to the need for controlled sample preparation and accurate characterization, the BOSS concept described in Chapter I cannot be tested. Therefore, an effort has been made to develop material fabrication and diagnostic techniques. This effort has resulted in a demonstration of controlled compensation of silicon doped GaAs with copper. The subsequent effect of changing the compensation on the photoconductive properties of the material will be discussed in later chapters. This chapter will describe the fabrication process for the switch samples used in this investigation, as well as catalog and interpret the evidence from diagnostic experiments designed to elicit basic data from the samples.

Sample preparation

It is well known that the diffusion of copper into silicon doped GaAs can lead to closely compensated, highly resistive semi-insulating GaAs crystals with resistivities as high as 10^8 Ω cm [13]. In fact, close compensation can be achieved with a relatively simple doping process involving the thermal annealing of GaAs with a solid source of copper previously deposited onto the crystal. The sample preparation technique used to achieve the compensation of crystals used in this investigation will now be described.

A two-inch diameter GaAs wafer taken from an ingot grown using the horizontal Bridgman technique was procured from the manufacturer [34]. The crystal was doped by the manufacturer with silicon, a shallow donor, to a concentration of 5×10^{16} cm^{-3}. The wafer was provided by the manufacturer polished on one face only. This wafer was placed into a vacuum evaporator after which a thin layer of copper was deposited onto the polished side of the wafer. The copper layer had an approximate thickness of 1 μm. The wafer was then scored and diced into many pieces, most of which had a nominal rectangular shape of 5 mm on a side and a thickness of 0.27 mm. Some of these samples were then assigned a sample number and subjected to the next step in the preparation process: thermal annealing.

The samples were thermally annealed at various temperatures in order to drive copper into the samples by diffusion. All of the samples were annealed for two hours at temperatures between 500 °C and 600 °C. Two hours were considered sufficient to uniformly saturate the samples with copper to the concentration given by the solid solubility of copper at that temperature. This assumption is supported by calculations which were in turn based on the known diffusion parameters of copper in GaAs [35].

The annealing procedure was performed as follows. The sample was first degreased with methanol and blown dry with nitrogen (only one sample was annealed at a time). The quartz reaction tube was also degreased and cleaned with various solvents (acetone, methanol, and freon) and blown dry. The sample was then placed into the reaction tube on a predetermined mark accompanied with a small nugget of pure arsenic (weighing approximately 10 mg). The arsenic, when vaporized by the heat of the furnace, prevents the GaAs from decomposing. A quartz stopper

with a long 1/4 inch diameter quartz access tube attached on one end was mated to the end of the reaction tube, where it sealed against a ground glass joint. The reaction tube/stopper assembly was then placed into the cool end of a Model #55342 Lindberg tube furnace. This configuration is illustrated in Fig. II-1.

In order to evacuate the reaction tube before moving it into the hot region of the furnace, a vacuum hose was attached to the end of the stopper access tube and thence to a vacuum pump. The vacuum pump was able to evacuate the reaction tube to a pressure no less than a few hundred millitorr due to leaks at the ground glass joint. However, since the arsenic was expected to raise the internal pressure of the reaction tube to a pressure greater than a few hundred millitorr after it sublimated in the hot zone of the furnace, this vacuum was considered sufficient. In addition, since the ground glass joint was firmly seated by thermal expansion during the annealing, it was assumed that the leaks were reduced during this period. However, the outer tube in which the reaction tube is installed (see Fig. II-1) was filled with nitrogen, thus hopefully reducing any contamination resulting from leaks into the reaction tube during annealing.

Prior to moving the reaction tube into the hot zone of the furnace, the reaction tube was sealed from the outside environment by closing a valve on the pump side of the vacuum hose. Consequently, except for leaks, the sample was annealed in a closed environment. At this time, the reaction tube was pushed to a pre-determined point in the furnace. Placement of the sample was determined before each sample was annealed by measuring the magnitude and spatial profile of the temperature in the furnace with a type K thermocouple. By placing the sample on a special mark in the reaction tube, it was guaranteed that the sample would be

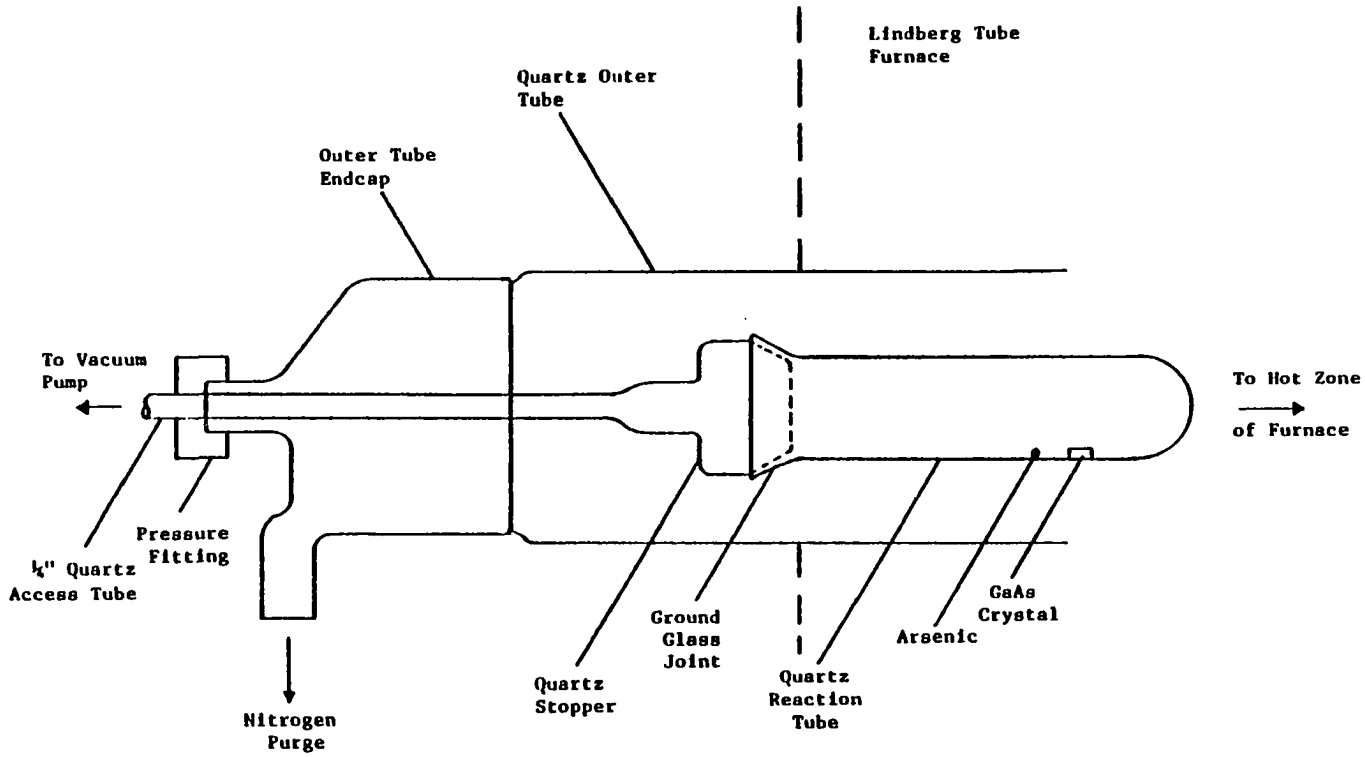

Figure II-1 Schematic diagram of the diffusion furnace apparatus.

within the 5 cm wide temperature flat zone of the furnace. During the time the sample was annealed, the temperature was controlled by the furnace to within ± 1 °C. After two hours, the reaction tube was quickly pulled back to the cool end of the furnace (a procedure known as rapid quenching) and allowed to cool. The sample was then removed from the reaction tube.

The samples, once annealed, were lapped to remove the copper residue and then polished on both sides with a non-contact, laminar flow polisher [36] in a 0.5% solution of bromine in methanol. After polishing, the samples were cleaned as a prelude to contact deposition according to a procedure developed at Sandia National Laboratories [37]. The samples then had pre-alloyed Au-Ge contacts evaporated onto one side in a planar geometry such that a gap typically 2 to 2.5 mm wide was formed on the surface between the contacts. As will be discussed in the next section, these contacts have been demonstrated to be injecting (ohmic).

Ultimately, six samples were successfully manufactured. Table II-1 lists the annealing temperature, dark conductivity at room temperature, σ, and critical dimensions for all six samples. Figures II-2(a)-(c) contain illustrations of the three samples used in the photoconductivity experiments. The illustrations indicate that small differences in device geometry exist either due to breakage during processing, or because of differences in contact geometry caused by different contact masks. Nevertheless, an idealized geometry was used for calculating reduced quantities (electric field, current density, conductivity, etc.). This geometry assumes uniform electric fields in the gap between the contacts (parallel plate contacts), an assumption not valid near the edge of the contacts at the surface, but otherwise

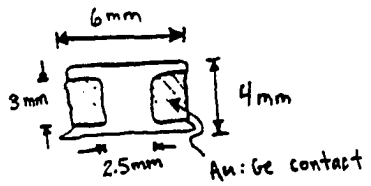

Sample 14-8-6(b)

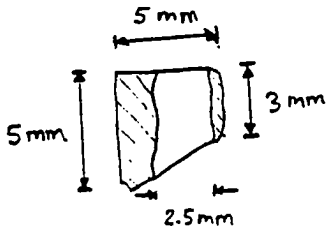

Sample 14-8-9(e)

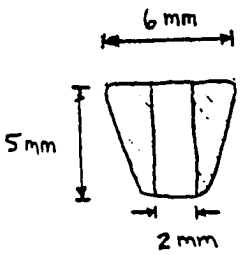

Sample 14-8-9(f)

Figure II-2 Illustrations showing the dimensions of the three samples used in the photoconductivity experiments.

Table II-1 Important sample characteristics.

Sample	Annealing Temperature [°C]	Sample Thickness [mm]	Effective Cross Section [mm^2]	Effective Contact Spacing [mm]	σ [$(\Omega\ cm)^{-1}$]
14-8-9(d)	540	0.24	1.2	2.2	1.5×10^{-2}
14-8-9(e)	549	0.24	0.9	2.5	1.4×10^{-3}
14-8-9(f)	552	0.24	1.2	2.0	1.4×10^{-6}
14-8-9(h)	572	0.24	0.7	2.0	3.8×10^{-6}
14-8-6(a)	575	0.24	1.0	2.5	8.4×10^{-5}
14-8-6(b)	575	0.23	0.9	2.5	1.0×10^{-5}

reasonably valid elsewhere in the bulk because of the small ratio of sample thickness to gap spacing.

Compensation results

In order to determine the results of the compensation experiments, the bulk dark conductivity of the samples must be measured. This can be accomplished by direct electrical measurement of the sample resistance only if the electrical contacts are sufficiently non-rectifying. This condition is presumed to be met as long as the current-voltage (*I-V*) characteristics of the sample are resonably linear (ohmic) at "low" electric fields (e.g., less than 500 V/cm), in which case the slope of the *I-V* curve at a given temperature represents the bulk resistance of the sample. The bulk conductivity of the material is calculated from this slope using the idealized geometry described above.

The *J-E* (current density vs. electric field) curve (derived from the *I-V* characteristics at a temperature of 300 K) for a representative sample [sample 14-8-9(f)] is shown in Fig. II-3. Clearly, the sample meets the linearity criterion over this range of electric field. It should be noted in passing that it would be more satisfying if the dark conductivities derived from the *I-V* characteristics could be verified with Hall measurements; however, the contact geometry precludes Hall measurements on these samples. Nevertheless, the direct electrical measurements are considered adequate to the first order.

The room temperature dark conductivity of all six samples [in addition to the sample above, this includes samples numbered 14-8-6(a), 14-8-6(b), 14-8-9(d), 14-8-9(e), and 14-8-9(h)] is plotted versus annealing temperature in Fig. II-4. The relative positions of the data points in Fig. II-4 can be interpreted as follows. The

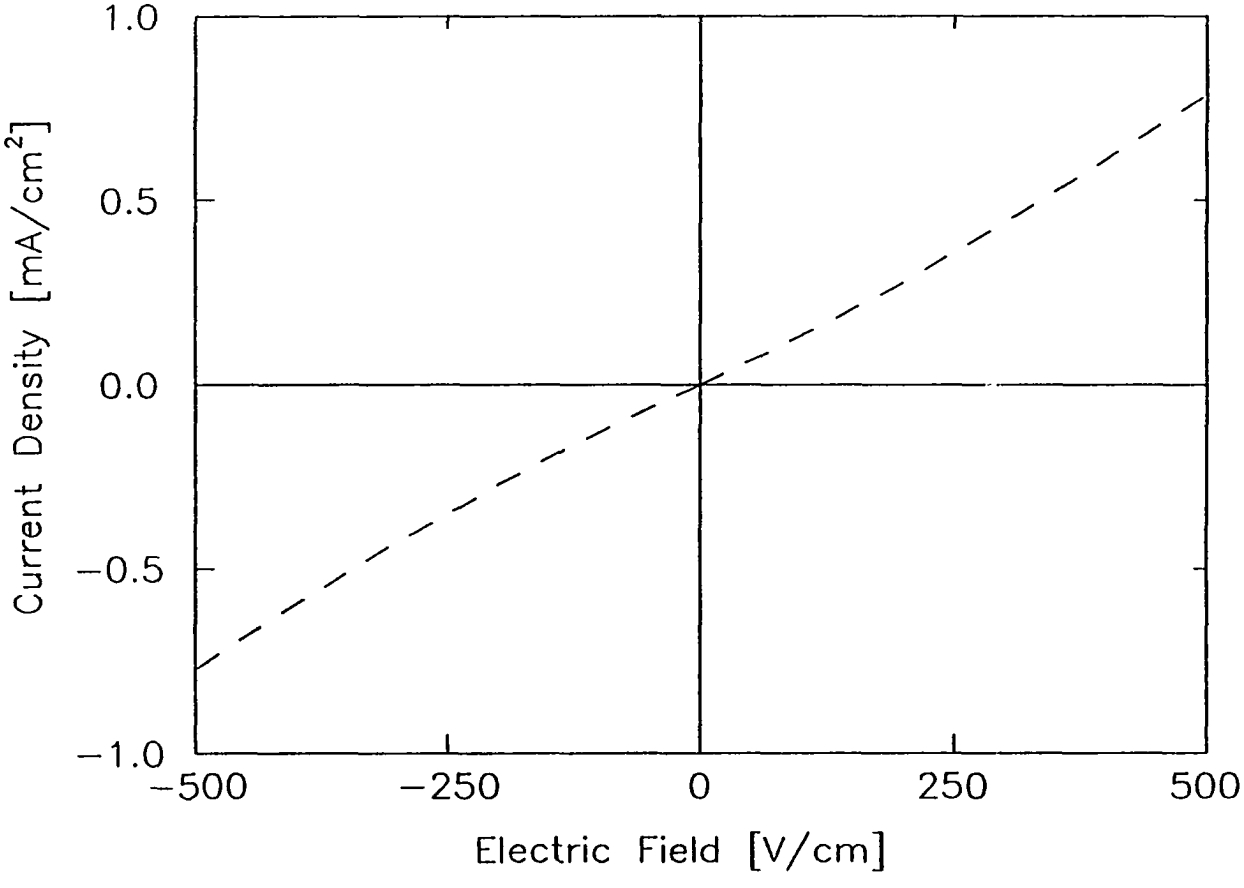

Figure II-3 Characteristic dark J vs. E curve for sample 14-8-9(f).

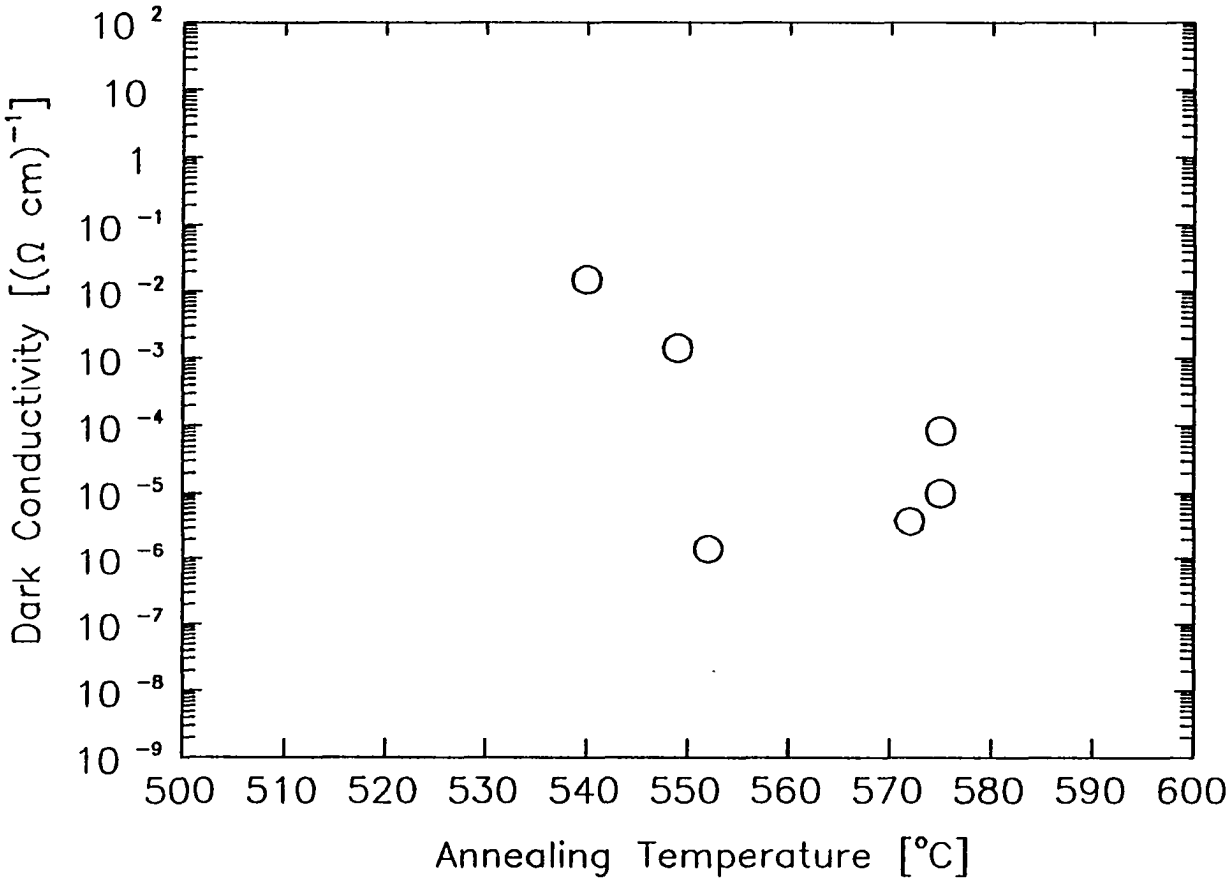

Figure II-4 Dark conductivities of the six samples vs. annealing temperature.

low resistivity of sample 14-8-9(d) implies that at relatively low annealing temperatures (less than 550 °C) insufficient compensation occurs. As the annealing temperature increases, the dark conductivity dramatically decreases [sample 14-8-9(e)], culminating in the semi-insulating sample [sample 14-8-9(f)] at an annealing temperature of 552 °C. At a substantially higher annealing temperature (575 °C), the remaining samples have a higher dark conductivity than 14-8-9(f), but less than 14-8-9(d) or 14-8-9(e). These remarkable results can be explained by a relatively simple compensation model involving the relative concentrations of the shallow donor (silicon) and deep acceptors introduced by the thermal diffusion of copper into the GaAs crystals. This model will now be presented.

Compensation model

Copper is known to form two dominate acceptor levels in GaAs [12]. These levels are sometimes referred to as Cu_A and Cu_B. Cu_A and Cu_B are typically reported to have thermal activation energies of 0.14 eV and 0.44 eV, respectively. These energies are referred to the valence band at room temperature (see Refs. [12], [13], and [38]). The partition of the total Cu concentration into these two levels (or any other levels associated with copper) is not known exactly, and is expected to vary with processing technique. A discussion of the possible origins of Cu_A and Cu_B and the resulting partition of the total copper concentration is provided in Appendix A for the interested reader. For the compensation model that will now be presented, the partition remains a variable.

Since both Cu_A and Cu_B are acceptors, their introduction into an n-type GaAs crystal doped with shallow donors should lead to compensation, regardless of the partition between the two levels. Various models of electrical compensation have

been reported for EL2 and chromium compensated materials [39-41], as well as for Cu-doped GaAs [13]. The model for copper compensation predicts that a transition from n-type to p-type dark conductivity is expected as the annealing temperature during Cu diffusion is increased. This is a consequence of the increasing solubility of Cu in GaAs as the annealing temperature increases. Blanc, et al. [13] have postulated that the Cu solubility is enhanced in the presence of shallow and deep donors, thus explaining the relatively close compensation of their samples (to a few parts per million) which cannot be explained by temperature control of the furnace alone.

To explain the annealing temperature dependence of the dark conductivity demonstrated in Fig. II-4, a simple calculation has been performed using a model of the deep level configuration for Cu:Si:GaAs presented by Ko [33] (see Fig. II-5). This model includes the EL2 and EL5 deep donor levels, the Cu_A and Cu_B deep acceptor levels, and the Si shallow donor level. The calculation finds the Fermi energy, E_F, at 300 K such that the neutrality condition is satisfied:

$$n + \sum_i n_{Ai} = p + \sum_j (N_{Dj} - n_{Dj}) \qquad \text{(II-1)}$$

where n and p are the free electron and hole densities respectively, n_{Ai} is the density of ionized states of the i^{th} acceptor level, and $(N_{Dj} - n_{Dj})$ is the density of ionized states of the j^{th} donor. The mass action law, given by

$$np = n_i^2 \qquad \text{(II-2)}$$

relates n and p to the intrinsic carrier concentration n_i.

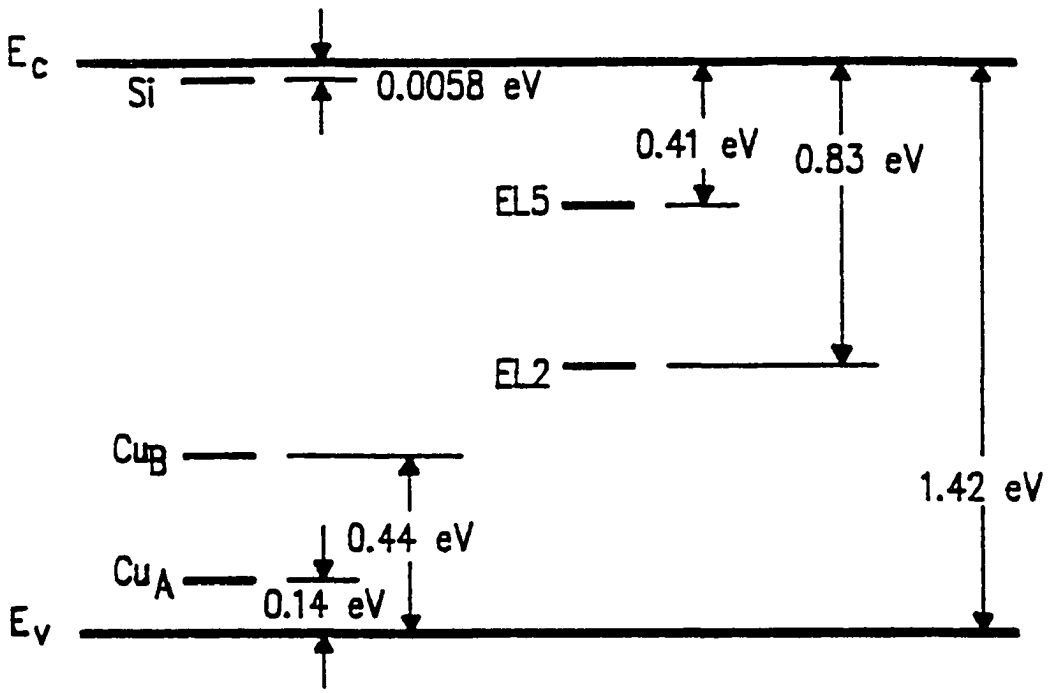

Figure II-5 Energy level diagram of the model used to simulate compensation in Cu:Si:GaAs (from Ref. [33]).

Equation (II-1) can be solved by introducing the Fermi distribution function for each term (including n and p)

$$n_j = \frac{N_j}{1 + g_j \exp[(E_j - E_t)/kT]} \qquad \text{(II-3)}$$

where E_j is the activation energy of the j^{th} level and g_j is the degeneracy. Equation (II-3) is used for both acceptors and donors. By fixing all values (i.e., known energy levels, known or assumed density of states for each level, and degeneracies), and iterating E_t until Eq. (II-1) is satisfied, then n, p, and the occupation probabilities at thermal equilibrium (the dark) can be found for all the levels.

The free electron and hole densities are calculated once E_t is known through the following expressions derived from Eq. (II-3):

$$n = N_c \exp[-\Delta E_t / kT] \qquad \text{(II-4)}$$

$$p = N_v \exp[-(E_g - \Delta E_t)/kT] \qquad \text{(II-5)}$$

N_c and N_v are the effective density of states in the conduction and valence band respectively, ΔE_t is the Fermi level referenced to the conduction band edge, and E_g is the band gap energy at temperature T. The dark conductivity can be calculated from the solution by using

$$\sigma = q(\mu_n n + \mu_p p) \qquad \text{(II-6)}$$

where $\mu_{n,p}$ is the mobilitity for electrons or holes respectively, and q is the electronic charge.

Table II-2 contains basic data used in the compensation calculation. Data for EL2 and EL5 come from Ref. [33]. The total copper density, $N_{Cu} = N_{CuA} + N_{CuB}$, and the partition, $\mathbf{p} = N_{CuA}/N_{CuB}$, are considered parameters for this calculation. Increasing N_{Cu} for constant values of **p** is considered a reasonable model of the actual effect of increasing the annealing temperature in this experiment. This is because the solubility of both Cu_A and Cu_B are expected to increase in proportion over the relatively small temperature range actually used (540 °C to 575 °C).

Figure II-6 contains the calculated change in dark conductivity as a function of total copper content. N_{Cu} was varied by a factor of ten, centered on the known silicon density of 5×10^{16} cm^{-3}. Five curves are presented, differing only in the value of **p**, the partition. The first value of the partition is that used by Ko [33]: **p** = 0.2; the other values are 1.0, 2.0, 4.0, and 10. The family of curves shown in Fig. II-6 have been divided into three areas: the n-type, semi-insulating, and p-type regions. These regions represent different levels of compensation.

The n-type region simply represents the case where too few acceptors have been introduced to trap electrons thermally freed from the shallow donor. At a silicon doping density of 5×10^{16} cm^{-3}, the uncompensated dark conductivity is very high [> 30 $(\Omega\ cm)^{-1}$]. As Cu is added to the system, the dark conductivity decreases slowly at first, and then decreases very rapidly with small changes in N_{Cu}. This is to be expected, since the Fermi level is above the middle of the band gap, and thus all of the copper related acceptors must be ionized. In order to achieve high resistivity

Table II-2 Parameters used in the compensation calculation.

Parameter	Value	Units
T	300	[K]
E_g	1.42	[eV]
N_{EL2}	1×10^{16}	[cm^{-3}]
N_{EL5}	3×10^{15}	[cm^{-3}]
N_{Si}	5×10^{16}	[cm^{-3}]
E_{EL2}	0.83	[eV]
E_{EL5}	0.41	[eV]
E_{CuA}	1.28	[eV]
E_{CuB}	0.98	[eV]

Note: All activation energies referred to the conduction band edge.

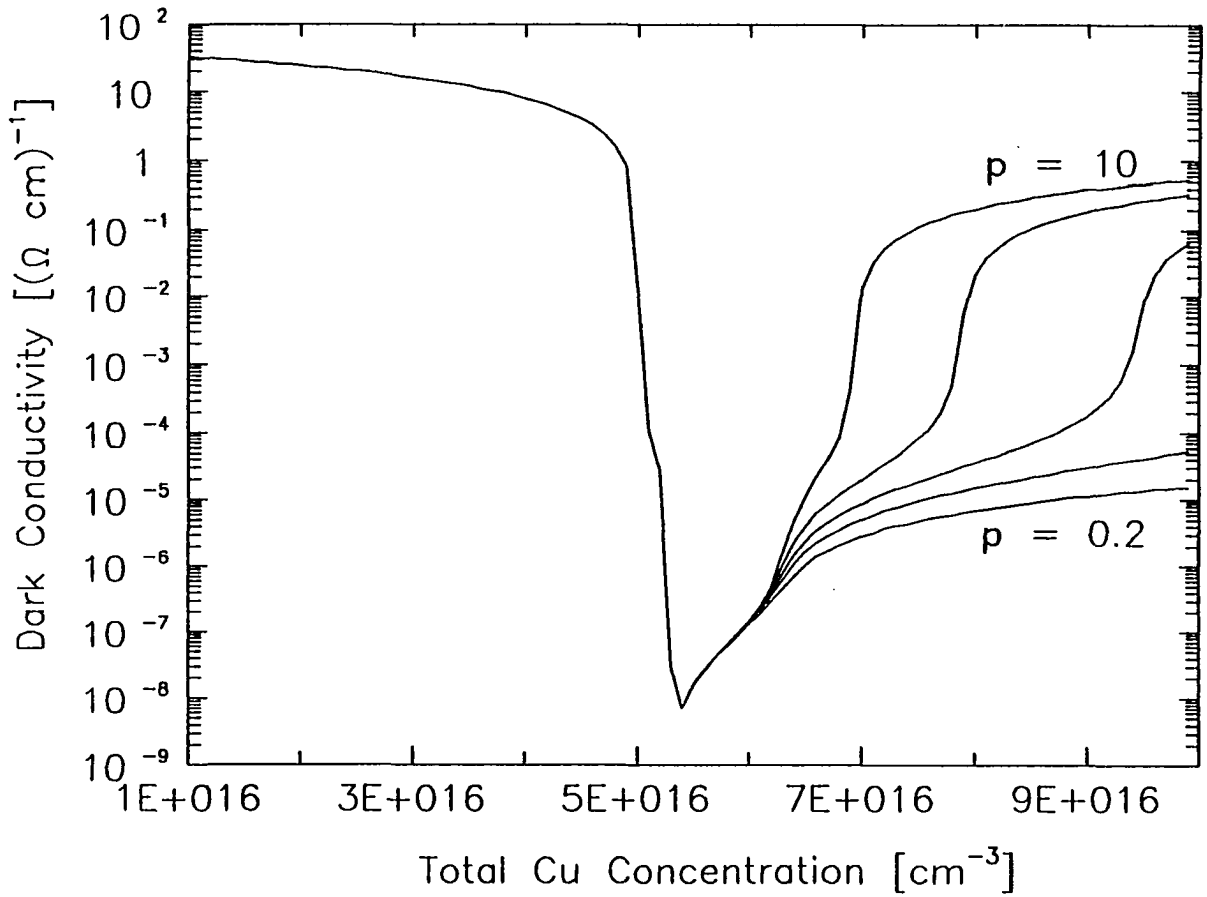

Figure II-6 Calculated dark conductivity vs. N_{Cu} for the following values of the partition: **p** = 0.2, 1, 2, 4, and 10.

n-type (undercompensated) material, the difference between the shallow donor density and the sum of the acceptor densities must be very small indeed (parts per million or better).

As the dark conductivity decreases below 10^{-6} $(\Omega\ cm)^{-1}$, the material begins to approach the intrinsic limit. In this region the material is considered semi-insulating; the destinction between n-type and p-type, while technically still possible, in practice becomes difficult, and perhaps, unimportant. On the p-type side of the minimum, the dark conductivity increases more slowly with increasing Cu concentration. This is partly a consequence of the much smaller hole mobility as compared to the electron mobility. However, the slope is also controlled somewhat by the thermal activation of the various deep levels, as can be seen throughout the curve.

Only as the further addition of copper drives the curves out of the semi-insulating region can a destinction between partitions be made. This is because the copper acceptors are fully ionized in the n-type and semi-insulating regions, regardless of partition. On the other hand, for a particular partition in the p-type region, Cu_B is initially electrically active at characteristically lower dark conductivities, followed by the electrical activation of Cu_A at characteristically higher dark conductivities.

The transition occurs rapidly after only a small increase in N_{Cu}, as is evident for partitions greater than one in Fig. II-6. In principle, the smaller partitions will also experience a transition to Cu_A controlled dark conductivity at very high values of N_{Cu}; however, for very small partitions, the required copper density may exceed the maximum solubility of copper in GaAs (approximately 10^{19} cm^{-3} [35]). Similarly,

for very large partitions, the activation of Cu_B will be indistinguishable amid the transition to Cu_A.

Now, returning to Fig. II-4, the experimental results qualitatively resemble the shape of the curves in Fig. II-6. Indeed, samples 14-8-9(d) through (f) would appear to confirm the steep decrease in dark conductitivity to be expected as close compensation occurs (while it appears that sample 14-8-9(d) has an anomalously low dark conductivity, it should be noted that the maximum dark conductivity that can be measured using *I-V* curves is probably limited by contact resistance). The other three samples were all annealed at around 575 °C, but they show a spread in dark conductivities. From Fig. II-6, one might be tempted to assign different partitions to the three samples. Indeed, annealing parameters other than temperature that may influence the partition, such as arsenic vapor pressure, were not controlled precisely during the anneal. However, no other independent evidence is available at this time to assign partitions to the different samples.

On the basis of similarities between the compensation experiments and theory, conductivity types have been assigned to the samples. Samples 14-8-9(d) and (e) are assumed to be n-type. Sample 14-8-9(f) has been labeled semi-insulating, and samples 14-8-6(a), 14-8-6(b), and 14-8-9(h) are assumed to be p-type. In the absence of hall measurements (which were not possible with this contact configuration) these assignments cannot be confirmed directly. However, three of the samples have been further characterized by measuring the temperature dependence of their dark conductivities, which reveals information about the defect level or levels controlling the dark conductivity. These measurements, which will now be described, tend to support the above assignments.

Characterization by thermal spectroscopy

As the sample temperature changes, so does the dark conductivity. As the temperature decreases, the occupation probabilities of the various deep levels change, thus moving the Fermi level closer to either the conduction band or the valence band, depending on whether donors or acceptors control the dark conductivity. The rate at which the dark conductivity decreases (increases) with decreasing (increasing) temperature is typically controlled by the activation energy of the impurity or defect level that is experiencing the greatest change in occupation probability. Thus by measuring the dark conductivity of a crystal at various temperatures, and then plotting this information versus reciprocal temperature, quite often a straight line over some temperature range is observed. As will now be shown, the slope of this line is proportional to the activation energy of the level.

Consider the following assumptions: First, that all donors in the crystal are closer to the conduction band than any acceptors; second, that all dominant energy levels (those with substantial concentration) are always separated by at least a few kT; third, that the degeneracy of each level is one; and fourth, that the temperature dependence of the mobility offsets the temperature dependence of the density of states of the appropriate band. The validity of these assumptions will be discussed later.

At any temperature T, the neutrality condition, represented by Eq. (II-1), must be satisfied in the bulk material. In high-resistivity material, n and p can often be neglected compared to the background concentration of ionized donors and acceptors. Equation (II-1) can be further simplified by assuming that all levels are

fully ionized but one, which is the effect of invoking the first two assumptions above. As a result Eq. (II-1) becomes

$$n_A = \sum_j N_{Dj} - \sum_i N_{Ai} \qquad \text{(II-7)}$$

where n_A is the concentration of ionized states of the single level (assumed to be an acceptor) that is only partially ionized. The right-hand side of Eq. (II-7) simply represents the compensation due to the other fully ionized donors and acceptors.

If the Fermi distribution function given by Eq. (II-3) is substituted for n_A, in which ΔE_f and ΔE_a (the Fermi energy and activation energy respectively) have been referenced to the valence band edge and the degeneracy has been assumed to be one, then

$$\frac{N_A}{1 + \exp[(\Delta E_a - \Delta E_f)/kT]} = \Delta N_D \qquad \text{(II-8)}$$

where N_A is the total density of the active acceptor and ΔN_D is the right-hand side of Eq. (II-7). Solving Eq. (II-8) for ΔE_f results in the expression

$$\Delta E_f = \Delta E_a + kT \ln\left(\frac{\Delta N_D}{N_A - \Delta N_D}\right) \qquad \text{(II-9)}$$

If the conductivity is assumed to be dominated by hole transport (i.e., ΔE_f is not too close to the middle of the band gap) and the natural logarithm of Eq. (II-6) is differentiated with respect to reciprocal temperature (reciprocal temperature = $1/T \equiv x$), then it is found that

$$\frac{d}{dx}\ln(\sigma) = \frac{T}{k}\frac{d\Delta E_t}{dT} - \Delta E_t/k \qquad \text{(II-10)}$$

which is the slope of the plot of ln(σ) versus reciprocal temperature. Equation (II-10) assumes that the product $\mu_p N_v$ is only a weak function of temperature (the fourth assumption).

By substituting Eq. (II-9) and its derivative (with respect to T) into Eq. (II-10), the slope of the dark conductivity curve becomes

$$\frac{d}{dx}\ln(\sigma) = \frac{T}{k}\frac{d\Delta E_a}{dT} - \Delta E_a/k \quad . \qquad \text{(II-11)}$$

If it is assumed that the thermal activation energy varies in proportion to the band gap energy as the temperature is changed, then an estimate for $d\Delta E_a/dT$ can be found such that the solution of Eq. (II-11) has the form

$$\Delta E_a = (\text{constant})\ [-k\frac{d}{dx}\ln(\sigma)] \qquad \text{(II-12)}$$

where the constant represents a temperature dependent correction factor for the "apparent" activation energy given by [$-k\frac{d}{dx}\ln(\sigma)$]. This correction factor is calculated to be 0.934 at room temperature in GaAs.

The magnitude and slope of the curve ln(σ) vs. $1/T$ represent independent information that can be used to determine ΔE_t and ΔE_a at a given temperature. This information can then be used to find $\Delta N_D/(N_A - \Delta N_D)$ from Eq. (II-9), which gives an idea of the degree of compensation in the crystal. Equation (II-12) also holds if

the material is n-type, in which case ΔE_a and ΔE_t are referred to the conduction band. In addition, the compensation term of Eq. (II-9) becomes $N_D/(N_D - \Delta N_A)$.

The curve $\ln(\sigma)$ vs. $1/T$ has been measured for each of the three samples used in the photoconductivity experiments to be described in Chapters III and IV. These samples are 14-8-9(e), 14-8-9(f), and 14-8-6(b). The results are plotted on a semi-log scale versus reciprocal temperature in Fig. II-7. The curves for the first two samples demonstrate substantial structure, while the curve for the last sample has a single slope over this temperature range. These features fit well from what would be expected if the conductivity types assigned from the compensation data are valid.

Consider the curve in Fig. II-7 for sample 14-8-9(e). This sample is believed to be n-type, however, from its dark conductivity at 300 K the Fermi level is estimated to be 0.33 eV from the conduction band edge, which implies a significant level of compensation. As a result, it would be surprising if the activation energy of the electrically active level at 300 K was as shallow as silicon (6 meV). Indeed, the activation energy at 300 K is a fairly deep 0.28 eV.

The identification of this level is not known, but it must exist in fairly small concentration since a modest decrease in temperature causes the curve $\ln(\sigma)$ vs. $1/T$ to transition to a very shallow slope. The activation energy for this level is, within the resolution of the technique (about a kT), consistent with the silicon donor level. The conclusion drawn from this curve is that the Si donor content of sample 14-8-9(e) has only just been compensated by the Cu doping, thus activating deeper donor levels that arise from native and impurity defects that exist in small concentrations in any bulk grown GaAs.

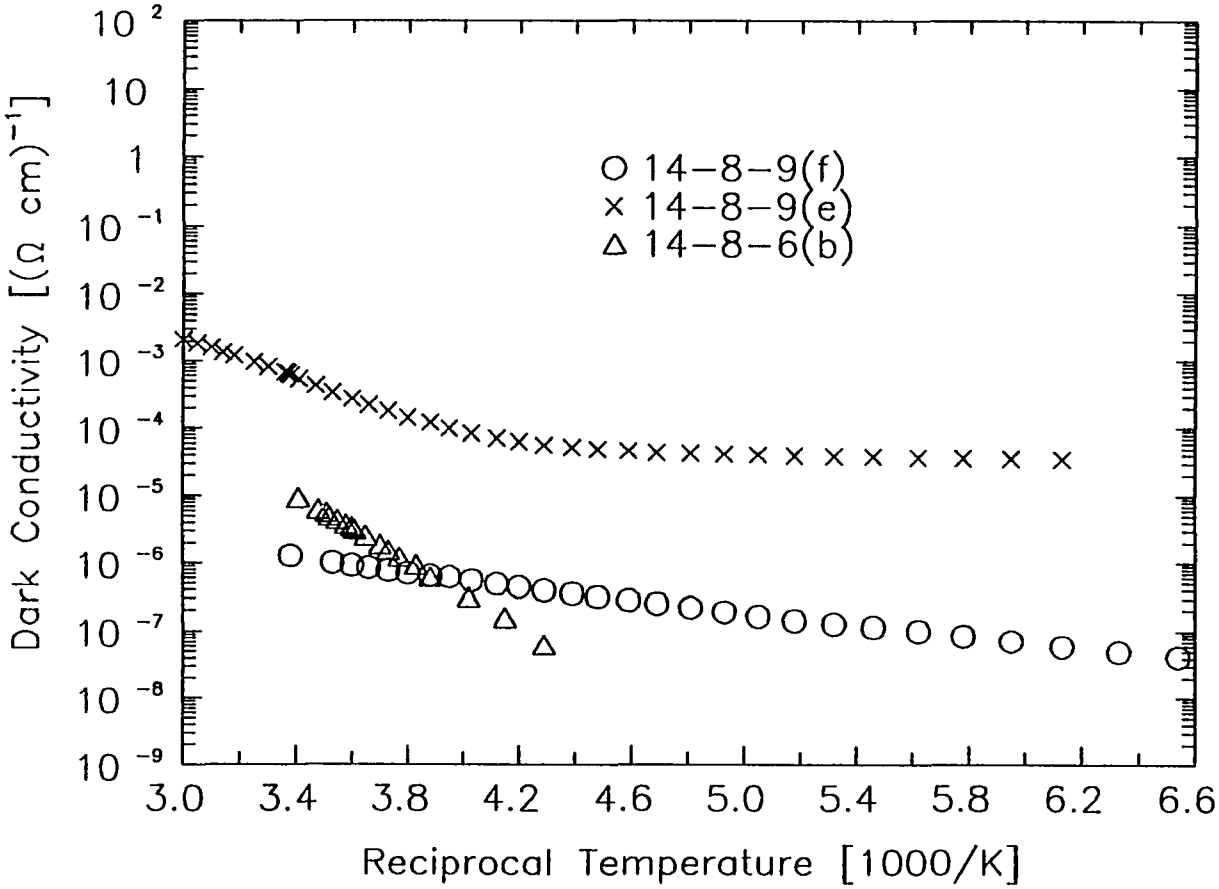

Figure II-7 The curves $\log_{10}(\sigma)$ vs. $1/T$ for three different samples.

The Fermi level at 300 K for sample 14-8-9(f) is estimated to be 0.51 eV from the conduction band, assuming the sample is on the n-type side of the compensation curve. This is in marked contrast with the slope of the curve $\ln(\sigma)$ vs. $1/T$ at 300 K, from which an activation energy of 0.097 eV is calculated. At first it seems surprising that a level with activation energy less than 0.28 eV is controlling the conductivity in a sample with lower dark conductivity than sample 14-8-9(e); however, it should be noted from Eq. (II-9) that in a closely compensated crystal, the term $kT \ln[N_D/(N_D - \Delta N_A)]$ can become significant, in which case ΔE_f and ΔE_a become substantially separated.

In fact, it would be expected that defect states existing in relatively low concentration should be resolved in closely compensated crystals, and it may well be that the 0.097 eV level, and the shallower level at 0.077 eV observed at lower temperatures, are defects existing in very small concentration in sample 14-8-9(f). However, the significant separation between ΔE_f and ΔE_a casts doubt on the premise that only one level is partially ionized at a time. If this assumption is no longer valid in the semi-insulating limit, then the calculated activation energies for this sample may suffer from significant error. Nevertheless, the apparent spread in activation energy and Fermi level is still considered a good indicator of semi-insulating material.

Finally, sample 14-8-6(b) has a Fermi level estimated to be 0.46 eV from the valence band edge. However, unlike the responses of the other two samples, the curve $\ln(\sigma)$ vs. $1/T$ for sample 14-8-6(b) has only one slope over the experimental temperature range. From this curve an activation energy of 0.45 eV at 300 K is

calculated. This level is indentified as Cu_B, which is known to have a thermal activation energy of 0.44 eV from the valence band at room temperature. The fact that the Fermi level and the activation energy are so close supports the assumption that this sample consists of a substantially over-compensated, p-type crystal. The fact that the slope of the curve $\ln(\sigma)$ vs. $1/T$ is monotonic over a substantial temperature range implies that Cu_B exists in significant concentrations in sample 14-8-6(b).

These measurements are, of course, subject to error. The validity of the assumptions made in deriving Eqs. (II-9) and (II-12) represent the most likely systematic error, since variables like dark current and sample temperature were measured accurately. The first two assumptions concerning the relative placement of donors and acceptors in the band gap were introduced so that only one defect level would be electrically active at a given temperature. In chromium and EL2 compensated material, this assumption is invalid since both deep levels can be active [39]. In this case, a more complete model presented by Zucca [40] is required to interpret the curve $\ln(\sigma)$ vs. $1/T$. However, for the Cu:Si:GaAs material used in this investigation, EL2 and Cr can be assumed to have only a minor effect because of their low concentrations.

Perhaps the two most obvious systematic errors concern the degeneracy of the deep levels and the assumption that the temperature dependence of the mobility offsets the temperature dependence of the density of states in the bands. As for the degeneracy, a value of one was chosen in the absence of better data on deep levels [40]. It is expected that the degeneracy terms will have little effect on the calculated activation energies, because they do not show up in the exponent of the Fermi functions.

According to theory, the temperature dependence of the mobility of the free carriers can follow one of two possible functions. A $T^{3/2}$ dependence at low temperature and relatively high impurity concentration is attributed to impurity scattering of free carriers moving through the otherwise periodic lattice potential. At higher temperature or low impurity concentration, a $T^{-3/2}$ dependence can be expected from free-carrier/phonon interactions (lattice scattering). It is this dependence that is assumed to offset the $T^{3/2}$ dependence of both N_c and N_v. Fortunately, experimental evidence [11, pp. 33-34] indicates that within the typical temperature range used here, the $T^{-3/2}$ dependence can be expected to dominate the mobility in Cu:Si:GaAs with impurity concentrations on the order of 5×10^{16} cm^{-3}. Even if the mobilities of electrons and holes were independent of temperature, the resulting error in the calculated activation energies would be no more than 10% [13] [40]. Since some offsetting temperature dependence is expected, the error in the calculated activation energies are believed to be less than 5%.

The measurement of the temperature dependence of the dark conductivity is a simple technique that can yield limited information about the deep level content in a crystal. More accurate and complete thermal spectroscopy techniques exist, such as deep level transient spectroscopy (DLTS) and photo-induced current transient spectroscopy (PICTS). However, only PICTS is suitable for direct measurements on the six samples available. A PICTS experiment on sample 14-8-9(h) will be performed in the future, but this experiment is beyond the scope of this thesis.

Summary

The critical first step in testing the BOSS concept is the successful compensation of low-resistivity, silicon-doped GaAs crystals to form high-resitivity,

semi-insulating crystals. A process that relies on the diffusion of copper into these crystals has been described. The systematic introduction of copper in increasing densities has been shown to result in compensation as demonstrated by the fabrication of six samples, some of which were found to have a high dark resistivity. The distribution of dark conductivity of the six samples as a function of annealing temperature was shown to support a simple model, involving primarily the compensation of shallow donors with copper related deep acceptors, thus forming the Cu:Si:GaAs crystal.

In particular, it was possible to determine the conductivity type (n-type, semi-insulating, or p-type) of the three samples used in the photoconductivity experiments by observing their level of compensation; which, as will be seen, allows differences in the samples' photoconductivity response to be explained. Measurements of the temperature dependence of the dark conductivity in these three samples have been shown to support the assignment of conductivity type. In the case of sample 14-8-6(b), Cu_B has been found to exist in substantial concentration, which is crucial to the success of the BOSS concept.

CHAPTER III

EXPERIMENTAL SETUP

The BOSS concept is based on the application of certain photoconductive properties of the compensated Cu:Si:GaAs material. That Cu:Si:GaAs crystals with different, and controllable, levels of compensation can be produced is demonstrated in the last chapter. Optogalvanic experiments that measure some of the photoconductive properties of these crystals have been performed. These experiments demonstrate the feasibility of the BOSS concept.

This chapter will briefly describe the important components of the experimental apparatus used to make the optogalvanic measurements. The discussion will cover the characteristic specifications of the lasers, as well as describe the electrical apparatus used to measure the rapidly time-varying sample conductance (proportional to conductivity) at both low and high electrical power. The bandwidth limitations of the electrical circuits will be considered in the discussion.

Laser light sources

Two independent laser light pulses were required for the photoconductivity experiments. One to "turn on" or activate the sample and one to "turn off" or deactivate the sample. These two laser pulses were generated by two independent lasers. One laser, known as the "mini-YAG," is a small, single wavelength laser used for the activation pulse. The second is a commercial laser capable of being tuned

over a considerable range of wavelength, which was used to study the infrared quenching effect in Cu:Si:GaAs. Infrared quenching is the mechanism used in the BOSS concept to deactivate the switch photoconductivity. In some separate experiments the commercial laser was used alone to activate the photoconductivity when features of this laser, such as short pulse width and high intensity, were experimentally necessary.

The mini-YAG laser is a single-shot, flashlamp pumped Nd:YAG solid state laser. The laser is Q-switched and operates at the fundamental wavelength of the Nd:YAG crystal: 1064 nm ($h\nu$ = 1.17 eV). A typical output pulse of this laser is presented in Fig. III-1. The pulse has a roughly gaussian temporal profile with a full width half maximum (FWHM) of 26 ns. The peak photon flux of the laser is about 10^{24} cm^{-2} s^{-1} ($\approx$ 190 kW/cm^2), but a typical photon flux is 5×10^{23} cm^{-2} s^{-1}. The typical energy per pulse is 1 mJ. The spatial intensity profile of the beam is approximately uniform, and at a distance of a couple of meters the spot diameter is about 1 cm.

The commercial laser system was supplied by Spectra Physics. The system is built around the DCR-3 pulsed Nd:YAG laser. This laser operates at 1064 nm. The temporal envelope of the pulse is roughly Gaussian with a FWHM of 7 ns in the "slow" mode, and 3 ns in the "fast" mode (see Fig. III-2 for an illustration of both pulses). The maximum energy per pulse is nearly 1 J. The output of the DCR-3 can be frequency doubled to 532 nm ($h\nu$ = 2.33 eV) with a conversion efficiency of 40%. Both the green beam and the residual (60%) infrared beam can be used separately.

A Spectra Physics PDL pulsed dye laser can be pumped with the green beam. The PDL can operate with a variety of dyes and the oscillator frequency of the PDL can be tuned over the gain bandwidth of the laser dye by adjusting a diffraction

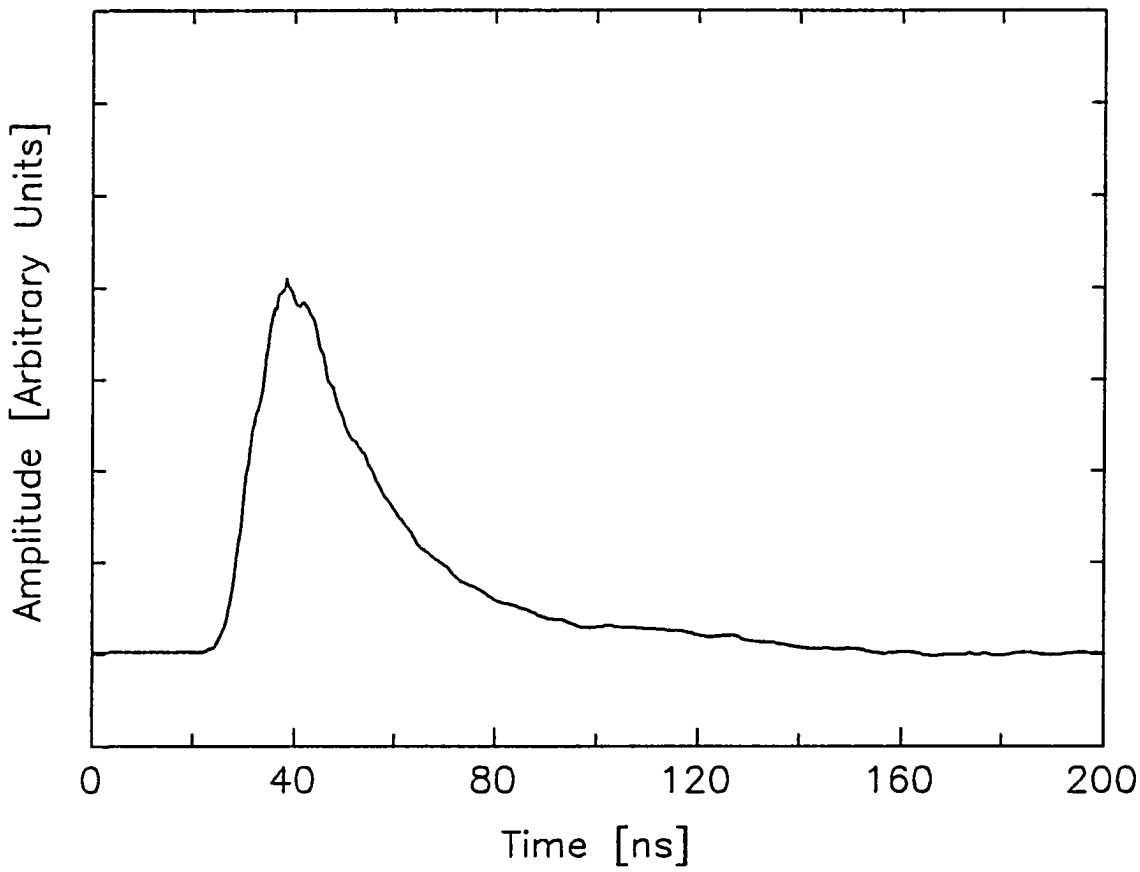

Figure III-1 Typical mini-YAG laser pulse (λ = 1064 nm).

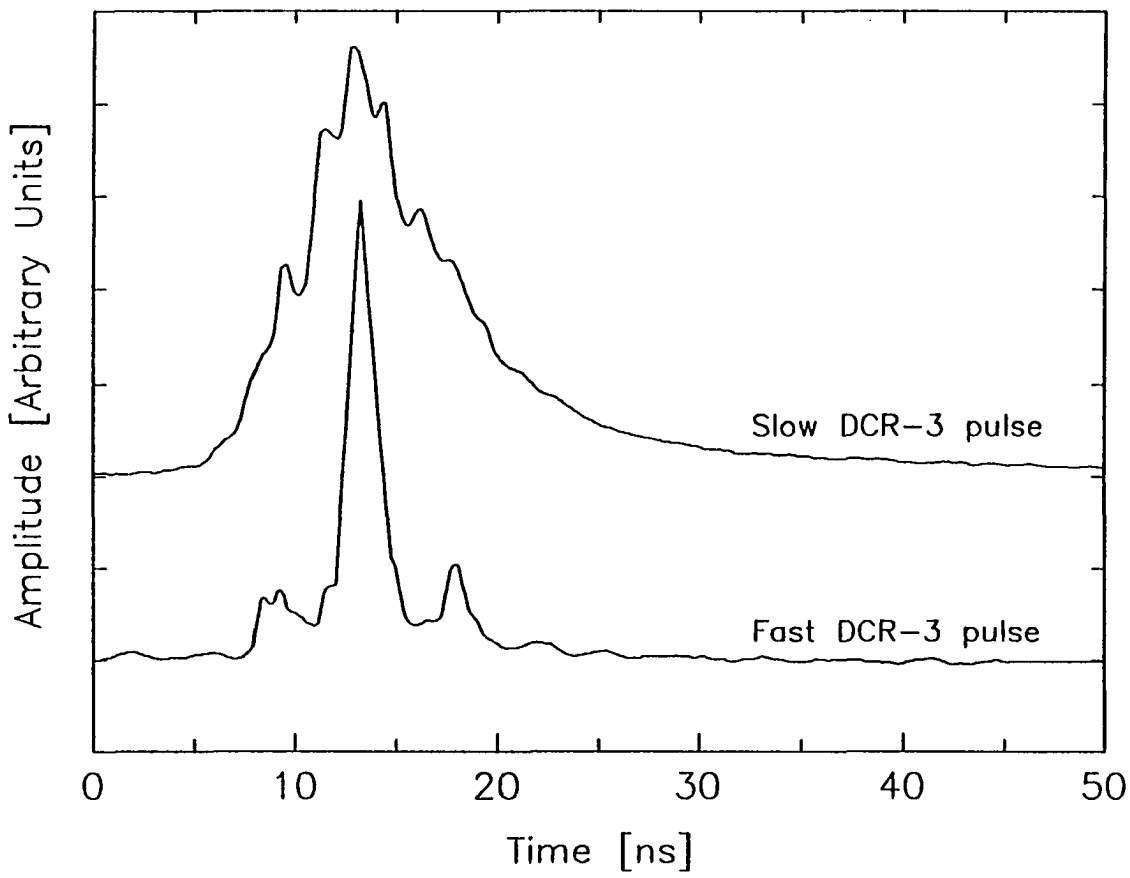

Figure III-2 Typical DCR-3 Q-switched laser pulses (λ = 1064 nm).

grating. Thus, the PDL allows continuous laser wavelength tuning within the discrete gain bandwidths of the available laser dyes. In practice only one laser dye was used; this dye, known as DCM, results in a wavelength range centered at 650 nm in the visible red.

A $LiNbO_3$ crystal contained in a Spectra Physics infrared wavelength extender (IR-WEX) was used to perform two-wave mixing with the output of the PDL and the residual 1064 nm laser beam from the DCR-3. The difference frequency is generated by the mixing, and the resultant laser beam is provided at the output of the IR-WEX. If the PDL output wavelength is in the red, then a near-infrared laser pulse can be generated that is continuously variable over the tuning range of the laser dye loaded in the PDL. For example, when the PDL is loaded with DCM, the IR-WEX can generate a laser pulse over an infrared band centered at 1.62 μm and tunable $\pm$ 0.18 μm ($h\nu$ = 0.77 eV $\mp$ 0.08 eV).

The maximum energy per pulse from the IR-WEX was recorded at the center wavelength to be approximately 3 mJ. This measurement was made with a Scientech Model 361 laser power meter equipped with a surface absorbing calorimeter while the laser was operated at its optimum repetition rate of 10 Hz. The IR-WEX laser pulse has a temporal profile very similar to the output of DCR-3. The DCR-3 was operated in the slow pulse mode (7 ns FWHM) for all experiments involving the IR-WEX. By focusing the output of the IR-WEX to a spot approximately 3 mm in diameter, a peak photon flux of 5×10^{25} cm^{-2} s^{-1} could be generated at the sample. This photon flux could be reduced in steps to a value of 10^{23} cm^{-2} s^{-1} by inserting neutral-density filters into the beam.

The relative timing between the two laser pulses can be carefully controlled since each laser can be Q-switched independently. Thus a valuable property of the BOSS can be demonstrated directly, namely that the electrical pulse length generated by the BOSS can be arbitrarily varied over the hundreds of nanoseconds to microseconds regime.

Low-power setup

The purpose of the low-power experiment was to investigate both the closing (turn-on) and opening (turn-off) properties of the samples, and compare them to computer calculations designed to simulate the Cu:Si:GaAs material. Relatively modest electrical power levels were used to demonstrate the principles of operation; bias voltages ranged from tens of volts to a few hundred volts, and currents ranged from tenths of an ampere, to a few amperes.

The three samples used in the photoconductivity experiments [14-8-9(e), 14-8-9(f), and 14-8-6(b)] have planar contacts on one surface; therefore, they can be most naturally integrated into a stripline based fast diagnostic circuit. An illustration showing the major components of the optical and electrical system used to test the samples at relatively low power is shown in Fig. III-3. The sample is imbedded in a 50 Ω microstripline that is in turn connected to a long length of RG-58 50 Ω coaxial cable on one end, and a length of semi-rigid 50 Ω cable on the other (see the detail in Fig. III-4). The RG-58 cable (two-way transit time = 275 ns) is connected to a charged capacitor terminated in 50 Ω. This capacitor is capable of biasing the sample up to 1 kV. The semi-rigid cable leads to a Tektronix 7912 digitizer terminated in 50 Ω, which acts as a current viewing resistor (CVR). Since the sample is in series

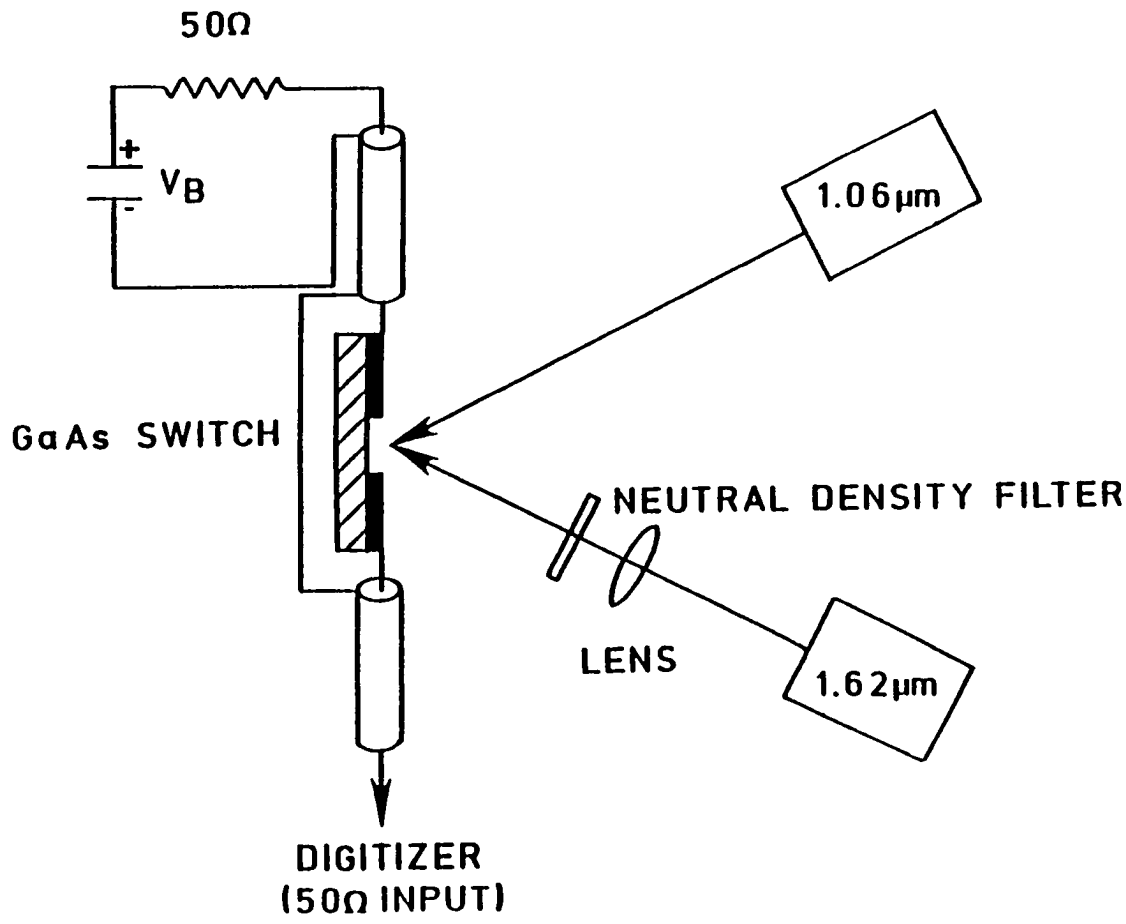

Figure III-3 Low-power setup showing optical and electrical components.

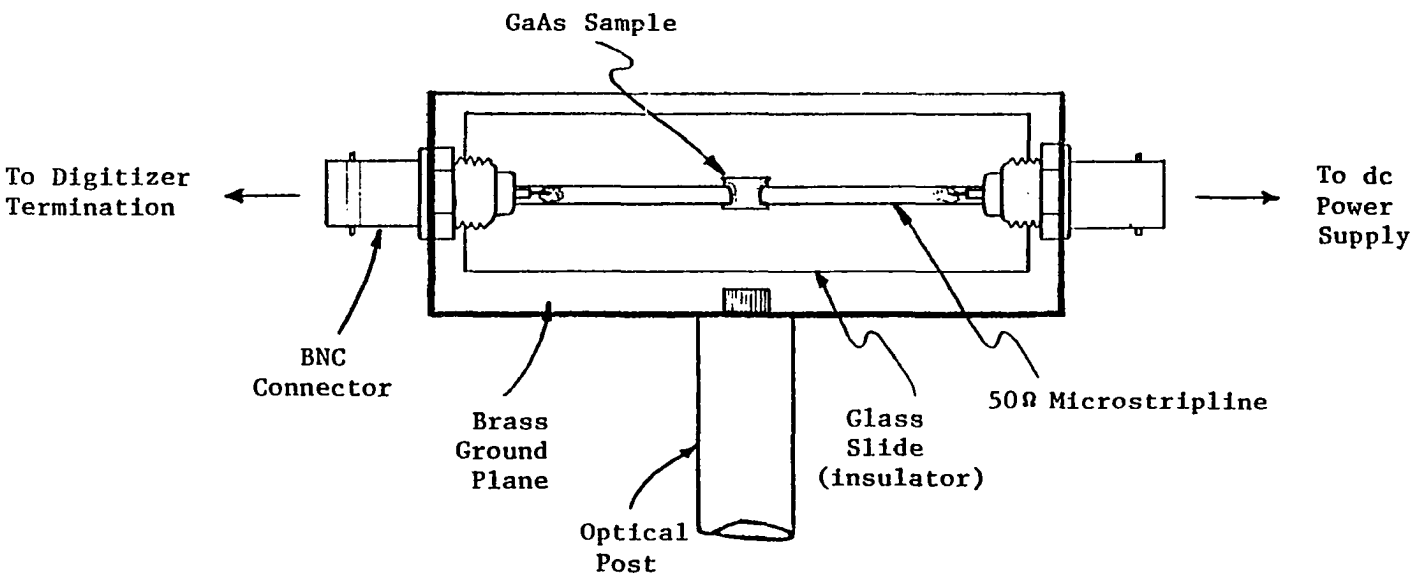

Figure III-4 Physical details of the microstripline diagnostic apparatus used in the low-power setup.

with both the CVR and the characteristic impedance of the RG-58 source cable, a 100 Ω load line is imposed on the sample's *I-V* characteristics.

Figure III-3 indicates that both laser pulses illuminate the contact side of the sample in the active region between the contacts. The change in the sample resistance due to illumination by the two laser pulses was determined by digitizing the sample current and then calculating the time-dependent sample conductance $G(t)$ (reciprocal of the resistance) from knowledge of the external circuit parameters: the capacitor bias voltage V_B and the circuit load line of 100 Ω. By solving the voltage loop equation about the equivalent circuit it is found that

$$G(t) = \frac{i(t)}{V_B - 100\, i(t)} \qquad \text{(III-1)}$$

The sample current is denoted by $i(t)$ and is measured at the digitizer termination.

Of course, Eq. (III-1) is an idealization of the true system response in which it is assumed that the bandwidth of the external circuit exceeds the bandwidth of the parameter to be measured, namely, $G(t)$. Such factors as cable connector inductance, transmission line dispersion, and digitizer bandwidth all conspire to reduce or limit the external circuit bandwidth. Ultimately, the bandwidth of the system is limited by the ability of the digitizer to follow $i(t)$. The digitizer used to measure current in the low power experiments has a bandwidth of 750 MHz, corresponding to an approximate rise time of 0.37 ns. The response of the cable connector/microstripline assembly that the sample is imbedded in has been measured to be down less than 1 dB at 500 MHz. Thus, it is believed that this component has a -3 dB bandwidth in excess of 750 MHz. The dispersion of the semi-rigid cable, through which the

current pulse $i(t)$ must travel, is sufficiently small to ensure at least a 750 MHz bandwidth. While the dispersion of the RG-58 source cable can lead to droop in V_B during long conduction pulses, it has no other effect on measurement bandwidth. From this analysis it is clear that the external diagnostic circuit can resolve 1 ns features in the response of the sample current.

Whether or not the sample can be modeled as a simple time-varying conductance is another matter. At the very least, a lumped capacitance between the contacts on the surface of the crystal should be considered. However, the capacitance between the contacts is estimated to be less than 1 pF, a value too small to produce appreciable distortion of the photocurrent over a nanosecond time frame [42]. Therefore, it is concluded that Eq. (III-1) is a reasonable characterization of the sample's response as measured from $i(t)$.

High-power setup

Photoconductivity measurements at power levels an order of magnitude larger than those used in the low-power measurements were conducted at Sandia National Laboratories. Only sample 14-8-6(b) was used in this experiment. The purpose of the higher power measurements was to look for deviations in the on-state of the Cu:Si:GaAs material (i.e., the tail current) as the sample voltage and current was scaled upward. Of particular interest were the threshold conditions for the appearance of "lock on" in Cu:Si:GaAs, a phenomenon observed at "high" fields in other semi-insulating GaAs materials [21].

Lock on is a conduction mode characterized by constant voltage operation, as opposed to the resistive operation of the photoconductive mode valid at low fields (i.e., the sample changes from a photosensitive resistor at low fields, to a constant

voltage device, like a Zener diode, at higher fields). This transition is typically observed as the initial bias field (before the application of the "turn-on" laser pulse) exceeds 10 kV/cm, although this is a material dependent parameter.

The high-power setup at Sandia is illustrated in Fig. III-5. A Marx bank is used to charge a pulse forming line (PFL) consisting of a 50 Ω coaxial cable. The PFL (two-way transit time = 160 ns) is connected to the sample through a 37 Ω load resistor, R_T, and thence through a short 50 Ω transition to the sample. The Marx bank charges the PFL with an overdamped voltage waveform that reaches peak voltage in about 2 μs. This charging voltage is fully applied across the sample. At some point on the waveform, a 1064 nm laser pulse from a Spectra Physics DCR-2 Nd:YAG laser (with a pulse shape virtually identical to the DCR-3 "slow" pulse) uniformly illuminated the non-contact side of the sample. At this time, the generation of photoconductivity in the sample caused the voltage to collapse, and current from the PFL began discharging through the sample. The sample current was measured by a CVR that has an impedance less than an ohm. Therefore, the load line imposed by this circuit is 87 Ω, not 100 Ω as in the low-power setup. The finite length of the PFL limited the source of current to a pulse length of 160 ns, after which the sample voltage and current collapsed.

Electric fields as high as 20 kV/cm (5 kV) were applied to the sample, which was kept in a pressurized container filled to 40 PSIG with SF_6. Surface flashover was not observed. A second laser capable of generating the longer wavelength radiation required to quench the photoconductivity of the crystal (i.e., turn it off) was not available, so this experiment concentrated on the generation of the tail conductivity only.

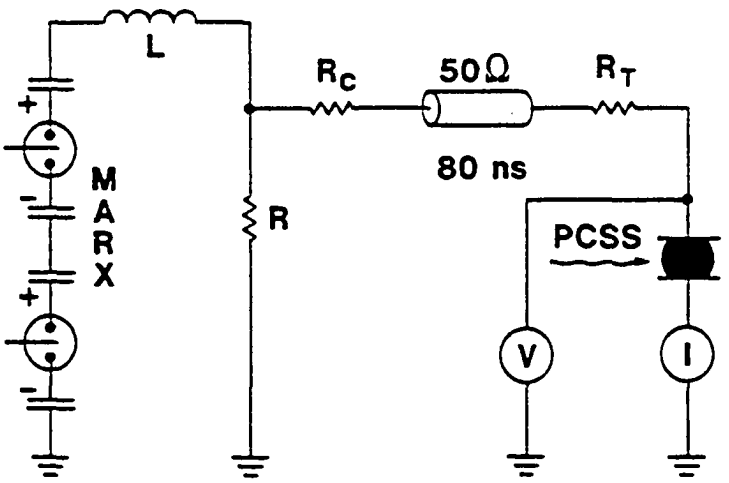

Figure III-5 High-power setup at Sandia National Laboratories (from Ref. [19]).

Unlike the low-power setup, the bandwidth of this system was restricted. In addition to the current, the sample voltage was measured with a resistive divider. Both current and voltage were recorded on a Hewlett Packard digitial sampling oscilloscope with a specified bandwidth of 250 MHz. Fortunately, this experiment was designed to investigate the relatively slow response of the sample after the laser pulse was extinguished; therefore, 250 MHz was considered adequate for the high-power setup.

Summary

This chapter has presented detailed information about the important equipment and techniques used to measure the photoconductive properties of three of the samples described in Chapter II. These samples are 14-8-9(e), 14-8-9(f), and 14-8-6(b). The results of both the low-power and the high-power experiments will be presented in the next chapter. The experimental apparatus were designed to faithfully measure both fast and slow features of the sample conductance as it responds to the illumination from the two laser light sources. However, it should be recognized that both setups represent plausible configurations for a light-activated pulsed power switch, one application of the BOSS concept.

CHAPTER IV

EXPERIMENTAL RESULTS

The photoconductive properties of samples 14-8-9(e), 14-8-9(f), and 14-8-6(b) were measured. It may be recalled from Chapter II that these samples have been assigned the labels "n-type," "semi-insulating," and "p-type" respectively, based upon their different levels of compensation.

In Chapter III, two different experimental setups were described. Most of the data to be presented in Chapter IV was provided by the low-power setup. Both the "turn-on" or closing effect and the "turn-off" or opening effect were investigated with this apparatus. The results of these experiments will be presented in four sections listed as follows: turn on versus level of compensation, turn on at different wavelengths, turn off versus level of compensation, and turn off versus intensity and wavelength. It will become clear that all of these parameters have an important influence on the photoconductive properties of Cu:Si:GaAs.

The results from the high-power setup will be presented in the final section. These results will demonstrate the promise of the BOSS concept as a pulsed power switch, and a problem with further scaling to higher power, namely, "lock on."

Turn on vs. level of compensation

This experiment was performed with an early version of the low-power setup and with samples 14-8-9(e) and 14-8-6(b). The early version of the low-power setup differed only in the termination of the bias capacitor (a short circuit instead of 50 Ω) and the length of the power supply cable (20 ns instead of 270 ns). Because the purpose of this experiment was to observe the differences in the long time constant conductivity decay of the two samples, the only significant impact of using the early apparatus was to impose a load line of 50 Ω instead of 100 Ω.

Samples 14-8-9(e) and 14-8-6(b) are the n-type and p-type samples respectively. These two samples were used because they have the greatest difference in their Cu_B occupation probabilities, and are accordingly expected to have the greatest contrast in turn-on properties.

The bias voltage applied to sample 14-8-9(e) was 15.3 V, and that applied to sample 14-8-6(b) was 16.5 V (the difference in the bias voltages is a result of the larger dark resistance of the p-type sample). Both samples were illuminated with identical laser pulses from the mini-YAG laser, whose beam diameter was reduced to the approximate size of the sample by focusing with a lens. Consequently, the peak photon flux was estimated to be 4×10^{24} cm^{-2} s^{-1} at the sample. There was no second laser pulse in this experiment. The resulting photocurrent pulses for both samples are shown in Fig. IV-1.

It is clear from Fig. IV-1 that there are substantial differences in the important characteristics of the tail currents. In particular, the ratio of the tail current to the peak current is considerably better (larger) for the n-type sample than for the p-type sample. In addition, the conductivity decay is much longer for the

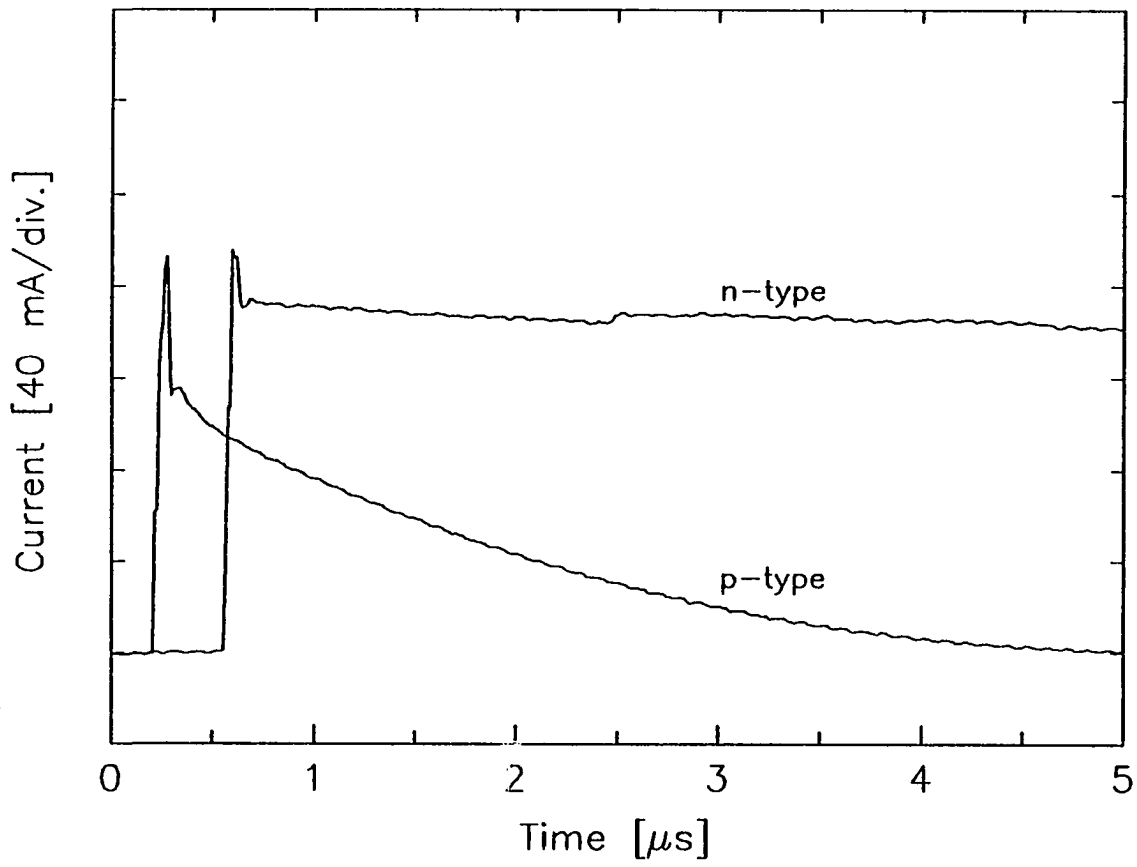

Figure IV-1 Comparative single-pulse current responses for the p- and n-type samples under similar conditions of voltage and light intensity (λ = 1064 nm).

n-type sample than for the p-type sample. The decay of the n-type sample's conductivity shown in Fig. IV-1 is nearly 30 μs, while for the p-type sample it is only about 1 μs.

Turn on at different wavelengths

The dynamics of the turn-on process were investigated under illumination by laser light of two other wavelengths besides 1064 nm. The first wavelength was 532 nm produced by doubling the output of the DCR-3 Nd:YAG laser. The laser was operated in the "fast" mode (see Fig. III-2) to provide the greatest excitation bandwidth possible. The other wavelength was provided by the IR-WEX pumped by the DCR-3's 1064 nm output and the PDL loaded with the DCM dye. The PDL was tuned such that the IR-WEX operated at a wavelength of 1760 nm. The DCR-3 was operated in the "slow" mode (see Fig. III-2) while pumping the IR-WEX. Only sample 14-8-6(b) was illuminated by the laser pulses. The sample was illuminated by first one laser pulse and then the other during separate shots. The corresponding photocurrents were measured in the low-power setup described in Chapter III. The purpose of this experiment was to demonstrate the temporal properties of the two processes critical to the BOSS concept; namely, electron-hole pair recombination, and hole capture at Cu_B. Because the photon energy at 532 nm exceeds the band gap energy of GaAs, it is certain that this laser pulse succeeded in generating a large electron-hole pair plasma. Figure IV-2 contains the digitized waveforms for both the 532 nm laser pulse and the resulting sample photoconductance. Clearly, the initial portion of the photoconductance pulse shares some of the nanosecond features of the "fast" DCR-3 laser pulse. In Chapter V, an analysis based on the deconvolution of the laser-pulse frequency response from the photoconductivity frequency response

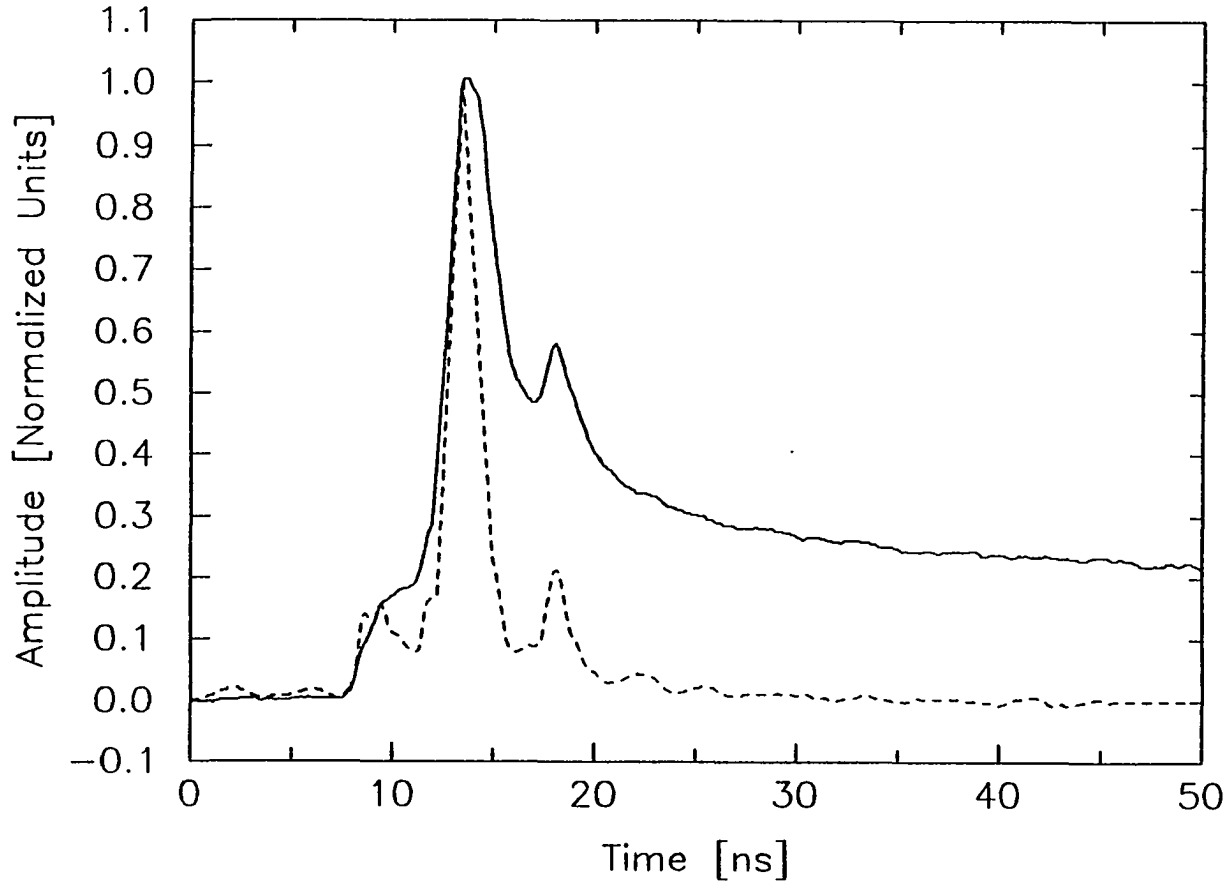

Figure IV-2 A comparison of the photoconductance (the solid line) of sample 14-8-6(b) resulting from illumination by a 532 nm laser pulse (the dashed line) shown superimposed on the photoconductance trace.

will demonstrate that the electron-hole pair lifetime is shorter than that which can be measured with this laser (i.e., subnanosecond).

On the other hand, the 1760 nm laser pulse has a photon energy of 0.70 eV, which is less than half the band gap at room temperature. Consequently, this laser pulse is restricted to the excitation of electrons and holes directly from deep centers. It is assumed that this laser pulse primarily excites holes from Cu_B to the valence band. The rapid recapture of holes back into Cu_B should result in a rapid decay of the laser-induced photoconductivity. Figure IV-3 contains the digitized response of sample 14-8-6(b) to the 1760 nm "slow" laser pulse. Although an actual measurement of the 1760 nm laser pulse temporal envelope is not available, as it was for the 532 nm pulse, the close similarity between the photocurrent response and the "slow" laser pulse shown in Fig. III-2 should be noted. Clearly, hole capture is also a subnanosecond phenomenon in Cu:Si:GaAs.

Although it will be discussed in further detail in Chapter V, it is mentioned here that the rapid hole capture observed in Fig. IV-3 helps explain the persistent current tail observed in Fig. IV-2 after the initial current peak. This current tail is the result of the competition between fast hole capture at Cu_B and fast recombination through centers; the same process that generates a tail current at λ = 1064 nm.

Turn off vs. level of compensation

Perhaps the most unique property of the BOSS is the ablility to turn it off with infrared radiation, an effect known as optical quenching. While optical quenching of photoconductivity has been known for sometime [43], the results presented here and in Refs. [29] and [30] represent the first demonstration of the

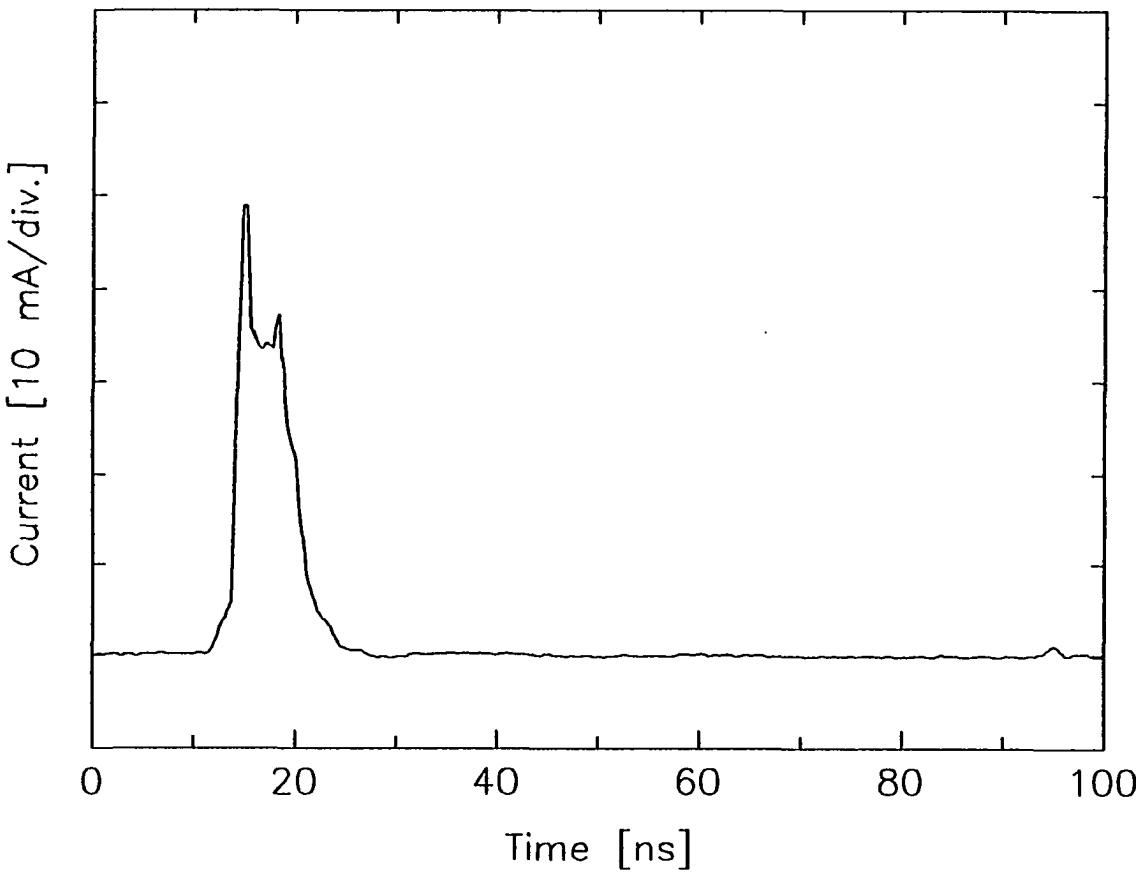

Figure IV-3 Photocurrent response of sample 14-8-6(b) to illumination by a 1760 nm laser pulse whose temporal properties are similar to the "slow" DCR-3 laser pulse.

feasibility of a nanosecond opening switch that utilizes fast optical quenching in GaAs.

Optical quenching is achieved after an initial photoconductivity is generated by illuminating the sample with, for example, Nd:YAG laser radiation of wavelength λ = 1064 nm. At any time prior to the complete decay of the photoconductivity (which occurs over microseconds) a laser pulse of photon energy less than 1 eV (at room temperature) can be directed onto the Cu:Si:GaAs sample in order to interrupt the photoconductivity and "open" the switch. Since the process of optical quenching (hole excitation from Cu_B and subsequent electron-hole recombination through recombination centers) depends on the availability of bound holes at Cu_B, which in turn depends on the level of compensation, it is expected that level of compensation will have a definite effect on the strength of optical quenching. This notion was tested in the following experiment.

Three different samples, 14-8-9(e), 14-8-9(f), and 14-8-6(b), were placed into the low-power setup one at a time. These three samples were chosen because of their different levels of compensation. Sample 14-8-9(e) is undercompensated (n-type), sample 14-8-9(f) is closely compensated (semi-insulating), and sample 14-8-6(b) is overcompensated (p-type). Once the sample was imbedded into the microstripline and a voltage bias applied, it was then illuminated with a light pulse from the mini-YAG laser. The sample was illuminated on the face containing the contacts with a beam whose diameter exceeded the sample dimensions. This led to the uniform illumination of the entire sample. The laser pulse had a peak photon flux of about 5×10^{23} cm^{-2} s^{-1}.

The illumination by the mini-YAG laser pulse induced photoconductivity in the sample; however, instead of allowing the photoconductivity to persist, as in the "turn-on" experiments, a second laser pulse from the IR-WEX was applied to the sample after a 200 ns delay. The IR-WEX pulse had a wavelength of 1620 nm. The output of the IR-WEX was focused to a spot 3 mm in diameter that illuminated the active region between the contacts. The peak photon flux of the IR-WEX laser pulse at the sample was estimated to be 1×10^{25} cm^{-2} s^{-1} by measuring the average energy per pulse.

Characteristic digitized photocurrent responses for samples 14-8-9(e), 14-8-9(f), and 14-8-6(b) are presented in Figs. IV-4, IV-5, and IV-6 respectively. There are three distinct features that should be observed: First, the relative value of the tail with respect to the peak; second, the apparent rate of decay of the tail; and third, the level of photocurrent after the second laser pulse. In the first case, as the sample goes from undercompensated to overcompensated, the tail becomes a smaller percentage of the peak current. Recall that this phenomenon was described in the first section of this chapter. Note that the actual "undisturbed" photocurrent tail does not occur until about 140 ns into the pulse because this is the point where the tail of the Q-switched mini-YAG laser pulse is cutoff (see Fig. III-1).

The second phenomonon is the decay of the photocurrent tail that was also discussed in the first section of this chapter. Notice that the decay accelerates as the sample changes from undercompensated to overcompensated. Again, the best comparison should be made after 140 ns but before the onset of the second laser pulse.

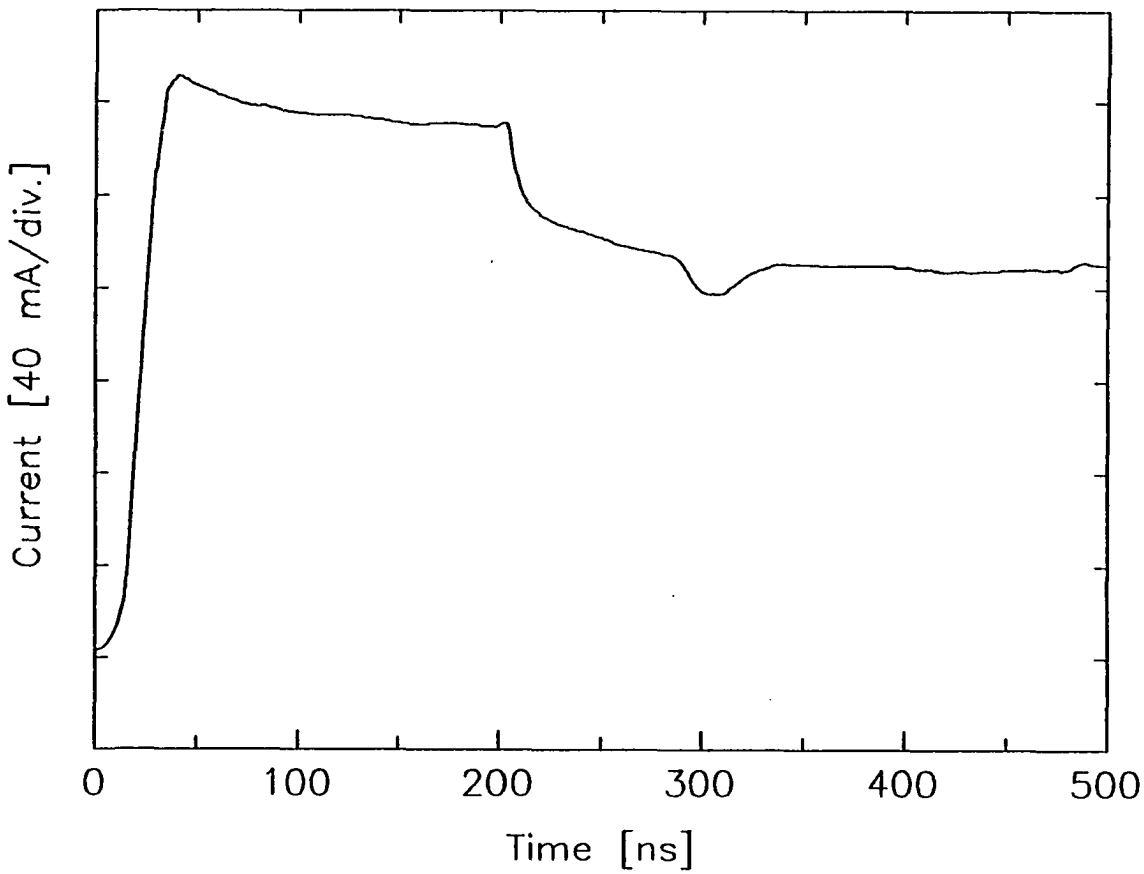

Figure IV-4 Typical photocurrent response of sample 14-8-9(e) to illumination first by a 1064 nm laser pulse, and then by a 1620 nm laser pulse 200 ns later. V_B = 39 V, Φ = 1 × 10^{25} cm^{-2} s^{-1} (second pulse).

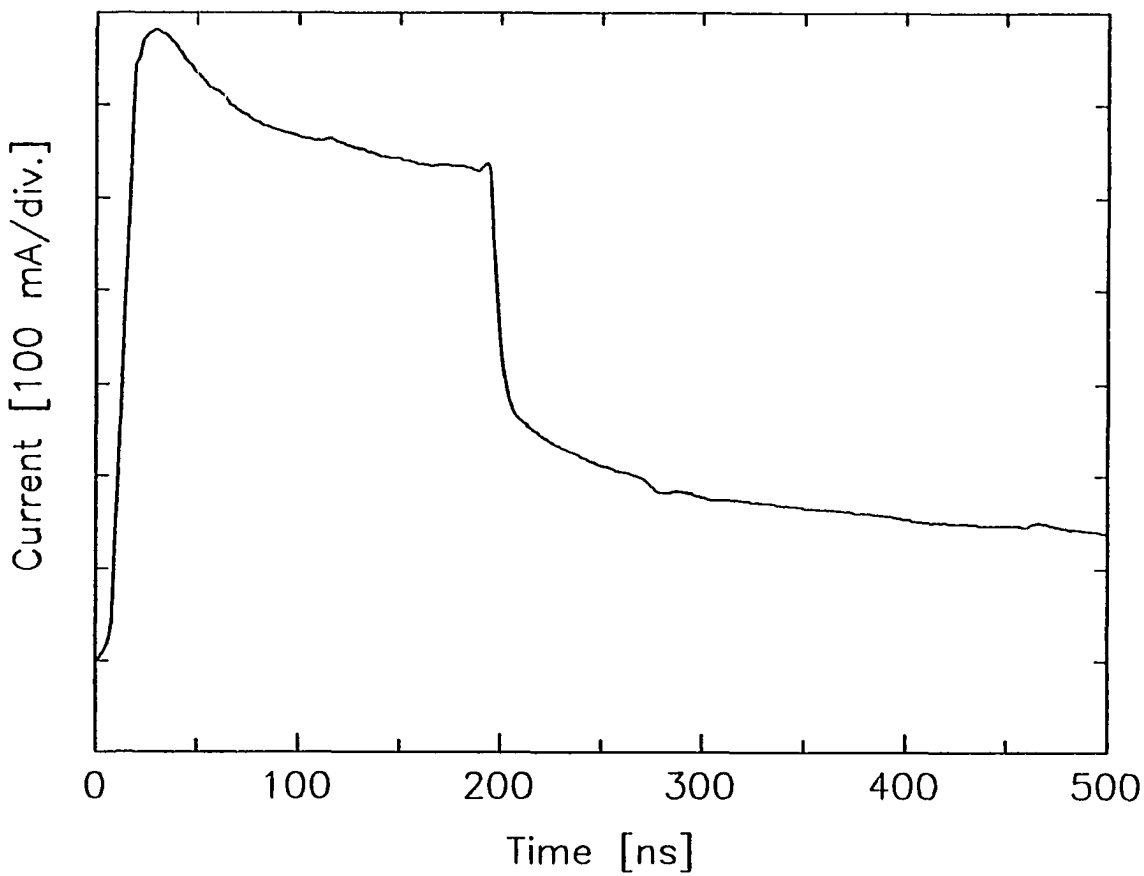

Figure IV-5 Typical photocurrent response of sample 14-8-9(f) to illumination first by a 1064 nm laser pulse, and then by a 1620 nm laser pulse 200 ns later. V_B = 80 V, Φ = 1×10^{25} cm^{-2} s^{-1} (second pulse).

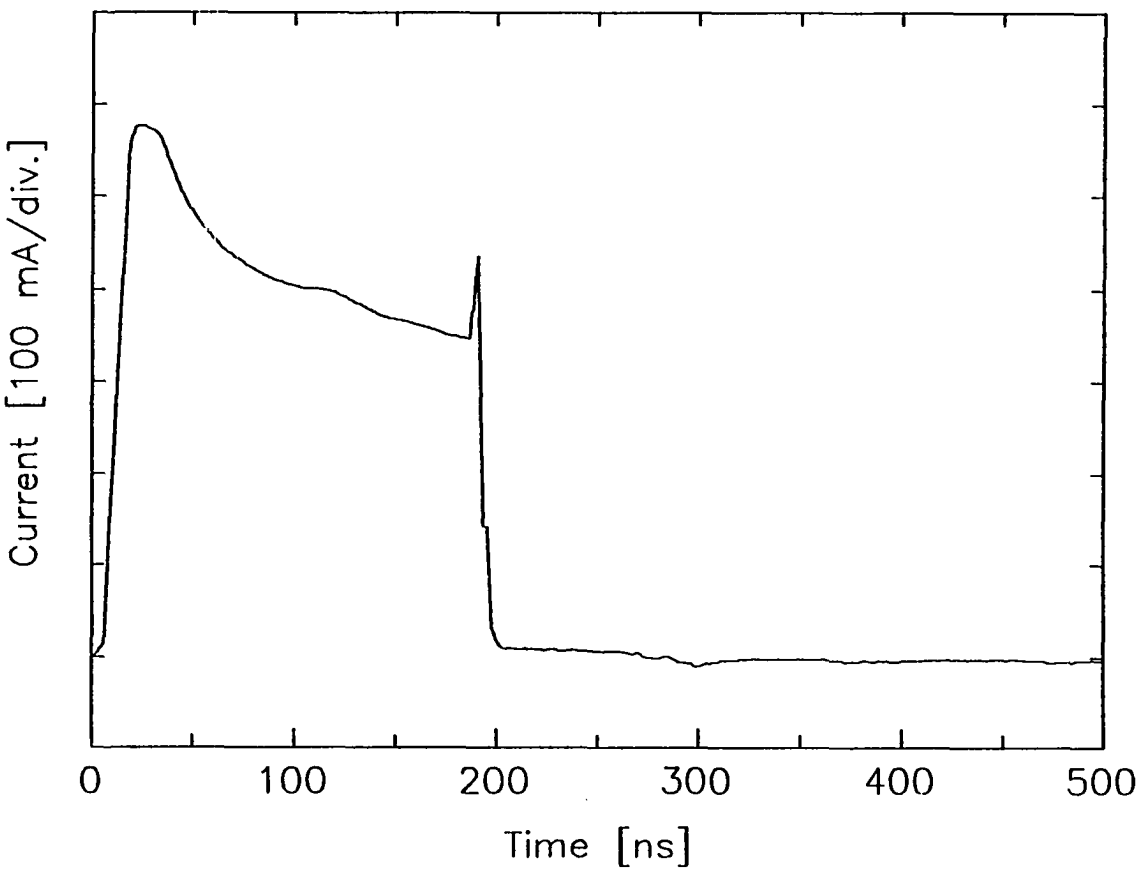

Figure IV-6 Typical photocurrent response of sample 14-8-6(b) to illumination first by a 1064 nm laser pulse, and then by a 1620 nm laser pulse 200 ns later. V_B = 80 V, $\Phi = 1 \times 10^{25}$ cm^{-2} s^{-1} (second pulse).

Last but not least is the effect of the second laser pulse. It is clear from Fig IV-6 that the 1620 nm laser pulse induces strong optical quenching which, within the resolution of the digitizer, virturally extinguishes the photoconductivity. Indeed, the photocurrent is quenched over the time scale of the laser pulse itself (i.e., $\approx$ 10 ns). This remarkable result is believed to be the first demonstration of nanosecond optical quenching in GaAs, and is a direct verification of the BOSS concept. However, as the sample is changed from overcompensated to undercompensated the influence of the second laser pulse diminishes, and the level of the tail current remaining after the second laser pulse increases from unmeasurably small in Fig. IV-6 to about 75% of the initial tail current in Fig. IV-4.

A couple of other effects may be noticed, notably a dip in the photocurrent at 270 ns in Figs. IV-4 and IV-5. This dip is due solely to a reflection at the opposite end of the power supply cable caused by interconnection inductance. However, the rather large spike in Fig. IV-6 (and the smaller ones in the other two figures) that is coincident with the second laser pulse is a photoconductivity effect related to intensity and wavelength dependent phenomena that will be discussed in the next section.

Other turn-off parameters

Two other parameters were varied to see their effect on the photoconductivity of the p-type sample [14-8-6(b)]. The first parameter was the wavelength of the second laser pulse, and the second parameter was the peak intensity of the second laser pulse. Data were recorded at three particular second laser pulse wavelengths: λ = 1500 nm ($h\nu$ = 0.83 eV), λ = 1620 nm ($h\nu$ = 0.77 eV), and λ = 1760 nm ($h\nu$

= 0.70 eV). Notice that the photon energy descends through the half-band-gap mark of 0.71 eV at room temperature.

Other than the change in second laser pulse wavelength, the experimental conditions were the same as described in the last section. Figures IV-7 and IV-8 represent the digitized photocurrent responses of sample 14-8-6(b) to the 1620 nm and 1760 nm laser pulses, both with a photon flux of approximately 1.5×10^{25} cm^{-2} s^{-1}. While the sample response at 1500 nm was virtually indistinguishable from the response at 1620 nm, it is clear that the response at 1760 nm is different; primarily because of the lack of a substantial spike in current coincident with the second laser pulse.

After the wavelength experiment, the second laser pulse intensity was adjusted by introducing neutral density filters into the IR-WEX beam (the mini-YAG beam was left undisturbed). The beam was focused (see Fig. III-3) and had a peak (unattenuated) photon flux at the sample of 6×10^{25} cm^{-2} s^{-1}. The beam was attenuated to a minimum photon flux of 1×10^{23} cm^{-2} s^{-1} without changing the spot size on the sample. The wavelength during this experiment was fixed at 1620 nm.

Many data points were taken between the two intensity extremes. For each data point, the tail conductivity just prior to the second laser pulse, σ_T, and the final conductivity after the second laser pulse, σ_F, were measured (except when σ_F could not be distinguished from the zero baseline). These two values were used to form the "quenching factor," which is defined as

$$Q \equiv \frac{\sigma_T - \sigma_F}{\sigma_T} = \Delta\sigma/\sigma_T \quad . \quad \text{(IV-1)}$$

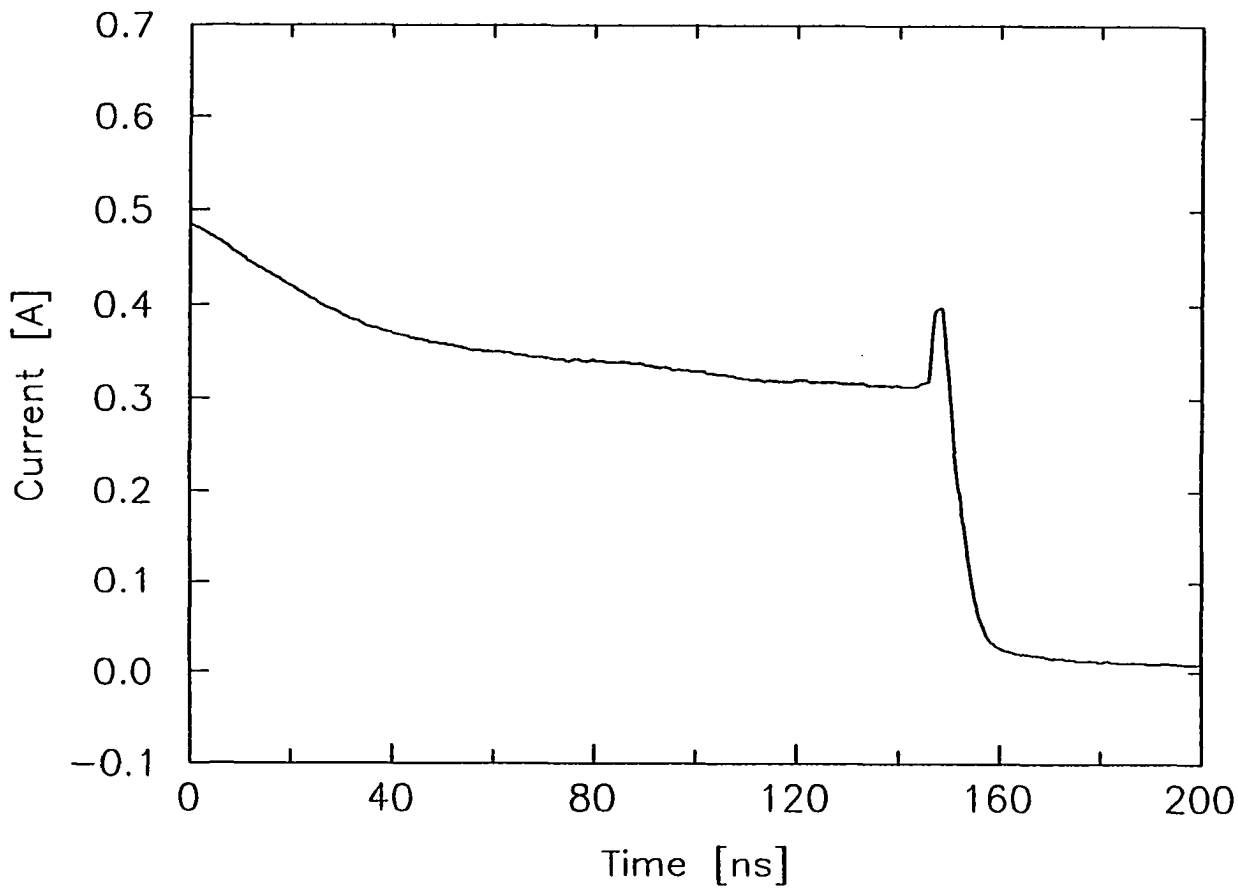

Figure IV-7 Expanded view of the photocurrent quench. Sample 14-8-6(b) is first illuminated by a 1064 nm laser pulse, and then by a 1620 nm laser pulse 200 ns later. V_B = 55 V, Φ = 1.5 × 10^{25} cm^{-2} s^{-1} (second pulse).

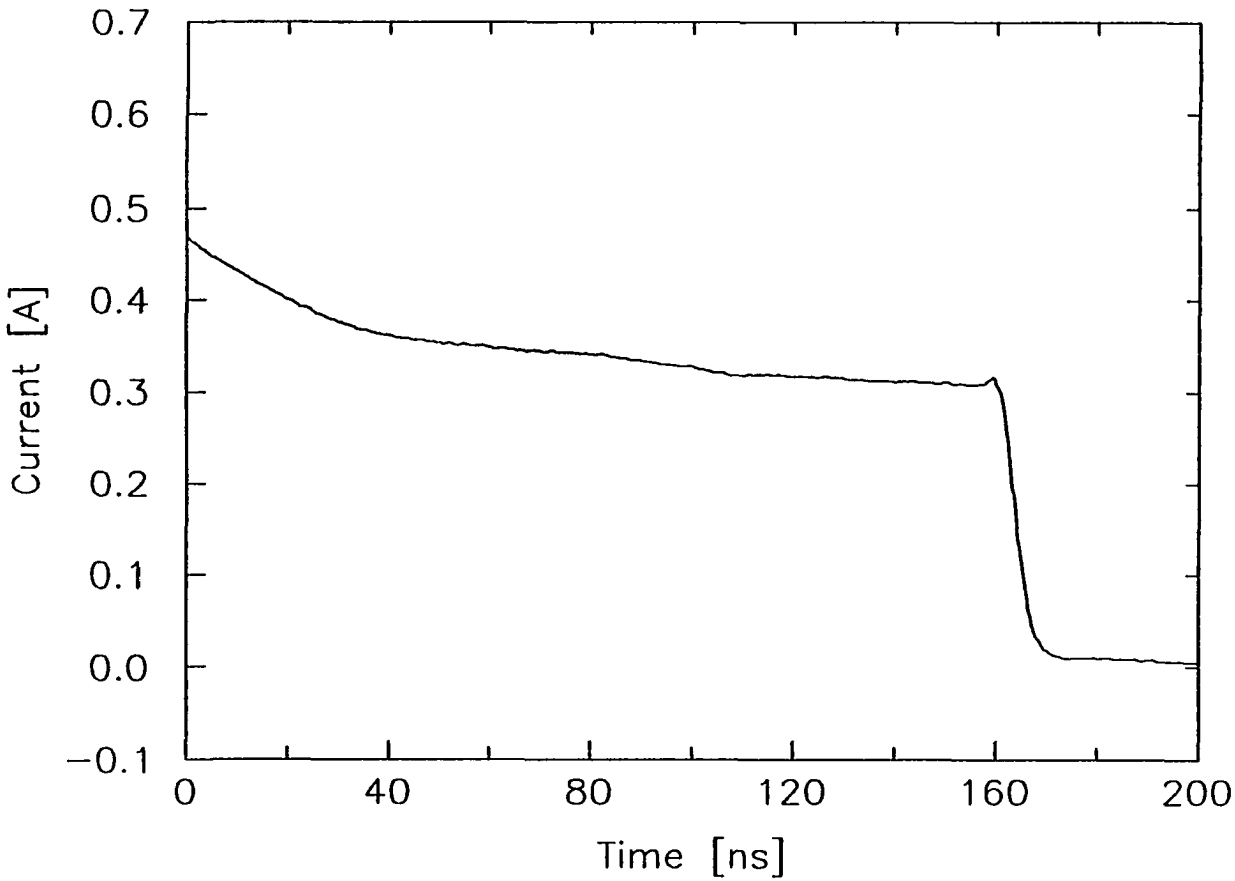

Figure IV-8 Expanded view of the photocurrent quench. Sample 14-8-6(b) is first illuminated by a 1064 nm laser pulse, and then by a 1760 nm laser pulse 200 ns later. V_B = 55 V, $\Phi = 1.5 \times 10^{25}$ cm^{-2} s^{-1} (second pulse).

Because values of σ_F only so small can be resolved from the digitized current traces, the maximum value of Q that could be resolved was 98%. Figure IV-9 is a plot of peak intensity of the second laser pulse (expressed as a photon flux) versus measured quenching factor. The maximum value of Q plotted in Fig. IV-9 is 98% in keeping with the limited resolution; however, the quenching factor of the shots at the higher intensities probably exceeded 98%. At a photon flux of 3×10^{24} cm^{-2} s^{-1} the quenching factor breaks below 98% and then uniformly decreases as the photon flux approaches 10^{23} cm^{-2} s^{-1}. The trend gives every sign of continuing to even lower intensities.

An interesting change in the quenching portion of the photocurrent response occurred as the photon flux decreased below 10^{25} cm^{-2} s^{-1}. Recall from Figs. IV-6 and IV-7 that there occurred an overshoot or spike in the current coincident with the second laser pulse at wavelengths of 1620 nm or less. During this experiment, the spike disappeared when the photon flux went below the 10^{25} cm^{-2} s^{-1} threshold, even though the wavelength did not change from 1620 nm.

High-power performance

Of course, the purpose of this work is to demonstrate the feasibility of the BOSS concept, which is expected to be used as a high-power switch in pulsed power applications. Consequently, measurements have been performed to investigate the "scalability" of the properties measured in the low-power setup to higher voltages and currents.

The measurements were compiled on the high-power test bed described in Chapter III. Only sample 14-8-6(b) was used in this experiment. Figure IV-10 demonstrates a typical switching event for peak fields on the order of, or less than,

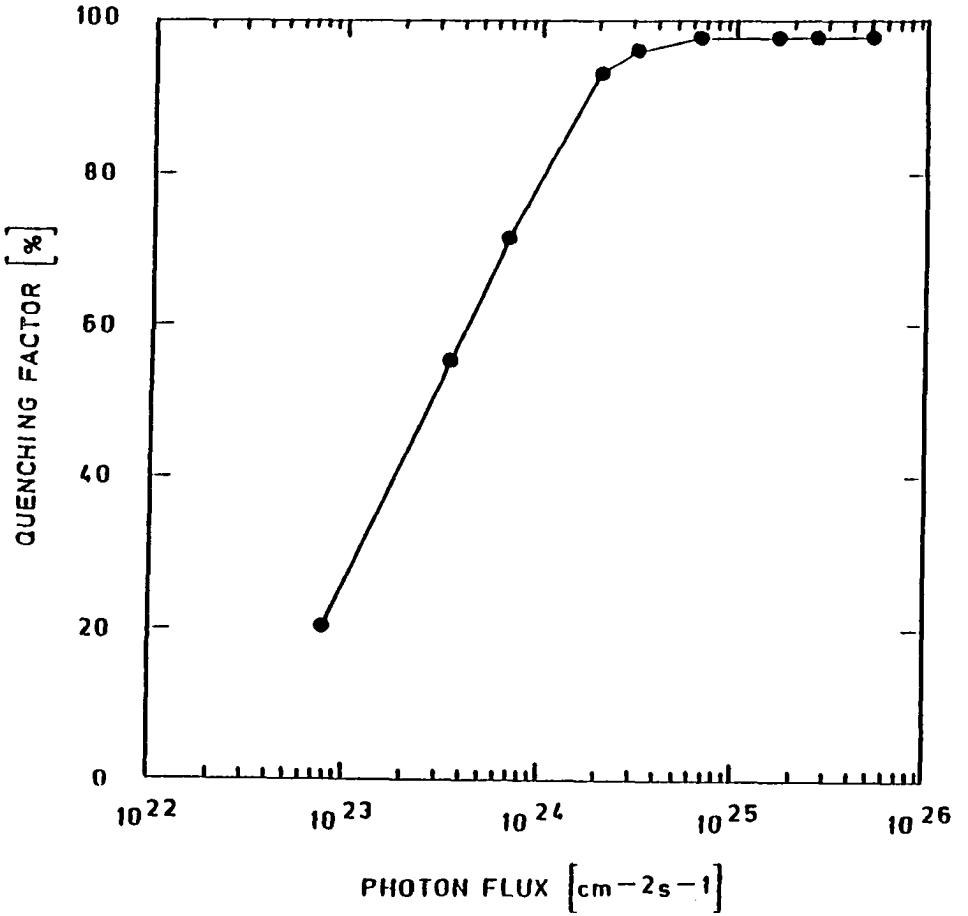

Figure IV-9 Quenching factor as a function of the 1620 nm laser pulse peak intensity. The maximum quenching factor that could be resolved was 98%.

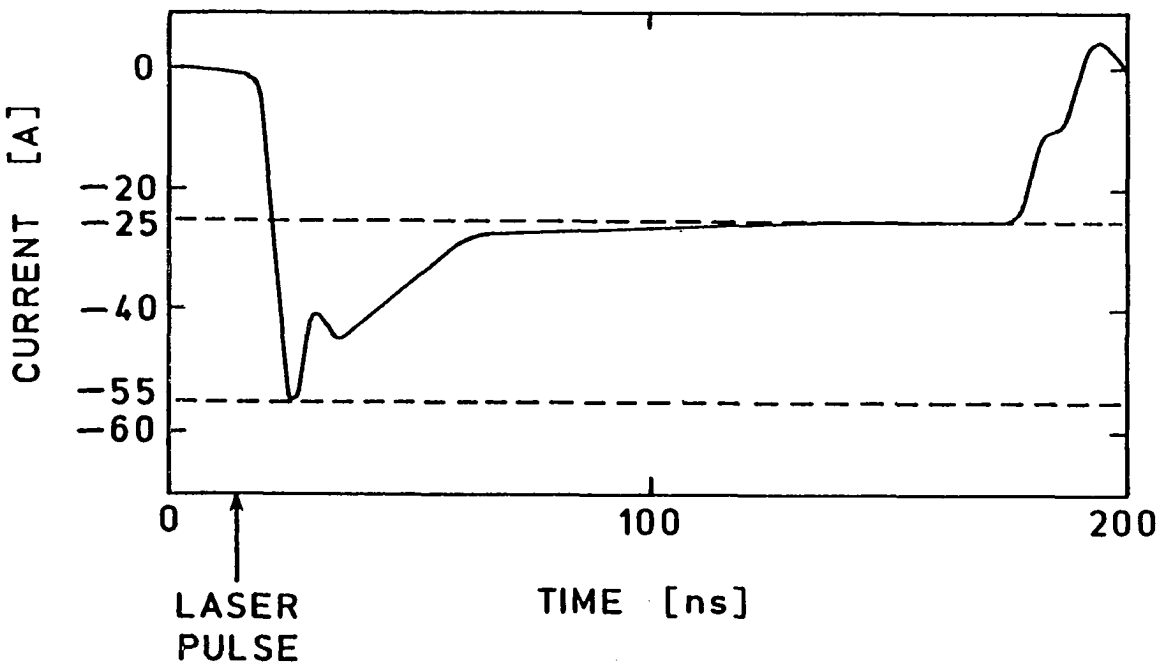

Figure IV-10 Photocurrent response of sample 14-8-6(b) to illumination by a 1064 nm laser pulse (note that the collapse of the current after 160 ns is due to the end of the transmission line voltage pulse).

10 kV/cm (in this case, the charging voltage was 3 kV, ≈ 12 kV/cm). Upon application of the laser pulse (the beginning of the pulse is indicated by the arrow), the current rapidly rises to 55 A and then decays to a long-time constant "tail current," which after 160 ns has settled to 25 A. This represents an approximate tail current density of 3.7 kA/cm^2. The current then collapses, not because of a second laser pulse (there was none), but because the pulse forming line (PFL) voltage pulse has been exhausted. The load was separated by a short distance from the chamber containing the sample, hence a reflection at the end of this separation is revealed by a dip in the current a few nanoseconds past the peak. This reflection heralds the transition between a 50 Ω circuit limit (which restrains the peak current), and an 87 Ω circuit limit (37 Ω load plus 50 Ω cable impedance) that is in effect during the tail conduction.

During the experiment, a maximum of 4.7 kV was placed across the sample without failure, corresponding to a maximum electric field of 19 kV/cm. When the sample was uniformly illuminated with a 10 ns FWHM 1064 nm laser pulse on the non-contact side of the crystal (the photon flux exceeded 5×10^{25} cm^{-2} s^{-1}), the sample conducted a peak current of 92 A, corresponding to a current density of 10 kA/cm^2.

The discussion in the above paragraph is intended to present the maximum performance achieved so far with the Cu:Si:GaAs samples. However, it should be noted that *tail* conduction as observed at fields on the order of 10 kV/cm or less did not occur as the field went above this threshold. Instead, the sample went into a state known as "lock on" which has been observed in other semi-insulating GaAs materials [19], [21]. The lock-on state is characterized by a constant voltage across the sample (as in a Zener diode) instead of a slowly decaying photoconductance

observed at the lower fields. Indeed, the lock-on state is clearly revealed in the *I-V* characteristics of the sample.

The *I-V* characteristic of sample 14-8-6(b) can be resolved from Fig. IV-11. This figure contains a plot of peak PFL charging voltage (which represents the source or open-circuit voltage that drives current in the circuit) versus the sample current just prior to the voltage collapse at 160 ns. Clearly, at the lower voltages (less than 3 kV) the data points fall on a line localized at the origin. This resistive load line includes both the sample impedance and the external circuit impedance. Above this voltage, however, the *I-V* characteristics break to a new line that has a non-zero intercept. This intercept represents the lock-on voltage of the sample, which is about 1.2 kV (the average field is 4.7 kV/cm). The slope of the new line is substantially steeper because it is determined by the external circuit impedance only.

Summary

This concludes the chapter on experimental results. Chapter IV has provided a close look at the experimental photocurrent data so far collected on samples 14-8-9(e), 14-8-9(f), and 14-8-6(b). The data cover several parameters that have been included in a rate equation model of this switch material [31-33], including level of compensation and laser pulse intensity. The next chapter will discuss the similarities between the modeling results and the experimental results just provided.

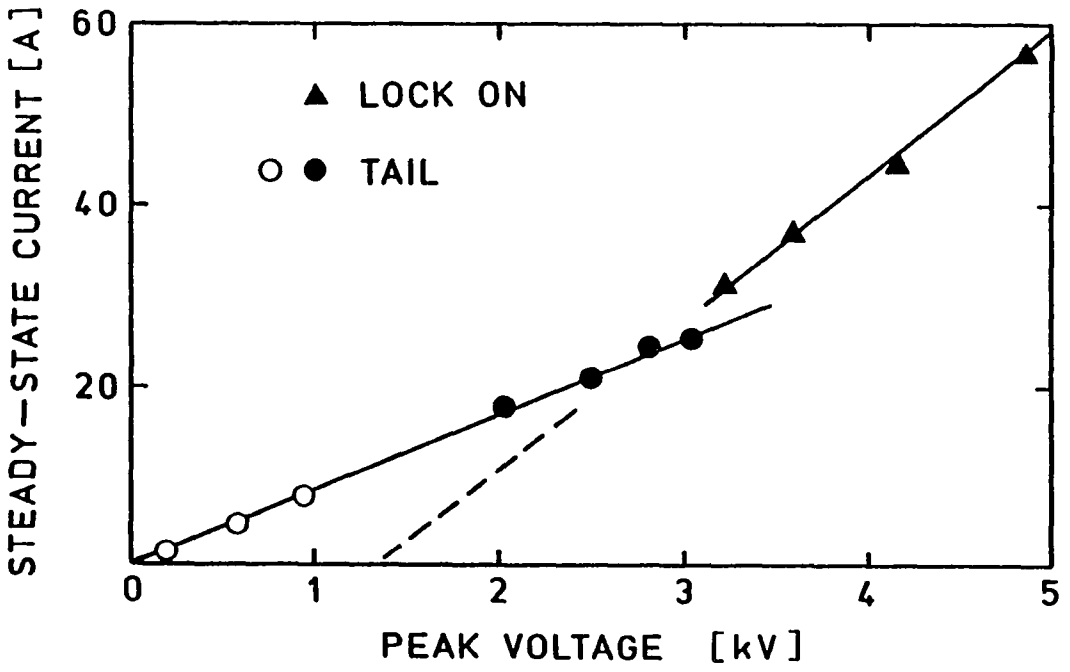

Figure IV-11 Peak voltage vs. tail/lock-on current. Open circles represent data measured with a low-voltage apparatus, while closed symbols represent data obtained with the higher voltage apparatus described in the paper.

CHAPTER V

DISCUSSION OF RESULTS

The results of the optogalvanic experiments described in the last chapter are the subject of this discussion. The purpose of the discussion will be to understand the photoconductivity properties of the Cu:Si:GaAs crystals used in this investigation. Extensive reference will be made to the results of various theoretical calculations by S. T. Ko found in Refs. [31-33]. These calculations involve the solution of zeroth-dimension rate equations which model the kinetics of the capture and emission of free carriers in Cu:Si:GaAs. It will be seen that many of the quantitative and qualitative predictions produced by these calculations describe the experimental results well. However, in addition to the numerical calculations that will be cited, analytical computations will also be presented when they are illustrative of the underlying principles controlling the behavior of the observed photoconductivities. In order to complete the discussion, some consideration of the measured photo-conductivities from a switching view point will be provided, including the topics of optical efficiency and power scaling.

Rather than discuss each experiment in the order given in Chapter IV, the arguments that follow will be grouped by the events that occur in a typical switching response, like that shown in Fig. IV-6. The events have causes, which will be explained by the optical and thermal processes occurring in the crystal. Before the

discussion begins, it would be useful to first review the various phenomena revealed by the optogalvanic experiments.

- During illumination by the laser pulse, the photoconductivity always overshoots the final tail conductivity. This is called the initial conductivity peak. The ratio of the conductivity peak to the tail conductivity was largest for the n-type sample and smallest for the p-type sample.
- A persistent or tail conductivity always lingered long after the initial laser pulse terminated. The tail conductivity decayed slowest for the n-type sample ($1/e \approx 30\ \mu s$), but fastest for the p-type sample ($1/e \approx 1\ \mu s$).
- Tail conductivity was generated with either 1064 nm or 532 nm laser radiation. Tail conductivity was not generated with 1760 nm laser radiation, instead the conductivity decayed so quickly that the resulting current pulse appeared to have the same temporal envelope as the laser pulse.
- With the onset of the second laser pulse (typically 200 ns after the first laser pulse) a fast decay of the photoconductivity began. The decay continued as long as the second laser pulse illuminated the sample (~ 7-10 ns). The strength of the photoconductivity quench depended on the compensation of the sample. The p-type sample had the strongest reduction in photo-conductivity while the n-type sample had the weakest. Of course, the semi-insulating sample was in between these two extremes.
- In some cases, the photoconductivity initially increased during illumination by the second laser pulse, but, eventually, the photoconductivity always strongly decreased. The initial overshoot was restricted to cases where the second

pulse wavelength was less than or equal to 1620 nm and the photon flux was significantly above 5×10^{24} cm^{-2} s^{-1}. Otherwise, no overshoot was observed.

- Persistent conductivity was observed in the p-type sample up to an initial field stress of 12 kV/cm. At higher fields, the sample's *I-V* characteristics broke to a new curve marked by a constant voltage across the sample (like a Zener diode) rather than a slowly decaying photoconductor. This new state is called "lock on."

This list can be gathered into three groups: effects associated with "turn on," effects associated with "turn off," and effects associated with high electric field. Hence, the following discussion will deal with each group one at a time, and, hopefully, in the process a clear understanding of the origins of all of these phenomena will emerge. At the end of this chapter the discussion will turn to issues related to switch performance, including efficiency of optical excitation and scaling to higher power.

Generation of tail conductivity

The description of the BOSS concept found in Chapter I was very general. While the experimental evidence is clear: tail conductivity can be generated in Cu:Si:GaAs after the application of sub-band-gap radiation, the dominant processes that allow this to happen have not been explained in detail. Indeed, other semi-insulating GaAs materials besides Cu:Si:GaAs can exhibit persistent conductivity (e.g., EL2 compensated GaAs [44, p. 68]). It is the properties of the dominant deep level or levels that dictate many of the properties of the observed photoconductivity.

In order to demonstrate that the generation of tail conductivity in Cu:Si:GaAs is dominated by two competing processes, namely, recombination and hole capture

at Cu_B, a simplified rate equation model is proposed. This model includes one hole trap (Cu_B), and one fast recombination center. Optical excitation of both holes and electrons will be allowed from Cu_B. Bimolecular direct recombination will be neglected, since this is usually a slow process compared to recombination at centers. Although the recombination center is not identified, parameters for the center (i.e., the density of states of the center and its electron and hole capture cross sections) will be taken from the more complete model by S. T. Ko [31-32]. In addition, all thermal emission processes will be neglected, because it is assumed that over the time scale of the first laser pulse these slow processes are not important.

The purpose of this model is to generate an analytical solution for the electron occupation number of the Cu_B level *after* illumination by the first laser pulse, because this determines the concentration of electrons depleted from compensated Cu_B centers which then contribute to the tail conductivity. Since Cu_B is a strong hole trap, it is very unlikely that hole transport produces a significant contribution to the tail conductivity. However, the purpose of this model is not to produce close quantitative agreement with experiment; instead, at the end of this section the more exact (but less illustrative) numerical calculations found in Refs. [31-33] will be compared directly to the experimental data.

The calculation begins by writing the set of first-order, non-linear rate equations that describe the processes of optical excitation, hole capture at Cu_B, and electron-hole recombination at a recombination center.

$$\frac{dn}{dt} = \Phi \sigma_n n_T - C_R n (N_R - n_R) \quad \text{(V-1)}$$

$$\frac{dn_T}{dt} = -\Phi \sigma_n n_T + \Phi \sigma_p (N_T - n_T) - C_{pT} p n_T \quad \text{(V-2)}$$

$$\frac{dn_R}{dt} = C_R n (N_R - n_R) - C_R p n_R \quad \text{(V-3)}$$

$$\frac{dp}{dt} = \Phi \sigma_p (N_T - n_T) - C_R p n_R - C_{pT} p n_T \quad \text{(V-4)}$$

The numerous variables found in these equations have been summarized in Table V-1 to acquaint the reader to their meaning.

It could be imagined that two situations may arise. The first would occur for a relatively "low" intensity laser pulse. In this case, the set of equations (V-1) through (V-4) would remain dynamic (i.e., constantly changing) because not enough photons would have been absorbed to force the system to reach the steady state. On the other hand, for the case of a "high" intensity laser pulse, the rates of hole capture and recombination become so fast that the system responds to changes in the illumination intensity "instantaneously," that is, the rate equations can be assumed to always be in the steady state. This means that at high intensity, the total rates of change given by the first derivatives of all four variables (n, n_T, n_R, and p) are zero. Both experimental evidence and numerical calculations [32] indicate that the later case occurs at intensities in excess of 3×10^{25} cm^{-2} s^{-1}. It will now be shown that if the system reaches steady state, then the occupation number of the Cu_B state after illumination by the laser pulse (given by n_T/N_T) is independent of the photon flux; in other words, the tail conductivity saturates.

Table V-1 List of variables used in the analytical model.

Variable	Description	Value	Units
n	Free electron density.		[cm^{-3}]
p	Free hole density.		[cm^{-3}]
n_T	Electron occupation of Cu_B.		[cm^{-3}]
n_R	Electron occupation of the recombination center.		[cm^{-3}]
N_T	Total density of Cu_B defects.		[cm^{-3}]
N_R	Total density of recombination centers.	3×10^{14}	[cm^{-3}]
C_{pT}	Hole capture parameter at Cu_B.	3×10^{-7}	[cm^3/s]
C_R	Electron and hole capture parameter at the recombination center.	10^{-6}	[cm^3/s]
σ_n	Photoexcitation cross section for electrons at Cu_B.	10^{-17}	[cm^2]
σ_p	Photoexcitation cross section for holes at Cu_B.	10^{-16}	[cm^2]
Φ	Photon flux of the laser radiation.		[$cm^{-2}\ s^{-1}$]

The left-hand side of Eqs. (V-1) through (V-4) are zero if the system is in steady state. The equations are written below in slightly rearranged form.

$$\Phi \sigma_n n_T - C_R n(N_R - n_R) = 0 \qquad \text{(V-5)}$$

$$[\, \Phi(\sigma_n + \sigma_p) + C_{pT} p \,]\, n_T = \Phi \sigma_p N_T \qquad \text{(V-6)}$$

$$n N_R - (n+p)\, n_R = 0 \qquad \text{(V-7)}$$

$$(\, \Phi \sigma_p + C_{pT} p \,)\, n_T + C_R p\, n_R = \Phi \sigma_p N_T \qquad \text{(V-8)}$$

Electron depletion of Cu_B

Equation (V-6) is the governing equation for the electron occupation of the Cu_B level, hence it can be solved directly for

$$\frac{n_T}{N_T} = \frac{\Phi \sigma_p}{\Phi(\sigma_n + \sigma_p) + C_{pT} p} \quad , \qquad \text{(V-9)}$$

which is the occupation number at any time after saturation. Equation (V-9) can be simplified. Take, for example, the case where hole capture is negligible [i.e., $C_{pT}p \ll \Phi(\sigma_n + \sigma_p)$], in this case Eq. (V-9) reduces to

$$\frac{n_T}{N_T} = \frac{\sigma_p}{\sigma_n + \sigma_p} \simeq 0.91 \qquad \text{(V-10)}$$

which, from the values given in Table V-1, is 91% regardless of the photon flux. Clearly, a 91% occupation number represents a filling of Cu_B with electrons, rather than depletion, when compared to the equilibrium occupation number of p-type material (~ 50%), and only a slight depletion for undercompensated material. This

high occupation number results from the order of magnitude greater probability of hole photoexcitation than electron photoexcitation. Surely, hole capture is vital to the depletion of Cu_B, and the consequent excitation of persistent photoconductivity in Cu:Si:GaAs.

Hole trapping, however, is not independent of the photon flux because optically induced changes in the Cu_B occupation number are fed back through the hole trapping rate. The influence of this process on Eq. (V-9) can be determined by equating Eqs. (V-6) and (V-8). In the resulting expression several terms cancel, and the free hole density, p, can then be extracted to form

$$p = \frac{\Phi \sigma_n n_T}{C_R n_R} \quad . \qquad \text{(V-11)}$$

Equation (V-11) is substituted back into Eq. (V-9), replacing p in the denominator, and thus forming Eq. (V-12):

$$\frac{n_T}{N_T} = \frac{\Phi \sigma_p}{\Phi(\sigma_n + \sigma_p) + \Phi \sigma_n C_{pT} n_T / C_R n_R} \quad . \qquad \text{(V-12)}$$

Interestingly enough, the photon flux Φ exists in each term, and thus cancels. Rearranging like terms allows Eq. (V-9) to be written in its final form:

$$\frac{n_T}{N_T} = \frac{\sigma_p}{\sigma_p + (1 + C_{pT} n_T / C_R n_R)\sigma_n} \quad . \qquad \text{(V-13)}$$

Note that σ_n is now multiplied by a factor that is *always* greater than one. This enhances the cross section,* and results in an enhancement of the optical depletion

*$(1 + C_{pT} n_T / C_R n_R)\sigma_n$ can be thought of as the effective optical cross section.

of electrons from the Cu_B state as compared to the weak effect predicted by Eq. (V-10).

Indeed, Eq. (V-13) demonstrates quite simply the effect of the competition between the two dominant processes associated with the generation of tail conductivity. Because the hole trapping parameter and the recombination term appear as a ratio, the effect of fast hole trapping, which tends to minimize n_T/N_T and thus increases turn-on efficiency, is offset by fast recombination, which is important for good turn-off efficiency, but clearly degrades the turn-on performance. Therefore, care must be taken when selecting alternate GaAs material for use as bulk optically controlled switches (such as chromium doped GaAs) not to enhance recombination too much.

Of course, n_T/N_T cannot be driven arbitrarily low because the hole capture term in Eq. (V-13) contains n_T. In other words, hole capture is eventually controlled by electron depletion of the Cu_B state. This feedback results in a quadratic equation in n_T that can be solved if n_R is known. Fortunately, n_R is known for the special but interesting case of the undisturbed tail conductivity.

Consider Eq. (V-7). The recombination center is partially filled with holes (i.e., $n_R < N_R$) only during illumination. This is because p decays considerably faster than n (at least when fast electron trapping can be neglected); therefore, it takes constant illumination to maintain a free-hole population against both recombination and trapping. After the laser pulse has decayed to insignificant levels, however, the free hole density disappears and the recombination center fills with electrons. Thus, the undisturbed tail conductivity is defined to occur when $n_R = N_R$.

Rewritting Eq. (V-13) into the quadratic form, and assuming that the system is in the tail conductivity phase, it is found that

$$n_T^2 + \sigma' C' N_R \, n_T - C' N_T N_R = 0 \qquad \text{(V-14)}$$

where $C' \equiv C_R/C_{pT}$, and $\sigma' \equiv 1 + \sigma_p/\sigma_n$. Equation (V-14) has a positive and negative solution, but only the positive solution for n_T is physical. This solution is written as

$$n_T = \sqrt{(\sigma' C' N_R/2)^2 + C' N_T N_R} - \sigma' C' N_R/2 \qquad \text{(V-15)}$$

If, from data supplied in Table V-1, $C' \approx 3.33$ and $\sigma' \approx 11$, then values for n_T can be calculated. Values for n_T have been calculated for three different values of N_T, the total Cu_B density, assuming the partition between Cu_A and Cu_B used by Ko: **p** = 0.2 [31-33]. These values have been collected in Table V-2 where it can be seen that n_T hovers in the low to mid 10^{15} cm^{-3} range; which represents an occupation number of less than 10%. Contrast this to the 91% occupation probability found for the case of weak hole capture, and it becomes clear why strong hole capture (with respect to recombination) is vital to the efficient depletion of Cu_B.

The influence of the partition

Cu_A has not been included in the dynamic model, but it can have an important effect on the magnitude of the tail conductivity. This is because the shallow donor density determines the upper limit of the electron density that can contribute to the tail conductivity. As the total Cu density increases for a fixed value of N_{Si} (i.e., as the level of compensation progresses from undercompensated to overcompensated) more and more of the available electrons are trapped into the

unproductive Cu_A state (unproductive because these electrons cannot be elevated to the conduction band with Nd:YAG laser radiation). Consequently, the effect of electron depletion at Cu_B caused by the turn-on laser pulse must be placed into context with the compensation ratio in order to determine the actual tail conductivity that will be observed after irradiation. A representative index is provided in the last column of Table V-2, which is labeled "on-state efficiency." On-state efficiency is defined as

$$\eta = (n_{T_o} - n_T)/N_{Si} \qquad \text{(V-16)}$$

where n_{T_o} is the electron density at Cu_B in thermal equilibrium. Equation (V-16) represents that fraction of electrons introduced by the shallow donors (the maximum being N_{Si}) that can be excited from Cu_B and thus contribute to the tail conductivity. This definition of on-state efficiency takes into account both the effects of finite Cu_B depletion (through n_T) and the effects of electron capture at acceptors other than Cu_B (through n_{T_o}).

The first value of η in Table V-2 is 73%, which represents the maximum efficiency for a partition of 0.2. As N_T increases, η steadily decreases. For the case where $N_T = 2\,N_{Si}$ [probably close to the level of compensation in the p-type sample 14-8-6(b)], η = 48%, a reduction of 35% in the maximum saturation tail conductivity. Thus, the level of compensation has two effects on the observed tail conductivity, both resulting in the reduction of the tail conductivity as N_T increases (in agreement with the experimental results). The first effect is to increase the saturation occupation probablility of Cu_B, and the second is to increase the number

Table V-2 Cu_B electron occupation after saturation for various Cu_B trap densities and $N_{Si} = 5 \times 10^{16}$ cm^{-3}.

Partition	N_T [cm^{-3}]	n_T [cm^{-3}]	η
0.2	5.0×10^{16}	3.4×10^{15}	73%
0.2	7.5×10^{16}	4.7×10^{15}	61%
0.2	1.0×10^{17}	5.9×10^{15}	48%

of electrons from the shallow donor trapped at Cu_A, assuming that the partition remains constant.

A weakness of this calculation is that it does not include electron trapping. Fortunately, fast electron traps, such as EL2, are likely to exist in concentrations at least a factor of five to ten less than copper. Thus electron trapping is expected to be a small correction; probably reducing the observed tail conductivity somewhat. The numerical calculations of Ko, which include electron trapping, are in general agreement. For example the saturation tail conductivity, σ_{ss}, for the n-type sample can be estimated from Table V-2 to be

$$\sigma_{ss} \simeq \eta N_{SI} \mu_n q = 29\ (\Omega\ \mathrm{cm})^{-1} \quad .$$

Figure V-1 contains a plot of the tail conductivity as a function of peak photon flux at λ = 1064 nm produced by the more complete numerical simulation. It is seen that the value of σ_{ss} calculated above is only slightly greater than the conductivity reported for the n-type sample at intensities greater than 10^{25} cm^{-2} s^{-1} (where saturation begins). In addition, the numerical simulation predicts a reduction in the p-type saturation tail conductivity of about 50%, again, in reasonable agreement to the 35% reduction given by the analytical calculation.

Comparison of calculations to experiment

Unfortunately, a comparison of the saturation tail conductivities of all three samples (n-type, semi-insulating, and p-type) cannot be made because only the p-type sample was conclusively driven into saturation. However, the ratios of the tail conductivities of the semi-insulating and p-type samples to the n-type sample's tail

conductivity under conditions of similar (but below saturation) turn-on laser pulse intensity have been calculated.* The ratios are 0.83 and 0.55 respectively; the latter ratio is very close to that calculated from the theoretical saturation conductivities of the n-type and p-type samples, and the former ratio is consistent with the trend suggested by the data in Table V-2. A further consequence of the decreasing excitation efficiency of tail conductivity with increasing compensation ratio,† is the decreasing value of the ratio of tail conductivity to peak conductivity observed experimentally and theoretically for constant photon flux [31].

However, the magnitude of the saturation tail conductivity for the p-type sample [14-8-6(b)] does not give as good agreement as the relative data. Also plotted on Fig. V-1 (the open triangles) are tail conductivity measurements made with sample 14-8-6(b) as a function of peak laser-pulse intensity. The "slow" DCR-3 Nd:YAG laser (λ = 1064 nm) was used for the measurements. Clearly, the tail conductivity saturates as the photon flux exceeds 10^{25} cm^{-2} s^{-1}, but it saturates at a conductivity at least an order of magnitude below that predicted by the numerical calculation (represented by the closed triangles).

The reason for this disagreement is unclear at this time, but it is likely to be related to one (or both) of the following two deviations from the parameters used in the calculations. First, the partition may be underestimated. If the concentration of desirable Cu_B states is reduced while keeping the compensation ratio constant,

---

*Using Eq. (III-1) to calculate the tail conductances from the photocurrent data in Figs. IV-4, IV-5, and IV-6; which were then converted to conductivities using the geometry factors given in Table II-1.

†The compensation ratio = N_{Cu}/N_{Si}.

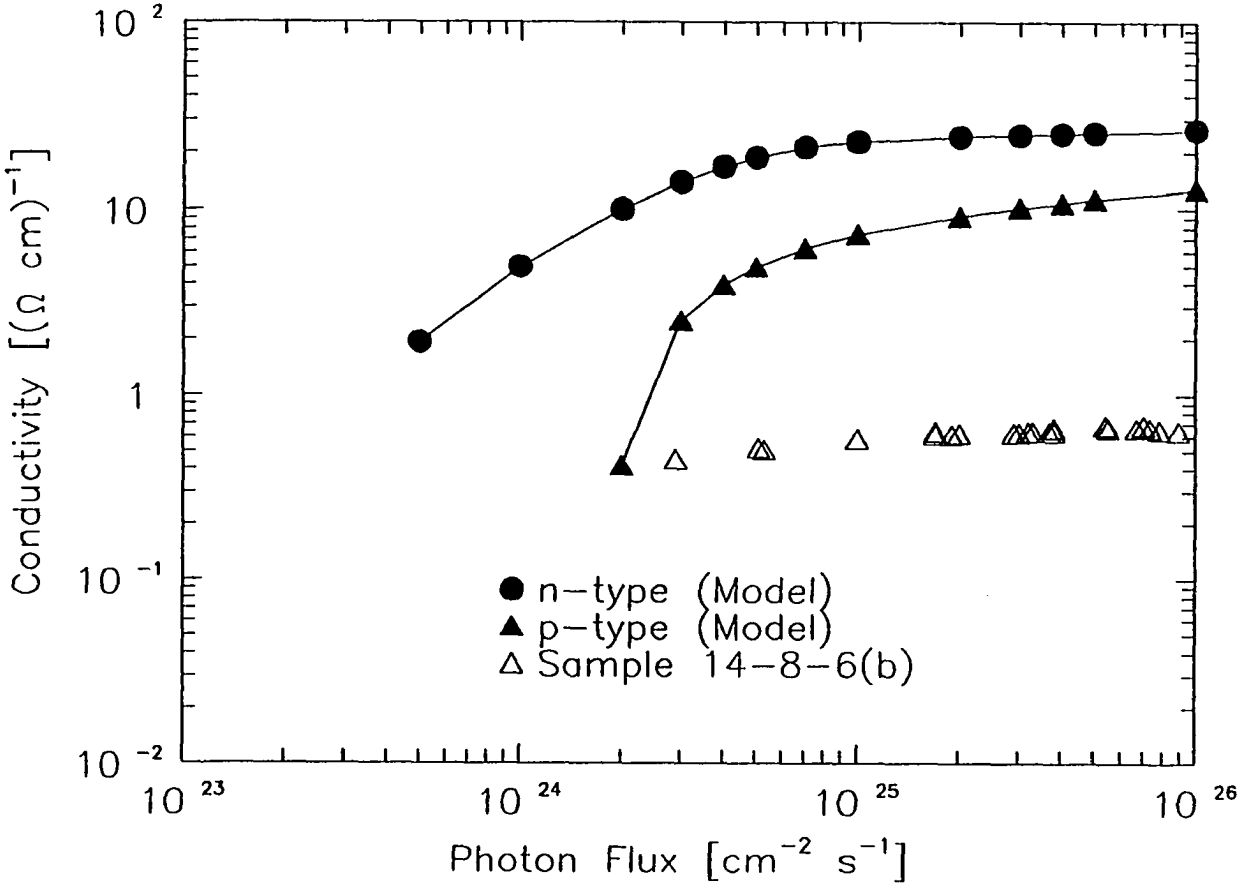

Figure V-1 Variation of the on-state conductivity as a function of the peak photon flux at 1064 nm. The closed symbols are calculated from the numerical simulation [32], the open symbols are measurements with sample 14-8-6(b).

then a corresponding decrease in the observed saturation tail conductivity is expected. For example, if the total copper density is 1.2×10^{17} cm^{-3}, as is assumed in Table V-2, but the partition is increased relatively little to $\mathbf{p} = 0.6$, then the "on-state efficiency" decreases from 48% to 0.5%; a corresponding reduction of the saturation on-state conductivity to about 0.2 $(\Omega\ cm)^{-1}$, well below the measured value. While it is admitted that the on-state conductivity of the more closely compensated crystals is less sensitive to the partition, even these crystals show a substantial reduction in the theoretical on-state conductivity when the partition is varied within the uncertainty described in Chapter II. Surely it is evident that control of the partition is important for achieving high on-state conductivity.

The other influence whose impact may be underestimated is that of recombination. Fast recombination has already been shown to increase the saturation occupation number of Cu_B, an effect that can reduce the observed tail conductivity. Unfortunately, the recombination parameters assumed in the numerical calculation are estimated from conductivity decay results in other semi-insulating material, not the Cu:Si:GaAs crystals used in this investigation. By nature the recombination centers exist in very low concentration in material where they have not been expressly added, consequently substantial variations in density (and cross sections if the centers arise from different defects) would be expected from different base materials and processing techniques.

An attempt has been made to measure the recombination lifetime of electron-hole pairs in sample 14-8-6(b), the p-type crystal. This experiment involved irradiation of the sample with 532 nm radiation, to ensure strong band-to-band absorption; and, as a result, a large electron-hole plasma. The result of this

experiment was presented in Fig. IV-2, in which the waveform of the "fast" DCR-3 frequency-doubled laser pulse is shown with the corresponding photoconductance response of the sample. The photoconductance response, determined from the photocurrent signal, has features that occur over the minimum time scale of the exciting laser pulse, as well as long-lived tail photoconductivity. The photoconductance data have been numerically deconvolved from the laser pulse so as to reveal the impulse response of the sample itself. Unfortunately, the deconvolution revealed that the impulse response of the sample has a bandwidth that considerably exceeds the maximum bandwidth of the laser pulse's intensity envelope, so that the minimum recombination lifetime cannot be determined with the laser diagnostics available. It can be determined that the impulse response has subnanosecond features; therefore, a picosecond laser facility is required to reveal the actual electron-hole pair lifetime.

The observation of tail photoconductivity with above-band-gap radiation is a repercussion of fast hole trapping. It doesn't matter if the supply of holes to be trapped is created by optical excitation from Cu_B (extrinsic absorption) or by optical excitation across the band gap (intrinsic absorption), the result will be the same. Indeed, augmenting Eqs. (V-1) and (V-4) with an $\alpha\Phi$ term, where α is the absorption coefficient at λ = 532 nm, simply modifies the denominator of Eq. (V-13) to form

$$\frac{n_T}{N_T} = \frac{\sigma_p}{\sigma_p + \left(1 + \frac{C_{pT} n_T}{C_R n_R}\right)\sigma_n + \frac{C_{pT}\,\alpha}{C_R n_R}} \quad . \qquad \text{(V-17)}$$

Since α is quite large,* the process of band-to-band absorption followed by trapping of optically-generated holes tends to dominate the electron depletion of Cu_B. Of

*From Ref. [18], $\alpha \approx 6 \times 10^4$ cm^{-1}.

course, the magnitude of the tail conductance was two orders of magnitude lower than that with the sub-band-gap radiation, because of the much smaller volume excited at the shorter wavelengths.

Decay of tail conductivity

The final topic to be covered in this section is the observed increase in the decay rate of the tail conductivity as the compensation ratio increases. There are two processes that can lead to the decay of tail conductivity. The first is the direct capture of an electron at a neutral Cu_B defect. The second is the thermal emission of a hole from a neutral Cu_B defect and its subsequent recombination with an electron at a recombination center. Because the electron capture parameter for Cu_B is so small, it is believed that the thermal emission process (at least at higher temperature) dominates the decay of the tail conductivity. The non-equilibrium thermal emission rate of holes from Cu_B depends on the hole capture cross section, the activation energy of the trap, and the temperature. In addition, the hole emission rate increases with the initial density of holes trapped at Cu_B [45]. Since this density is greater for increasing levels of compensation, it stands to reason that the repopulation of Cu_B (and, hence, the decay of the tail conductivity through recombination with the thermally emitted holes) should be faster with increasing compensation ratio.

Now that prior reasoning has established that the origin of the tail conductivity in Cu:Si:GaAs is associated with the depletion of electrons from compensated Cu_B centers by the turn-on laser pulse, thus leaving a large non-equilibrium density of electrons in the conduction band, the explanation for the

strong optical quenching observed experimentally with radiation of photon energy less than about 1 eV can be developed.

Optical quenching and switch turn off

The analytical model developed in the last section leads naturally to the optical quenching effect. Optical quenching is nothing more than the optical emission of the trapped holes at Cu_B so that they may recombine with the non-equilibrium electrons in the conduction band that are making up the tail conductivity. Therefore, the turn-off phase of the switch cycle can be modeled as a special case of the turn-on phase in which transitions from Cu_B to the conduction band are excluded *after* the Cu_B state has been depleted of electrons (i.e., during tail conduction). Excluding this transition is accomplished by making σ_n negligible, which is in turn accomplished by decreasing the photon energy of the incident radiation below the threshold given by the activation energy of Cu_B with respect to the conduction band. However, optical transitions from Cu_B to the valence band must still be allowed, thus the wavelength of the second laser pulse must not be too long. These constraints force the photon energy of the second laser pulse to a range given by $0.44\ \text{eV} < h\nu < 0.98\ \text{eV}$; or in wavelength, $2.8\ \mu\text{m} > \lambda > 1.3\ \mu\text{m}$.

The results of Chapter IV provide definitive proof of optical quenching in the range 1500 nm to 1800 nm. This effect also demonstrated a strong dependence on the compensation of the material. The numerical calculations cited in the previous section [31-33] are in qualitative agreement with this result.

Other parameters, however, are not in close quantitative agreement. For example, the break point* for the p-type sample in the experimental quenching factor versus photon flux curve found in Fig. IV-9 occurs at a photon flux of 3×10^{24} cm^{-2} s^{-1}, but the corresponding break point for a model of the p-type sample used in the numerical simulation is found to be 2×10^{25} cm^{-2} s^{-1} [33, p. 87], almost an order of magnitude higher. Part of the error can be blamed on the crude calibration used for the photon flux at the longer wavelengths (the spatial uniformity of the beam could not be guaranteed, thus altering the calibration based on average energy measurements). Nevertheless, both the nature of the recombination centers and the actual value of the partition significantly affect any quantitative predictions of the quenching process, hence, it is not possible to do better without improved knowledge of these influences.

Notwithstanding the above difficulties, the experimental observations can be shown to support, and certainly not contradict, the model developed in the last section. As an illustration consider the following thought experiment. Imagine a high-intensity, relatively short laser pulse whose wavelength falls in the range given above. The effect of this laser pulse is described in mathematical terms by rewriting the general model [given by Eqs. (V-1) through (V-4)] in the special form of the turn-off phase.

$$\frac{dn}{dt} = - C_R n(N_R - n_R) \qquad \text{(V-18)}$$

$$\frac{dn_T}{dt} = \Phi \sigma_p (N_T - n_T) - C_{pT} p n_T \qquad \text{(V-19)}$$

*The break point occurs when Q = 98%.

$$\frac{dn_R}{dt} = C_R n(N_R - n_R) - C_R p n_R \qquad \text{(V-20)}$$

$$\frac{dp}{dt} = \Phi \sigma_p (N_T - n_T) - C_R p n_R - C_{pT} p n_T \qquad \text{(V-21)}$$

Now, assume that the initial conditions of these equations are representative of the tail state, that is, $n \simeq \eta N_{Si}$, $n_T \simeq n_{To} - n$, $n_R \simeq N_R$, and $p \approx 0$. The high-intensity laser pulse suddenly throws the system out of its quasi-equilibrium. The valence band is rapidly flooded with holes. Even though some holes are inevitably retrapped back into Cu_B through the trapping term $C_{pT} p n_T$ in Eq. (V-19), others are trapped in the recombination center, causing the free electron lifetime to go from microseconds to subnanosecond upon application of the laser pulse.

If the laser pulse had a very high intensity or hole capture at Cu_B was weak, then virtually all of the holes stored at Cu_B after the turn-on laser pulse would be released into the valence band. In the case of closely compensated material, the electron occupation of Cu_B would be returned to its thermal equilibrium value (fully filled); barring hole retrapping, all of the tail conduction could eventually be extinguished. However, as more and more electrons recombine with holes, the electron-hole pair lifetime would gradually increase, thus slowing the conductivity quenching process. In short, the free hole density is not going to exceed the free electron density, thus keeping the free electron lifetime longer than the minimum given by $1/C_R N_R$ (i.e., $n_R << N_R$). If strong hole retrapping is included, as is the case in Cu:Si:GaAs, then p will always be less than n, regardless of how small n becomes (until Cu_B is fully repopulated, of course). Here, hole trapping is considered parasitic (in contrast to the turn-on phase), but fast recombination is essential. In fact, it

becomes inefficient to reduce the tail conductivity of closely compensated crystals more than an order of magnitude because the recombination rate for low values of n is substantially reduced while hole trapping approaches maximum efficiency (because n_T has approached within 10% of N_T).

The p-type, overcompensated crystals are another matter. In their case, the electron occupation of Cu_B can be increased substantially beyond the thermal equilibrium value (see, for example, Ref. [33], p. 90). This means that the free hole density can be maintained at concentrations near N_T, even though the free electron density may be orders of magnitude less. On the other hand, the hole trapping rate also increases compared to the closely compensated crystals, but it is offset by the reduction of the free electron lifetime to the minimum value, given by $1/C_R N_R$, when the recombination center fills with holes as n decreases below N_R. Hence, the corresponding quenching efficiency remains high enough that the overcompensated crystals can be driven back nearly to their dark conductivity* for the same turn-off laser pulse width and peak photon flux used to reduce the tail conductivity of an n-type crystal by only 50% [31].

The preceding discussion was meant to explain the observed and calculated variation of quenching efficiency with level of compensation. It is clear that the properties that make for good turn-on efficiency, such as high Cu_B thermal equilibrium occupation number and strong hole trapping, are not ideal for good turn off. However, these differences allow for the BOSS to be optimized for a given application by relatively simple changes in the processing parameters [32].

---

*Limited only by thermal emission from electron traps, such as EL2.

A process that was not included in the analytical model is two-photon absorption. This non-linear effect occurs at high intensity for laser radiation of photon energy equal to at least half the band gap of the material. Two-photon absorption is not distinguishable from single photon absorption during the turn-on phase, but it can result in an initial *increase* in the photoconductivity during the turn-off laser pulse. Therefore, the process is modeled by adding a $\beta h\nu\Phi^2$ term to Eqs. (V-18) and (V-21), where β = 30 cm/GW [46] when $h\nu \geq 0.71$ eV at T = 300 K. Calculations reveal that this term will generate conductivities comparable to that observed on the conductivity tail of the p-type material only when the photon flux approaches 10^{25} cm^{-2} s^{-1}. A two-photon process will not occur for photon energies less than half the band gap. The fact that the photocurrent spike coincident with the second laser pulse in Figs. IV-6 and IV-7 became negligible when the wavelength was increased to a value above 1750 nm or the intensity was decreased to a value below 10^{25} cm^{-2} s^{-1} leads to the conclusion that the spike is the result of two-photon absorption.

Effect of high electric field

Figure IV-11 demonstrates the change in the *I-V* characteristics of the p-type sample as the electric field increases above a threshold of about 12 kV/cm. The change in the sample's I-V characteristic is represented by a break in the circuit response from a line localized at the origin (the closed and open circles) to a line with a non-zero intercept (the triangles). The line with zero intercept can be modeled as

$$I_{ss} = \frac{V_p}{R_L + Z_o + 1/G_{ss}} \qquad \text{(V-22)}$$

where I_{ss} is the steady state tail current,* V_p is the peak PFL charging voltage, $R_L + Z_o = 87\ \Omega$, and G_{ss} is the saturation tail conductance of sample 14-8-6(b). Thus, the sample is modeled as a photoconductor with a slowly decaying conductivity. The slope of a least squares fit to the tail current data allows $1/G_{ss}$ to be calculated, which is found to be 33 Ω. From G_{ss} the saturation tail conductivity, σ_{ss}, is calculated to be 0.84 $(\Omega\ \text{cm})^{-1}$.

When the data in Fig. IV-11 breaks to the new curve at the higher initial fields, Eq. (V-22) is no longer adequate to model the system response. Instead, a "battery" must be included in the circuit to account for the non-zero intercept. The new model is written

$$I_{ss} = (V_p - V_{lo})/Z \qquad \text{(V-23)}$$

where V_{lo} is the "battery" or lock-on voltage and Z is the remaining circuit impedance. A least-square estimate of the slope of this line gives a value of Z close to the total external circuit impedance, which leaves none left for the sample. The sample obviously is maintaining V_{lo} across itself, but is contributing little further impedance to the circuit. V_{lo} is found from the least-square estimate to be 1.2 kV, which represents an average field of 4.7 kV.

---

*Measured just before the collapse of the PFL voltage at t = 160 ns.

Equations (V-22) and (V-23) model the experimental results shown in Fig. IV-11. This model can be used to estimate the on state J vs. E characteristics of the sample itself. Figure V-2 illustrates this estimate. The solid line with zero intercept represents the saturation tail conductivity of sample 14-8-6(b), which is about 0.86 $(\Omega\ cm)^{-1}$. The nearly vertical dashed line represents lock on, although the actual slope of the line cannot be resolved from the data in Fig. IV-11.

The explanation for lock on is elusive, and not considered the scope of this thesis. However, experimental work has been performed by other researchers [19], [21], [23-25]. Since lock on has only been observed in direct band gap semiconductors with satellite conduction band valleys (such as GaAs and InP) but never in silicon, the formation of stable space charge domains (Gunn domains) resulting from the transferred electron effect are suspected to play a role [24]. Another idea has charge injection from the ohmic contacts causing dark currents much higher than would be expected from the *low-field* dark conductivity [44, pp. 101-2]. The issue is not resolved, and the interested reader is referred to the references cited for more information on the many other interesting properties of lock on, such as low light level triggering, good voltage regulation, material dependences, and fast recovery characteristics.

Efficiency

Because the samples used in this experiment were not meant or designed to be high-power switching devices, but simply to be instruments of research on the Cu:Si:GaAs material, switching efficiency was not a concern. However, estimates of the actual laser energy required to activate and deactivate the electrical conductivity of the p-type sample will be made.

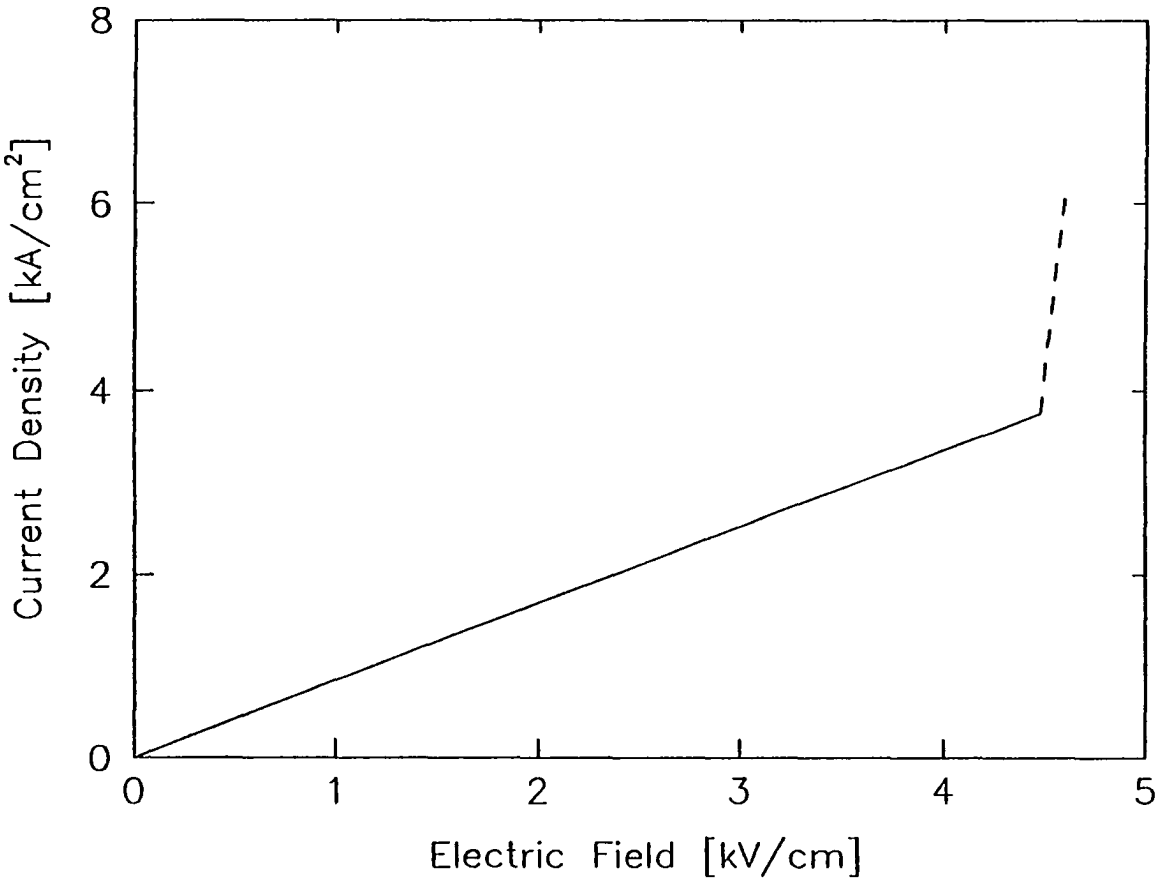

Figure V-2 On state J vs. E characteristics for sample 14-8-6(b) estimated from the circuit response shown in Fig. IV-11.

Sample 14-8-6(b) required approximately 1 mJ of 1064 nm laser energy to induce a tail conductivity of at least 0.5 $(\Omega\ cm)^{-1}$; however, because of the long absorption length for light at wavelengths exceeding the band-gap cutoff, only a fraction of the incident radiation was absorbed. Measurements of absorption in overcompensated, p-type Cu:Si:GaAs indicate a low-intensity (linear) absorption length of about 2.5 mm [47]. For the thickness of sample 14-8-6(b) (0.23 mm) this means a maximum absorption of 10%. This estimate implies, then, that about 100 μJ were required to induce conductivity in a volume of 2.3 mm^3.

At the break point on Fig. IV-9 ($\Phi = 3 \times 10^{24}\ cm^{-2}\ s^{-1}$), $\approx$ 0.3 mJ of laser energy at 1620 nm was expended to quench the photoconductivity to a final value of about 0.01 $(\Omega\ cm)^{-1}$. The absorption at this wavelength is expected to be similar to the absorption at 1064 nm or, perhaps, a bit stronger. Therefore, the energy required to turn off the switch is within the same order of magnitude as the energy required to turn it on.

Summary

This chapter has dealt primarily with the explanation for the observed photoconductive properties of the three samples investigated [14-8-9(e), 14-8-9(f), and 14-8-6(b)]. It has been shown with the aid of a simple analytical model, and a more complete numerical simulation from another source [31-33], that the generation of tail conductivity in Cu:Si:GaAs is dependent on strong hole trapping at Cu_B, but recombination is a parasitic effect reducing the turn-on efficiency. On the other hand, good turn-off efficiency depends on strong recombination, but hole trapping is undesirable. The tradeoff between these two processes can explain the observed variation in tail conductivity and quenching factor with compensation ratio.

Unfortunately, for all three samples the observed magnitudes of the tail conductivities were uniformly below predictions, indicating that either the partition was underestimated, the recombination lifetime was overestimated, or both.

CHAPTER VI

CONCLUSIONS

The purpose of this report has been to demonstrate some of the properties of copper compensated, silicon doped, gallium arsenide (Cu:Si:GaAs). The motivation for working with this material comes from the bulk optically controlled semiconductor switch (BOSS) concept. The BOSS concept is a proposal for utilizing the desirable properties of bulk GaAs switches, such as high dark resistivity and short electron-hole pair lifetime, while still achieving long conduction times without sustaining the conductivity with costly laser radiation. The option to terminate the photoconductivity is excercised by utilizing fast infrared quenching. A BOSS is manufactured by carefully compensating n-type, silicon doped GaAs with copper. The deliberate introduction of deep acceptors associated with copper into the band gap of GaAs allows the photoconductivity of the material to be tailored to high-power, closing and opening switch applications.

The first step in demonstrating the BOSS concept was to successfully compensate n-type GaAs with copper. By compensate it is meant that a bulk GaAs crystal grown with a substantial shallow donor density, such as silicon, has a comparable density of acceptor defects introduced into the crystal (uniformly) so that the free electrons that would otherwise be thermally ionized from the donor defects

and free to conduct, would instead be trapped at the acceptor sites and become immobile.

In this investigation it was shown that the quantity of copper acceptors introduced into the crystal by diffusion could be controlled by adjusting the temperature at which the samples were annealed. The annealing temperature is presumed to limit the total copper density that can be dissolved in the solid crystal, a limit known as the solid solubility. For a base material grown with a Si donor density of 5×10^{16} cm^{-3}, the temperature range in which significant dark resistivities were obtained was 549 °C to 575 °C. A total of five samples were found to be compensated to one degree or another. The highest dark resistivity was found to be 7×10^{5} Ω cm, but the dark resistivity as a function of annealing temperature was distributed in such a way as to confirm, in principle, the change of the material's conductivity by compensation from n-type, through semi-insulating, and finally p-type. However, it is not clear at this time how much of the total Cu density goes into the desirable Cu_B acceptor (E_a - E_v = 0.44 eV), and how much goes into the undesirable Cu_A acceptor (E_a - E_v = 0.14 eV). The distribution of the densities of the two defects is known as the partition, defined as $\mathbf{p} \equiv N_{CuA}/N_{CuB}$.

The photoconductive properties of Cu:Si:GaAs can be separated into two categories in a switching sense. The first category involves the activation or "turn-on" of the photoconductivity of the sample. Turn on is achieved by illuminating the sample with laser radiation of photon energy greater than 1 eV. This has been shown to deplete the Cu_B level of electrons trapped there by compensation, which, by and large, end up in the conduction band to produce photoconductivity. This photoconductivity is long lived (decay time constant ≥ 1 μs) compared to the

nanosecond laser pulse used as optical excitation. The second category involves the deactivation or "turn-off" of the photoconductivity. Turn off is realized by illuminating the sample with laser radiation of photon energy less than 1 eV, but greater than 0.4 eV. This radiation cannot deplete Cu_B of electrons, but it can ionize trapped holes at Cu_B into the valence band, which then recombine with free electrons at recombination centers to extinguish the photoconductivity.

The photoconductive properties of the Cu:Si:GaAs material have been shown to be strongly dependent on the compensation ratio, defined as the ratio of copper density to silicon density N_{Cu}/N_{Si}. In general, it was shown that overcompensated crystals ($N_{Cu}/N_{Si} > 1$) had lower on-state, or tail, conductivities but were more easily turned off than undercompensated or semi-insulating crystals ($N_{Cu}/N_{Si} \leq 1$). This result is a consequence of the different equilibrium electron occupation densities and the different Cu_B total trap densities from one sample to another.

The measured saturation tail conductivity of 0.8 $(\Omega\ cm)^{-1}$ for the p-type sample did not agree well with the calculations, both numerical and analytical, which predicted an order of magnitude higher tail conductivity. Two possible reasons have been given for this discrepancy, the first being that the partition was underestimated in the calculations, thus overestimating the number of electrons available at Cu_B defects. The other possiblility is that the recombination process for electrons and holes may be underestimated, thus predicting a greater electron depletion of Cu_B than is the case.

Experiments were conducted at electric field strengths in the p-type sample of up to 19 kV/cm. Peak current densities of 10 kA/cm^2 were conducted. At fields higher than about 12 kV/cm the slowly decaying tail conductivity predicted by the

calculations was no longer observed. Instead, a new conduction state known as "lock on" was observed, in which the sample voltage remained constant at 1.2 kV (4.7 kV/cm) instead of slowly increasing as the tail conductivity decayed. The lock on state is not understood at this time, but represents a serious scaling problem for the BOSS concept if III-V semiconductors are to be used.

As an example, consider the p-type sample in the 87 Ω circuit. Here, lock on represents a more efficient operating mode than tail conduction because of the relatively high on-state saturation resistance. However, if the circuit load line were increased or the saturation tail resistance were reduced to the levels predicted by the numerical simulation (a factor of 20 reduction) the two lines in Fig. IV-11 would not intersect, as they do now, but would be parallel. In this case lock on would represent a tremendous power dissipation in the switch, and an artificial limit to the current the external circuit could otherwise provide.

The future of the BOSS concept is predicated on solutions to several problems. Perhaps the most important shortcoming identified so far is the low tail conductivity. There would, in all likelihood, already be short term applications for this BOSS device if sub-ohm on resistance could be demonstrated with a package of similar dimensions to the samples used in this investigation. This is because the optical energy required to activate the conductivity (~ 100 μJ) is within the range that could be supplied by an optical source of comparable size to the switch: the semiconductor laser. A semiconductor laser would be the ideal choice to drive a BOSS in high-repetition-rate (hundreds of kilohertz), moderate peak power (tens of megawatts) applications which are now poorly served by both thyratrons and thyristors. However, the tail conductivity must be improved to at least the calculated

levels. This will happen only with further research into materials and processing technology, mainly to control the copper partition and to control the density of recombination centers.

To utilize the turn-off properties of the BOSS, which are highly desirable for command charging and inductive energy storage, a BOSS must have the ability to withstand high electric fields. This is mainly a device consideration, that is, finding device structures that will limit charge injection in the off state, while allowing electron injection during tail conduction so as to preserve the long conduction times. A device based on a n^+-*i*-n^+ structure capable of conducting bipolar currents is described in Appendix B. This device potentially should be able to control charge injection until such time as the intrinsic region is converted to n-type photoconductivity, after which the switch will have all of the properties of a BOSS photoconductor, including command turn off.

There are other ways in which the BOSS concept may be scaled to the needs of pulsed power applications. Several individual switches may be cascaded far easier than comparable devices. Since each switch may be truly optically isolated with fiber optic cables emanating from a single modest Nd:YAG laser, then switches with moderate voltage and current ratings (say 50 kV and 1 kA) could be placed in series and parallel without the usual isolation and trigger jitter problems associated with FET's and SCR's. Even these conservative ratings would allow a reduction in the number of devices stacked.

Longer term research will be required to take advantage of candidate materials other than Cu:Si:GaAs. For example, the BOSS concept has already been demonstrated in CdS using 532 nm radiation for turn on and 1064 nm radiation for

turn off [26-27]. The use of wider band gap materials, such as CdS, allows the wavelength of the laser radiation to be shifted into the visible. Instead of changing the host material, a different acceptor impurity could be used in place of copper in GaAs. Many of the transition metals, such as Fe, Ni, and Au, have properties similar to Cu. Perhaps these metals might have better partition properties between their shallow and deep acceptor levels.

That brings this work to a close. It has been gratifying and exciting to work on the BOSS concept, and to see all of the photoconductive properties of the Cu:Si:GaAs material at least qualitatively confirmed and understood. With luck, and hard work, the enthusiasm I have felt and seen at Old Dominion for the optically controlled switch project will grow and transfer to other researchers in other places. The potential payoff in improved medium-power high-repetition-rate switches for everything from linear accelerators to 60 Hz power transmission is worth every bit of the effort.

LIST OF REFERENCES

[1] E. M. Honig, "Inductive energy storage circuits and switches," in *Opening Switches*, A. Guenther, M. Kristiansen, and T. Martin, Eds. New York: Plenum, 1987, pp. 1-48.

[2] C. H. Lee, "Introduction: A historical overview," in *Picosecond Optoelectronic Devices*, C. H. Lee, Ed. Orlando, Florida: Academic, 1984, pp. 1-9.

[3] W. C. Nunnally, "Photoconductive switching," in *Proc. of the Workshop on Optically and Electron-beam Controlled Semiconductor Switches*, K. H. Schoenbach and M. Weiner, Eds. Norfolk, Virginia: Old Dominion University, 1988.

[4] H. Mehta, "Power electronics," *Electric Power Research Inst. J.*, vol. 13, no. 8, pp. 44-47, 1988.

[5] J. Douglas, "The future of transmission: switching to silicon," *Electric Power Research Inst. J.*, vol. 14, no. 4, pp.4-13, 1989.

[6] J. A. Oicles and J. R. Grant, "High performance modulators using MOSFETS," in *Proc. Eighteenth Power Modulator Symp.*, S. Levy and A. S. Gilmour Jr., Eds. New York: IEEE, 1988, pp. 34-38.

[7] C. H. Lee, "Picosecond optoelectronic devices based on optically injected electron-hole plasma," in *Picosecond Optoelectronic Devices*, C. H. Lee, Ed. Orlando, Florida: Academic, 1984, pp. 119-188.

[8] K. H. Schoenbach, M. Kristiansen, and G. Schaefer, "A review of opening switch technology for inductive energy storage," *Proc. IEEE*, vol. 72, pp. 1019-1040, 1984.

[9] W. C. Nunnally and R. B. Hammond, "Optoelectronic switch for pulsed power," in *Picosecond Optoelectronic Devices*, C. H. Lee, Ed. Orlando, Florida: Academic, 1984, pp. 373-398.

[10] K. H. Schoenbach, V. K. Lakdawala, R. Germer, and S. T. Ko, "An optically controlled closing and opening semiconductor switch," *J. Appl. Phys*, vol. 63, pp. 2460-2463, 1988.

[11] S. M. Sze, *Semiconductor Devices: Physics and Technology*. New York: Wiley, 1985, p. 23.

[12] N. Kullendorff, L. Jansson, and L-A. Ledebo, "Copper-related deep level defects in III-V semiconductors," *J. Appl. Phys.*, vol. 54, pp. 3203-3212, 1983.

[13] J. Blanc, R. H. Bube, and H. E. MacDonald, "Properties of high-resistivity gallium arsenide compensated with diffused copper," *J. Appl. Phys.*, vol. 32, pp. 1666-1679, 1961.

[14] D. H. Auston, "Picosecond optoelectronic switching and gating in silicon," *Appl. Phys. Lett.*, vol. 26, pp. 101-103, 1975.

[15] G. Mourou, W. H. Knox, and S. Williamson, "High-power picosecond switching in bulk semiconductors," in *Picosecond Optoelectronic Devices*, C. H. Lee, Ed. Orlando, Florida: Academic, 1984, pp. 219-248.

[16] C. H. Lee, "Picosecond optoelectronic switching in GaAs," *Appl. Phys. Lett.*, vol. 30, pp. 84-86, 1977.

[17] J. Agostinelli, G. Mourou, and C. W. Gabel, "Active pulse shaping in the picosecond domain," *Appl. Phys. Lett.*, vol. 35, pp. 731-733, 1979.

[18] W. C. Nunnally, "Photoconductive power switches: A review," in *Proc. Fifth IEEE Pulsed Power Conf.*, M. F. Rose and P. J. Turchi, Eds. New York: IEEE, 1985, pp. 235-241.

[19] F. J. Zutavern, G. M. Loubriel, and M. W. O'Malley, "Recent developments in opening photoconductive semiconductor switches," in *Proc. Sixth IEEE Pulsed Power Conf.*, P. J. Turchi and B. H. Bernstein, Eds. New York: IEEE, 1987, pp. 577-580.

[20] R. L. Druce, K. L. Griffin, W. W. Hofer, and M. D. Pocha, "Photoconductive switching at LLNL," in *Proc. of the Workshop on Optically and Electron-beam Controlled Semiconductor Switches*, K. H. Schoenbach and M. Weiner, Eds. Norfolk, Virginia: Old Dominion University, 1988.

[21] G. M. Loubriel, M. W. O'Malley, and F. J. Zutavern, "Toward pulsed power uses for photoconductive semiconductor switches: Closing switches," in *Proc. Sixth IEEE Pulsed Power Conf.*, P. J. Turchi and B. H. Bernstein, Eds. New York: IEEE, 1987, pp. 145-148.

[22] F. J. Leonberger and P. R. Moulton, "High-speed InP optoelectronic switch," *Appl. Phys. Lett.*, vol. 35, pp. 712-714, 1979.

[23] G. M. Loubriel, M. W. O'Malley, F. J. Zutavern, B. B. McKenzie, W. R. Conley, and H. P. Hjalmarson, "High current photoconductive semiconductor switches," in *Proc. Eighteenth Power Modulator Symp.*, S. Levy and A. S. Gilmour Jr., Eds. New York: IEEE, 1988, pp. 312-317.

[24] F. J. Zutavern, G. M. Loubriel, B. B. McKenzie, M. W. O'Malley, R. A. Hamil, L. P. Schanwald, and H. P. Hjalmarson, "Photoconductive semiconductor switch (PCSS) recovery," presented at the Seventh IEEE Pulsed Power Conf. (Monterey, California), June 11-14, 1989.

[25] G. M. Loubriel, F. J. Zutavern, H. P. Hjalmarson, and M. W. O'Malley, "Closing photoconductive semiconductor switches," presented at the Seventh IEEE Pulsed Power Conf. (Monterey, California), June 11-14, 1989.

[26] R. K. F. Germer, K. H. Schoenbach, and S. G. E. Pronko, "A bulk optically controlled semiconductor switch," *J. Appl. Phys.*, vol. 64, pp. 913-917.

[27] R. K. F. Germer and K. H. Schoenbach, "Stimulated switch-off and repetitive switching of a bistable optically controlled semiconductor switch," *J. Phys. D: Appl. Phys.*, vol. 22, pp. 398-403, 1989.

[28] M. S. Mazzola, K. H. Schoenbach, V. K. Lakdawala, R. Germer, G. M. Loubriel, and F. J. Zutavern, "GaAs photoconductive closing switches with high dark resistance and microsecond conductivity decay," *Appl. Phys. Lett.*, vol. 54, pp. 742-744, 1989.

[29] M. S. Mazzola, K. H. Schoenbach, V. K. Lakdawala, and S. T. Ko, "Nanosecond optical quenching of photoconductivity in a bulk GaAs switch," *Appl. Phys. Lett.*, vol. 55, pp. 2102-2104, 1989.

[30] M. S. Mazzola, K. H. Schoenbach, V. K. Lakdawala, and S. T. Ko, "Investigation of a photoconductive closing and opening bulk GaAs semiconductor switch," presented at the Seventh IEEE Pulsed Power Conf. (Monterey, California), June 11-14, 1989.

[31] S. T. Ko, V. K. Lakdawala, K. H. Schoenbach, and M. S. Mazzola, "Influence of copper doping on the performance of optically controlled GaAs switches," *J. Appl. Phys.*, to appear Jan. 15, 1990.

[32] S. T. Ko, V. K. Lakdawala, K. H. Schoenbach, and M. S. Mazzola, "Optimization studies of materials for optically controlled semiconductor switches," presented at the Seventh IEEE Pulsed Power Conf. (Monterey, California), June 11-14, 1989.

[33] S. T. Ko, *Study of direct semiconductor materials for an optically controlled switch*, Ph.D. Dissertation, Dept. of Electrical & Computer Eng., Old Dominion Univ., Norfolk, Virginia, 1989.

[34] Grown by Morgan Semiconductor Div., Ethyl Corp., Garland, Texas 75047-2376.

[35] R. N. Hall and J. H. Racette, "Diffusion and solubility of copper in extrinsic and intrinsic germanium, silicon, and gallium arsenide," *J. Appl. Phys.*, vol. 35, pp. 379-397, 1964.

[36] N. A. Ives and M. S. Leung, "Noncontact laminar-flow polishing for GaAs," *Rev. Sci. Instrum.*, vol. 59, pp. 172-175, 1988.

[37] J. Romero, private communication.

[38] D. V. Lang and R. A. Logan, "A study of deep levels in GaAs by capacitance spectroscopy," *J. Electronic Materials*, vol. 4, pp. 1053-1066, 1975.

[39] G. M. Martin, J. P. Farges, G. Jacob, J. P. Hallais, and G. Poiblaud, "Compensation mechanisms in GaAs," *J. Appl. Phys.*, vol. 51, pp. 2840-2852, 1980.

[40] R. Zucca, "Electrical compensation in semi-insulating GaAs," *J. Appl. Phys.*, vol. 48, pp. 1987-1994, 1977.

[41] P. F. Lindquist, "A model relating electrical properties and impurity concentrations in semi-insulating GaAs," *J. Appl. Phys.*, vol. 48, pp. 1262-1267, 1977.

[42] D. H. Auston, "Picosecond photoconductors: Physical properties and applications," in *Picosecond Optoelectronic Devices*, C. H. Lee, Ed. Orlando, Florida: Academic, 1984, pp. 73-117.

[43] R. H. Bube, *Photoconductivity of Solids*. New York: Wiley, 1960, pp. 348-354.

[44] D. F. Stoudt, *The electrical characteristics of semi-insulating gallium arsenide: A material for high power switches*, Master's Thesis, Dept. of Electrical & Computer Eng., Old Dominion Univ., Norfolk, Virginia, 1989.

[45] J. C. Balland, J. P. Zielinger, M. Tapiero, J. G. Gross, and C. Noguet, "Investigation of deep levels in high-resistivity bulk materials by photo-induced current transient spectroscopy: II. Evaluation of various signal processing methods," *J. Phys. D: Appl. Phys.*, vol. 19, pp. 71-87, 1986.

[46] A. F. Stewart and M. Bass, "Intensity-dependent absorption in semiconductors," *Appl. Phys. Lett.*, vol. 37, pp. 1040-1043, 1980.

[47] R. A. Roush, private communication.

[48] C. C. Tin, C. K. Teh, and F. L. Weichman, "Photoinduced transient spectroscopy and photoluminescence studies of copper contaminated liquid-encapsulated Czochralski-grown semi-insulating GaAs," *J. Appl. Phys.*, vol. 62, pp. 2329-2336, 1987.

[49] S. S. Chiao, B. L. Mattes, and R. H. Bube, "Photoelectronic properties of LPE GaAs:Cu," *J. Appl. Phys.*, vol. 49, pp. 261-268, 1978.

[50] C. S. Fuller and J. M. Whelan, "Diffusion, solubility, and electrical behavior of copper in gallium arsenide," *J. Phys. Chem. Solids*, vol. 6, pp. 173-177, 1958.

[51] Z. G. Wang, H. P. Gislason, and B. Monemar, "Acceptor associates and bound excitons in GaAs," *J. Appl. Phys.*, vol. 58, pp. 230-239, 1985.

[52] B. G. Streetman, *Solid State Electronic Devices*. Englewood Cliffs, New Jersey: Prentice-Hall, 1980.

APPENDIX A

THE ORIGINS OF COMPENSATION BY COPPER IN GaAs

In order to fabricate a highly resistive semiconductor material, something must be done to compensate for the relatively large densities of impurities and native defects that exist in real semiconductors. For example, single crystal GaAs grown using the horizontal Bridgman technique is likely to contain silicon, arising from the crucible in which the crystal is grown [39], in concentrations greater than 10^{15} cm^{-3} [40]. Since silicon is a shallow donor, most of these donor states are ionized at room temperature. Contrast this donor density with the free electron density of typical n-type semi-insulating GaAs: less than 10^{9} cm^{-3}. Since real material contains other donors and acceptors, both shallow and deep, the Si density may or may not be partially compensated by acceptors. However it is clear that unwanted residual impurities must either be closely compensated by oppositely charged shallow states to a degree of at least 1 part in 10^{6}, or the uncompensated states must be deep enough to preclude significant thermal ionization.

Through careful control of the growth parameters, such as the ambient environment exposed to the crystal, the composition of the crucible, and the deliberate addition of impurities, the compensation of the crystal can be achieved during growth. This is how so called EL2 compensated (also known as "as grown") and chromium doped semi-insulating GaAs are manufactured [39]. However,

low-resistivity GaAs crystals, doped during growth with a shallow impurity, can also be made semi-insulating by subsequent introduction of suitable deep levels. For the case of GaAs grown with silicon, it is well known that this can be achieved by diffusing copper into the crystal [13]. To understand how copper diffusion results in semi-insulating GaAs, the properties of copper in GaAs must be examined.

The introduction of copper into GaAs can result in the creation of several energy states (or levels) in the band gap of the host. For example, copper diffusion can result in numerous acceptor levels including 0.14, 0.24, and 0.44 eV above the valence band [11]; also 0.5 eV [48] and 0.6 eV [49] above the valence band. In addition, a shallow donor has also been reported [35]. The acceptors are widely recognized to be the result of a copper substitutional on a vacant gallium site (denoted as Cu_{Ga}) perhaps in combination with other defects which form a so called complex. However, the exact nature of each different level is not clearly known. The donor level is associated with a copper interstitial (that is, a copper atom that takes a lattice position in between other host atoms, rather than occupying a proper lattice site, which is called a substitutional). The copper interstitial is widely believed to account for the rapid diffusion of copper in GaAs, but generally exists in a much smaller concentration than the copper substitutionals in GaAs [35].

The actual partition of the total copper content in the crystal into the different acceptor level concentrations is important for the BOSS concept for two reasons. First, the final resistivity of the material after copper diffusion will depend in part on the activation energies of the copper levels which compensate the shallow donors. Excessive formation of the Cu_A level at 0.14 eV, for example, would place greater restrictions on the compensation process, when compared to compensation

with the Cu_B level at 0.44 eV, because any over compensation with Cu_A would lead to a much larger concentration of thermally ionized free holes. Secondly, the photoconductive properties of the BOSS rely on the properties of Cu_B. If compensation is achieved predominately by other levels, degraded switching performance could result from the parasitic effects of these other levels. Therefore, it is important to consider briefly the origin of the various copper acceptor centers in GaAs, their typical partition in actual materials, and the means, if any, for enhancing Cu_B formation over its competitors.

The labels Cu_A and Cu_B, representing the copper acceptors at 0.14 eV and 0.44 eV above the valence band in GaAs, where coined by Kullendorff, Jansson, and Ledebo [12], who termed them the "dominant" copper levels in GaAs. Earlier investigators [35] [50] explained these two centers by invoking the expectation that copper could be singly or doubly ionized while substituting for a gallium atom in the host lattice. This explanation would require Cu_A and Cu_B to occur in equal concentrations; however it has been determined [12] that Cu_A and Cu_B exist in different concentrations, and are now considered independent.

If Cu_A and Cu_B arise from different physical mechanisms, what are their origins? It is widely accepted that copper can form complexes [48] with native defects and other impurities. These complexes (defined as copper substitutions on gallium vacancies which are surrounded by a variety of crystal defects as nearest neighbors) are in principle infinite in variety, but in practice only a few would be probable enough to exist in substantial concentration. There are many suggestions for identifying Cu_A and Cu_B, including Cu_{Ga} and $Cu_{Ga}V_{As}$ or $V_{As}Cu_{Ga}V_{As}$ and $Cu_{Ga}V_{As}$

[12] [51], where V_{As} is a vacancy on the arsenic sub-lattice. However, no definitive conclusions have been made.

The implication that Cu_A and Cu_B are related to copper complexes immediately suggests a way for controlling their relative densities. For example, consider the first possible identification in which Cu_A is the result of a copper atom occupying a simple gallium vacancy while Cu_B would be associated with a copper substitutional on the gallium sub-lattice and a single vacancy in the nearest arsenic sub-lattice. Clearly, processing the crystal in an arsenic poor environment that otherwise left the gallium vacancy concentration substantially unchanged could lead to an enhancement of Cu_B centers at the expense of Cu_A.

In fact, the actual partition of Cu_A and Cu_B is unknown, and would be expected to vary substantially with processing technique. Ko [33] used a partition of 20% Cu_A, 80% Cu_B in his rate equation model of the BOSS concept. However, in light of the nature of the complexes suggested for these defect states, it would seem advisable to assume, in general, that Cu_A would have the dominant concentration, since it is more likely to find V_{Ga} and V_{As} independent of each other (possibly necessary for Cu_A formation) than it is to find $V_{Ga}V_{As}$ complexes (possibly necessary for Cu_B formation). Indeed, Kullendorff [12] reported higher Cu_A concentrations than Cu_B concentrations in bulk InP grown using the liquid encapsulated Czochralski (LEC) technique (expected to be similar to bulk GaAs [12]). On the other hand, Lang and Logan [38] reported just the opposite case for their samples, which were grown using liquid phase epitaxy (LPE). Clearly, this important point should be studied further.

APPENDIX B

A HIGH-VOLTAGE OPTICALLY-CONTROLLED SWITCH

One of the difficulties of using a bulk photoconductor as a high-voltage switch is the "problem" of charge injection at the contacts. Charge injection is very important during conduction, because the bulk conductivity of the crystal can only be sensed by the external circuit if carrier sweepout is avoided. During the off state,* however, charge can be injected in excess of that necessary to maintain charge neutrality in the presence of dark current if the electric field at the contacts is high enough. This space charge is self limiting, that is, injected space charge tends to reduce the local field, and thus bring the charge injection rate (the current!) to equilibrium with the applied voltage. The process is described, of course, by Poisson's equation

$$\frac{\partial E}{\partial x} = \rho(x)/\varepsilon \quad . \qquad \text{(B-1)}$$

For the case of single charge injection, defined as the injection of predominately only one charge type (either electrons or holes), the so called

*The off state is the time *before* the first laser pulse in the BOSS concept. The off state should not be confused with the so called "dark" state, because conduction can occur long after the laser pulse is gone.

Lampert theory prevails [43, pp. 120-26], in which charge trapping of the injected carriers prolong the period of ohmic conduction predicted by the low-field dark conductivity of the material. Eventually, however, the traps fill and the dark current can dramatically increase (by orders of magnitude) for relatively little increase in voltage. If, as is thought to occur at fields in the 10^4 V/cm range, double injection becomes important (i.e., the injection of electrons at one contact *and* holes at the other) then the self-limiting condition is partially nullified and the measured dark current can increase so dramatically that thermal dissipation in the photoconductor will lead to breakdown and failure of the switch.

Unfortunately, operating at fields of the order 10^4 V/cm is precisely where the BOSS can make its best contributions at this time. Thus, a device based on a simple bulk photoconductor with ohmic contacts would be limited to pulse charged applications where the onset delay time of the dark injection current [44, pp. 54-57] would protect the device from breakdown. An alternative device structure is now proposed that retains the compact nature of the BOSS, is optically controllable, can be dc charged to levels that would otherwise be limited by double injection, and relies on the fabrication technology already developed for the bulk photoconductors used in this investigation.

Consider the device illustrated in Fig. B-1 (a). The device consists of an idealized n^+-p-n^+ structure with ohmic contacts on either end, where n^+ signifies a "large" donor concentration, while p signifies only weakly p-type material. Even though there are two junctions, only one is reverse biased. This junction is placed at the origin of the x-axis. A bias voltage, V, is assumed and the resulting depletion region extends a width, W, into the n^+ and p regions as indicated. The electric field

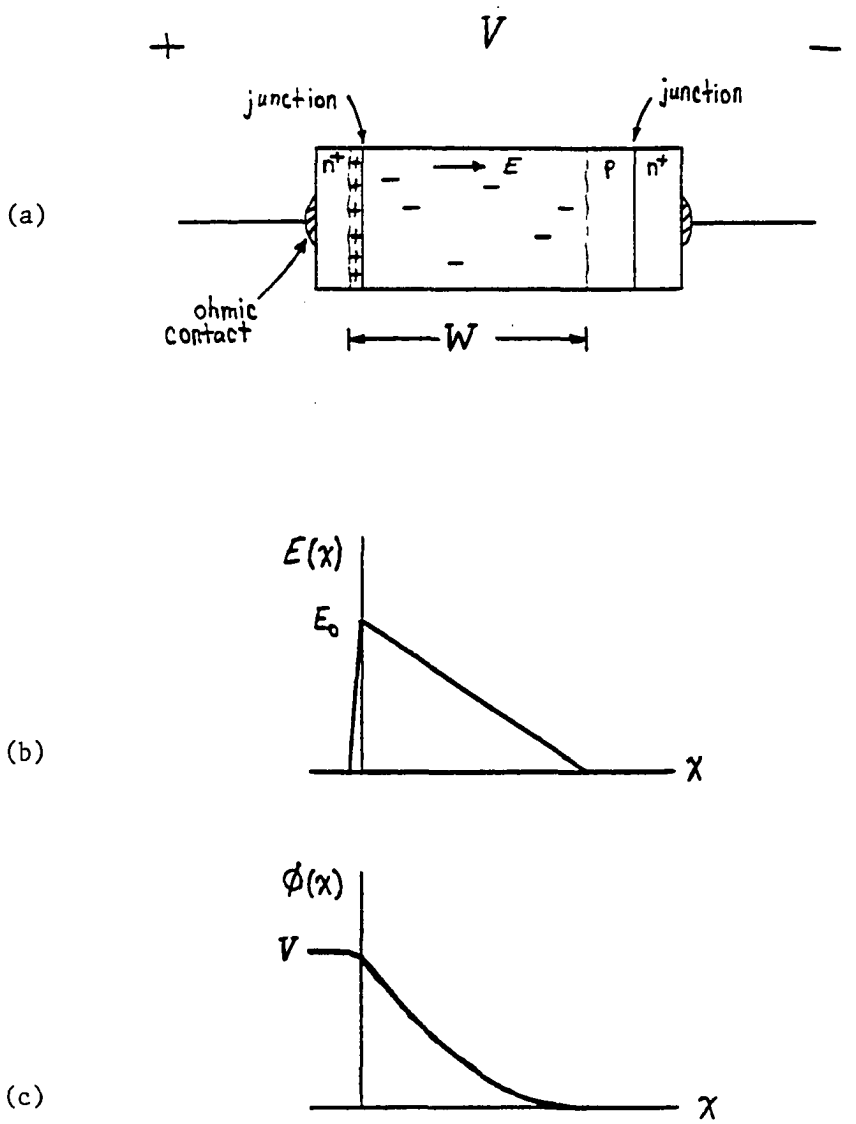

Figure B-1 An illustration of the device concept in which the idealized device geometry is shown in (a), the variation of the magnitude of the electric field in the device is shown in (b), and the distribution of the potential across the device is shown in (c).

is distributed in the device as is shown in Fig. B-1 (b), a distribution similiar to that in an n-p-n transistor. The magnitude of the field follows a rough triangle* whose apex is at the junction. Note from the potential distribution, shown in Fig. B-1 (c), that the vast majority of the bias voltage falls across the depletion region in the weakly p-type material. More importantly, the field at the ohmic contacts is virtually zero. In fact, the field at the contacts need only be large enough to support the very small thermal current (known as the leakage current) generated in the neutral regions on either side of the depletion region.

The theory of p-n junctions is well known, and can be reviewed in many texts [11], [52]. Suffice to say here that the peak electric field in the depletion region, which occurs at the junction, can be calculated from Poisson's equation to be

$$E_o = \frac{q}{\varepsilon} \Delta N_A^- \, W \quad . \qquad \text{(B-2)}$$

ΔN_A^- is the space charge density of that part of the depletion region extending into the p-type material (W_p). For the case of a weakly p-type material in contact with a strongly n-type material, it can be assumed that $W_p \approx W$. The expression for W is found in [52, p. 174] to be

$$W = \left[\frac{2 \varepsilon V}{q} \left(\frac{\Delta N_A^- - N_d^+}{\Delta N_A^- \, N_d^+} \right) \right]^{1/2} \quad . \qquad \text{(B-3)}$$

In order to use this expression, ΔN_A^- and N_d^+ must be defined. N_d^+ is the concentration of ionized donors (here the superscript '+' stands for positive charge state) in the

*Actually, this is only an estimate known as the *depletion approximation.*

n^+ region. Because the n^+ region is heavily doped with shallow donors, then $N_d^+ \simeq N_d$ where N_d is the density of shallow donors. The weakly p-type region is made high resistivity by overcompensation in a host material that was originally doped with N_d shallow donors. Thus the density of ionized acceptors is approximately equal to the concentration of acceptors compensated with donors plus the concentration of thermally ionized acceptors (those that have given a hole to the valence band to make the material p-type). In the depletion region extending into the p-type material, the uncovered space charge is given by $N_A^- - N_d \equiv \Delta N_A^- \simeq p$. But $p << N_d$, so that Eq. (B-3) reduces to

$$W \simeq \left[\frac{2 \varepsilon V}{q \Delta N_A^-} \right]^{1/2} \quad . \qquad \text{(B-4)}$$

Assuming a Fermi energy of 0.46 eV from the valence band, as in sample 14-8-6(b), so that p can be calculated from Eq. (II-5), several values of W are presented in Table B-1 for bias voltages ranging from 5 kV to 50 kV. Also included in the table are the E_o, calculated from the W. While in each case E_o exceeds the average field, it is still moderate for reasonable depletion widths, and increases only with the square root of the voltage.

The dark current is composed of thermally generated currents in the neutral regions and the depletion region, but injected currents are virtually non-existent. Since the thermally generated leakage currents in the large depletion region will probably be dominant, the leakage current is expected to increase with W, a scaling law far more suitable than the super-linear scaling that occurs with double injection.

Table B-1 Depletion width and peak field for several values of bias voltage.

Bias Voltage V [kV]	Depletion Width W [cm]	Peak Field E_o [kV/cm]
5	0.7	14
10	1.0	19
25	1.6	31
50	2.3	44

Because the junctions are symmetrical, the device can hold off the same voltage of either polarity.

Of course, this device appears to be the familiar n-p-n transistor, but it does not conduct like a transistor. As a result, it can have a large semi-insulating "base" to hold off large voltages without worry about poor current transfer characteristics, the limiting factor in real transistors. Instead of causing conduction by injecting minority carriers into the base, the weakly p-type material is converted into a strongly n-type photoconductor by optical illumination. Compensation by deep copper acceptors is used to make the semi-insulating p-type region. By depleting Cu_B of electrons with sub-band-gap radiation, the depletion region can be erased, leaving a bulk n-type photoconductor in series with two strongly n-type contact regions. The n^+ regions now serve as highly conductive transitions to the ohmic contacts which reduce the power dissipation in the contact region.

The resulting current flow is controlled by the bulk photoconductivity, not by junction effects. Since the tail conductivity can be sustained by electron injection from the ohmic contacts into the n-type photoconductor, current can flow *in either direction* as long as the photoconductivity will sustain it, just like in the original BOSS concept. The photoconductivity can be interrupted on command just as before by optically exciting holes from Cu_B. However, the exact process leading to the re-establishment of the reverse bias depletion region is not trivial, but it probably can be achieved against even strong electron injection during the high field stress of opening if sufficient turn-off radiation intensity is maintained.

Perhaps the most interesting feature of the proposed device is its ease of manufacture using the process already developed to produce Cu:Si:GaAs material.

A simplified description of the suggested process for manufacturing the structure in Fig. B-1 will now be discussed. Consider Fig. B-2. The first illustration [Fig. B-2 (a)] is of a rectangular wafer, say with dimensions of 0.5 cm × 3 cm and a thickness of 0.5 mm. This wafer is uniformly doped with a shallow donor (silicon) to a density of 5×10^{16} cm^{-3}.

The first step in the process is to cover about 5 mm of the material at either end of the sample with a heat resistant photoresist. Then, a thin layer of copper can be vacuum deposited on the space in between the masked regions, as shown in Fig. B-2 (b). When the sample is placed in a diffusion furnace at a temperature that will produce the appropriate level of compensation (550 °C to 575 °C), then copper will diffuse into the bulk material. However, since the masked regions are long compared to the thickness of the wafer, only a small portion of the region under the mask will be penetrated and compensated by the Cu (assuming relatively isotropic diffusion), but the region underneath the copper will be saturated with acceptor defects. This is illustrated by the arrows in Fig. B-2 (b).

After diffusion, the photoresist is stripped from the material, and Au:Ge:Ni contacts are made on opposite sides of the wafer, but over the regions previously masked. This will result in the structure shown in Fig. B-2 (c). The two n^+ regions should be close to their original conductivity because they were isolated from the Cu diffusion. Undercompensating the region in between the n^+ regions should be avoided because a junction will not form. Instead, the annealing temperature should be carefully chosen to stay on the p-type side of the compensation curve, as discussed in Chapter II. If the application calls for high tail conductivity, then the resistivity of the compensated region should be as close to intrinsic as possible. If the

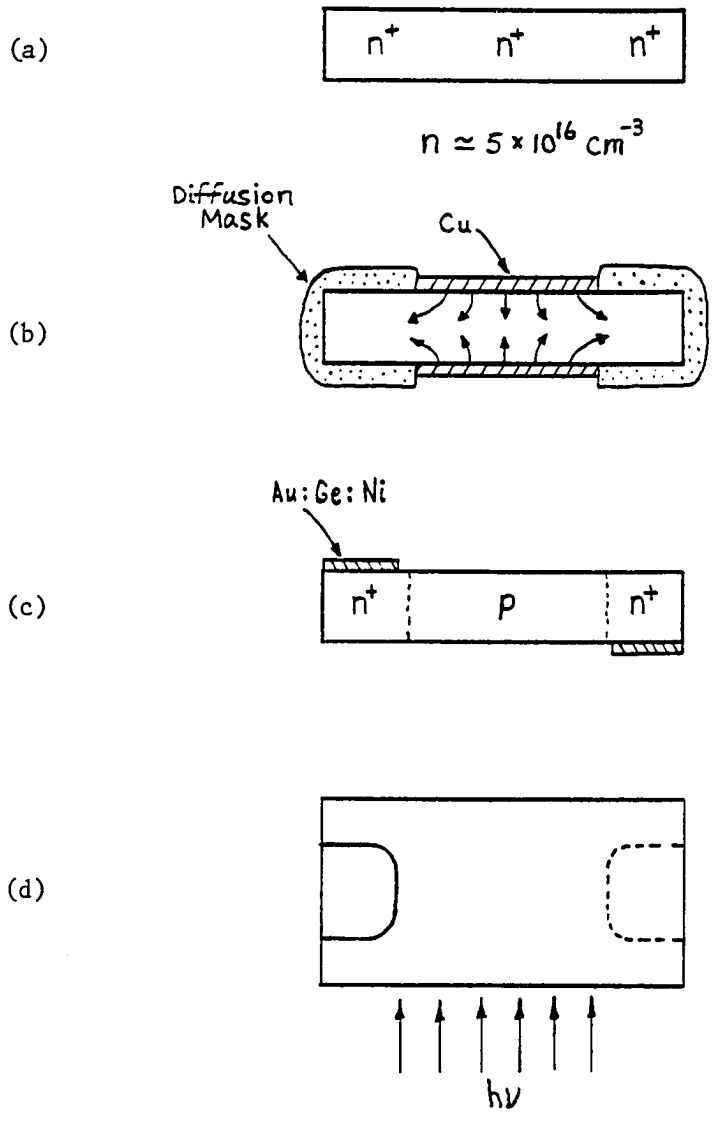

Figure B-2 An illustration of the important steps in fabricating the proposed device. The initial bulk crystal is shown in (a), the diffusion of copper into selected (unmasked) portions of the bulk crystal is shown in (b), and the finished device with contacts is shown in (c) and (d).

application requires good turn-off characteristics, then the material should be more strongly p-type. It should also be noted that the level of compensation controls the depletion width at a given bias voltage; therefore, care must be taken to select the length of the compensated region to accommodate the depletion width expected at a given level of compensation and bias voltage, so that depletion width "punch through" and resulting charge injection at the contacts is avoided.

Figure B-2 (d) is a top view of the device. The contacts are arranged in an offset over-under geometry to increase the surface flashover potential of the device. The device geometry is also an advantage during conduction, because the expected large conduction currents are supported through highly conductive n^+ transition regions to the ohmic contacts. Since hole currents are negligible during the tail conduction phase, only single carrier injection is required to sustain the current, and majority carrier (electron) injection at that. Thus minimal power dissipation is expected in the contact region.

Finally, the switch is to be activated by side pumping the depletion region as shown in Fig. B-2 (d). The advantage here is that the long absorption length (several millimeters) of the extrinsic radiation is fully absorbed traveling through the width of the switch, as opposed to traveling through the narrow thickness of the wafer. Thus a relatively high *intensity*, but low *power* laser pulse can be used to illuminate the small cross section presented by the side of the switch, and the laser pulse need only contain the minimum energy required to activate the conduction volume because of the efficient absorption. Of course, the same argument prevails for the deactivation of the switch with a second longer-wavelength laser pulse.

The optical efficiency can be further increased by coating the side of the sample with an anti-reflection coating so that the 30% reflection occurring at the surface of the crystal, due to the large ε of GaAs, is virtually eliminated. In this way, it is hoped to use compact, pulsed semiconductor lasers operating at 905 nm (or more) to activate tail conduction, but even if this is not feasible at first, then the radiation can be supplied by a central Nd:YAG laser whose output is fanned out to a stack of switches using fiber optic cables. The high voltage isolation between switches comes naturally, without the need for heavy, slow, isolation transformers or other equipment.

Michael S. Mazzola was born in Bethesda, Maryland, in 1961. He received the B. S. and M. E. degrees, both in electrical engineering, in 1984 and 1986, respectively, from Old Dominion University in Norfolk, Virginia.

From 1986 to 1989 he has been a Graduate Research and Teaching Assistant in the Department of Electrical and Computer Engineering at Old Dominion University. In January of 1990, he will join the Naval Surface Warfare Center in Dahlgren, Virginia, to continue his work in high-power photoconductive switching.

He has co-authored three journal articles, including "Nanosecond optical quenching of photoconductivity in a bulk GaAs switch," *Appl. Phys. Lett.*, vol. 55, pp. 2102-2104, 1989; "GaAs photoconductive closing switches with high dark resistance and microsecond conductivity decay," *Appl. Phys. Lett.*, vol. 54, pp. 742-744, 1989; and "Modeling of a dc glow plasma loudspeaker," *J. Acoust. Soc. Am.*, vol. 81, pp. 1972-1978, 1987. In addition, he has co-authored a number of conference papers.

In 1985 he was named a Texas Instruments Graduate Fellow, which supported his work toward a Master's degree. In 1986 he was given the Graduate Research Paper Award by the Tidewater Chapter of Sigma Xi for a paper that was later published in the Journal of the Acoustical Society of America. In 1989 he was honored with the Pulsed Power Student Award at the Seventh IEEE Pulsed Power Conference in Monterey California.

He was inducted into the Phi Kappa Phi Honor Society in 1986. He is a Member of the Institute of Electrical and Electronic Engineers and the American Physical Society.